

1197  
MANEUVER LOADS BRANCH SECTION C-1

P. 53

# NATIONAL ADVISORY COMMITTEE FOR AERONAUTICS

## TECHNICAL NOTE

No. 1197

### SOME INVESTIGATIONS OF THE GENERAL INSTABILITY OF STIFFENED METAL CYLINDERS

VIII - STIFFENED METAL CYLINDERS SUBJECTED TO  
PURE TORSION

By Louis G. Dunn

California Institute of Technology



Washington

May 1947

NATIONAL ADVISORY COMMITTEE FOR AERONAUTICS

TECHNICAL NOTE NO. 1197

SOME INVESTIGATIONS OF THE GENERAL INSTABILITY OF STIFFENED METAL CYLINDERS

VIII - STIFFENED METAL CYLINDERS SUBJECTED TO PURE TORSION

By Louis G. Dunn

SUMMARY

An experimental investigation of the general instability of reinforced thin-walled metal cylinders was carried out at the California Institute of Technology. The basic parameters involved were the spacing and sectional properties of the stiffening elements, the wall thickness, and the diameter of the cylinder. An analysis of the experimental data led to a suitable parameter for estimating the general instability stress of reinforced metal cylinders when subjected to pure torsion loading.

INTRODUCTION

The present report deals with the experimental investigation of the general instability of metal cylinders subjected to pure torsion loading. Reports on other loading conditions, that is, pure bending, combined bending and transverse shear, and combined bending and torsion, have been published previously (references 1 to 7).

Inasmuch as a condition of a pure torsional load seldom arises in the design of fuselage or wing structures, the problem of pure torsion as such might not warrant an investigation. However, under a combined loading of bending and torsion (reference 7) the ultimate load of the stiffened cylinder is dependent on the ratio of the shearing stress at failure for combined loading to the shearing stress at failure for pure torsion. Hence, in order to predict the ultimate strength of a stiffened metal cylinder subjected to combined bending and torsion, a knowledge of the ultimate strength of the cylinder when subjected to a pure torsion loading is necessary.

Because of the nonlinearity of the buckling problem of stiffened cylinders (cf. references 5 and 8), no attempt has been made to give a theoretical treatment of the problem. As given in the present report, the

parameter for predicting the ultimate strength of stiffened metal cylinders subjected to torsion loads is based on an analysis of the experimental results and on the existing theory of unstiffened metal cylinders. This method was preferred over that of a linearized theory which cannot correctly describe the behavior of the structure. The results of a linear theory would have to be modified and corrected to bring it into agreement with the experimental observations and thus the theory would immediately be rendered an empirical method.

This investigation was carried out by the California Institute of Technology under the sponsorship and with the financial assistance of the National Advisory Committee for Aeronautics.

#### SYMBOLS

$M_T$  applied torsional moment, inch-pounds

$M_{T_{cr}}$  applied torsional moment at skin buckling, inch-pounds

$M_{T_{max}}$  applied torsional moment at failure, inch-pounds

$\tau$  shearing stress in the sheet covering, pounds per square inch

$\tau_{cr}$  buckling shear stress of the sheet covering, pounds per square inch

$\tau_{max}$  shearing stress in the sheet covering at failure, pounds per square inch

$\sigma_t$  tensile stress of diagonal-tension field, pounds per square inch

$P$  tension load resulting from  $\sigma_t$  acting over a unit circumferential width of sheet; acts in the direction of  $\cos \alpha$ , pounds

$P_H$  longitudinal component of  $P$ , pounds

$P_V$  circumferential component of  $P$ , pounds

$\alpha$  angle of diagonal-tension field with reference to a longitudinal stiffener

$\epsilon_{st}$  strain in a longitudinal stiffener

$G$  shear modulus, pounds per square inch

$E$  Young's modulus, pounds per square inch

$G_E$  effective shear modulus, pounds per square inch  
 $t$  thickness of sheet covering, inches  
 $A$  area enclosed by sheet covering, square inches  
 $R$  radius of cylinder, inches  
 $L$  length of cylinder, inches  
 $b$  spacing of longitudinals, inches  
 $d$  spacing of frames, inches  
 $\rho_x$  radius of gyration of a longitudinal and effective sheet, inches  
 $\rho_y$  radius of gyration of a frame and effective sheet, inches

#### DESCRIPTION OF APPARATUS

All tests were conducted in the combined bending and torsion machine of the structures laboratory at GALCIT. This machine has a maximum capacity of 500,000 inch-pounds. A detailed description of the machine is given in reference 2. A photograph (fig. 1) shows a 10-inch-diameter cylinder mounted for a pure-torsion test.

The wire-strain-gage equipment, as used for the strain measurements, has been described in reference 6. The circumferential position of the various gages is shown in figure 2. Longitudinally the gage is mounted at the center of the specimen.

#### TEST PROCEDURE

The test specimens were all circular reinforced metal cylinders. Two sizes of specimens were tested, one series having a diameter of 32 inches and a length of 64 inches, and the other series, a diameter of 20 inches and a length of 40 inches. The sheet covering was 0.010-, 0.015-, and 0.020-inch-thick 24ST dural. The longitudinal reinforcing members consisted of round 24ST dural tubing drawn to an elliptical shape and the frames consisted of rectangular bars of 24ST Alclad. Longitudinals of three different wall thicknesses and frames of two different sizes were used. A sketch of the reinforcing members is presented in figure 3.

A diagram showing a sheet panel bounded by two longitudinal stringers and end mounting rings is presented in figure 4(a). The relationship of the forces acting on an element of sheet of unit width is given in figure 4(b). In table I the sheet thickness, the reinforcing members, and their spacing are listed for each specimen. Stress-strain curves of the materials used in the tests are shown in figures 5 to 12.

All test specimens were tested in the combined torsion and bending machine mentioned previously. In the pure torsion loading, the bending arms and one torsion arm were locked in place, the load being applied to the second torsion arm. In all tests, shear stresses in the sheet covering were not measured, inasmuch as it was assumed that a calculation of the shear stresses based on the classical formula

$$\tau = M_T / 2At \quad (1)$$

would be sufficiently accurate. Strain measurements of the induced stresses in the longitudinal members were made on all specimens, the strain measurements being made by means of electric strain gages as described in reference 6. For a number of specimens, the unit angular deflection as a function of the applied torque was measured. By measuring the differential displacement between two pointers mounted on the cylinder, the unit angular deflection could be calculated. The pointers consisted of triangular frame structures and are shown mounted on the specimen in figure 13. Mounting these pointers on the cylinder just in-board of the end-rings ensured that the entire measured deformation occurred in the cylinder.

The effective shear modulus was calculated in the following manner:

If

$l'$  length of the pointer measured from the center of the cylinder, inches

$\delta$  measured differential displacement between the two pointer, inches

$l$  distance between the pointers, inches

then the unit angular displacement is given by

$$\theta = \frac{\delta}{l l'}$$

and the effective shear modulus is

$$G_E = \frac{M_T l l^2}{2\pi R^3 t \delta} \quad (2)$$

Some attempts were made to measure the wave form of the buckled sheet as a function of the applied torque; however, considerable difficulty was encountered in these measurements, primarily because of the nonuniform buckling which occurred over the cylinder. It was found that, in the testing of a cylinder, buckling of individual panels, that is, a sheet panel bounded by two frames and two longitudinals, would vary by as much as 100 percent. For this reason it was thought that a measurement of the wave form and wave amplitude as a function of the applied load would be rather meaningless. Photographs of a number of typical failures are shown in figures 13 to 17.

#### TEST RESULTS

Results of the induced longitudinal strain as a function of the applied torsional moment are shown for 17 specimens in figures 18 to 34. Each curve represents the average of two strain gages mounted on diametrically opposite sides of the longitudinal stiffener.

The induced strain is associated with the shear buckles in the sheet covering. It can be readily seen that upon buckling of the sheet, longitudinal forces which act on the end mounting rings are introduced by the sheet covering. These forces have a tendency to pull the end mounting rings together and, since such a motion is resisted by the longitudinal stiffeners, the result is an induced strain in these members. In the appendix some calculations have been worked out on the magnitude of the resulting strains. The calculated values do not agree too well numerically with the measured values; however, the order of magnitude is correct.

The results of induced strain as a function of applied torque have been cross-plotted as shown in figures 35 to 46. The strain was plotted radially outward with the cylinder circumferences as the zero reference line. These curves indicate that in general the induced strain is distributed uniformly around the cylinder.

In addition to the foregoing test data, the measurements of the effective shear modulus as a function of the shearing stress in the sheet covering are given in figures 47 to 53. At the lower shear-stress values, the results are not very reliable because of the difficulty in measuring the resulting small deflections. At the higher values of  $\tau$  the results are sufficiently accurate to indicate the order of magnitude of the

effective shear modulus which may result in an actual structure. It is of interest to note that the effective shear modulus  $G_E$  is considerably less than  $0.625G$ , which is the theoretical value for the fully developed diagonal-tension field of a flat plate.

In presenting these experimental data, it would be more appropriate to use the ratio  $\tau/\tau_{cr}$  rather than  $\tau$  or  $M_p$  since all the measured quantities are associated with buckling. However, as previously mentioned, for the cylinders tested, buckling did not occur uniformly over the cylinder at a definite load. The buckling process was progressive and uniform buckling occurred, for some specimens, at more than twice the load at which the first buckles appeared. For this reason, it was not possible to establish a definite observed buckling value.

In determining a parameter for predicting the general instability failure in torsion, the same general procedure was followed as was used in the pure-bending investigation of reference 5. The variables to be considered are the same as those of the pure-bending problem and can again be divided into two groups, namely, those dealing with the geometry of the structure and those involving the sectional properties of the stiffening elements as well as the sheet covering. The geometrical variables are the longitudinal spacing  $b$ , the frame spacing  $d$ , the diameter, and the length of the cylinder. The second group of variables includes the section properties of the longitudinals and frames and the thickness of the sheet covering.

A number of specimens were tested in which the geometrical variables  $b$  and  $d$  were systematically varied while  $R$  was kept constant and equal to 16 inches. The results of these tests yielded a family of curves as shown in figure 54 where the shearing stress in the sheet covering at failure is plotted as a function of the longitudinal spacing  $b$  for constant values of  $d/b$ . An examination of these curves indicates that, if the abscissa value of each curve is multiplied by an appropriate expansion factor  $K$ , all curves can be made to coincide with, for example, the curve of  $d/b$  equal to 0.394. A log-log plot of the expansion factor  $K$  as a function of  $d/b$  indicated that  $K$  varies as  $\sqrt{d/b}$ . A plot of  $1/K$  as a function of  $1/\sqrt{d/b}$  gives the linear variation indicated in figure 55. A plot of  $\tau_{max}$  as a function of  $\sqrt{bd}$  is shown in figure 56 and indicates that the test results scatter about a common curve.

The next question is, in what manner does the radius  $R$  influence the failing load? For the buckling of unstiffened cylinders subjected to pure torsion, the experimental results of reference 9 indicate that for values of  $L/R$  equal to and greater than 3.2 the buckling stress  $\tau_{cr}$  varies approximately as  $(t/R)^{3/4} \sqrt{t/L}$  as shown in figure 57. It

was therefore assumed that, for identical values of  $b$ ,  $d$ ,  $\rho_x$ , and  $\rho_y$ , the critical shearing stress for the general instability of a stiffened cylinder would vary as the reciprocal of  $R^{3/4}$ . In order to verify this assumption, a number of tests were conducted on 16-inch-radius specimens and various values of  $d$  and  $b$ . A plot of  $\tau_{\max}$  as a function of  $\sqrt{bd} R^{3/4}$  for the 10- and 16-inch specimens is shown in figure 58. These results indicated that the assumption was justified and it was therefore concluded that the parameter for predicting general instability in torsion is of the form:

$$\frac{\sqrt{bd} R^{3/4}}{f(\rho_x, \rho_y)}$$

From dimensional reasoning, it follows that the function  $f(\rho_x, \rho_y)$  must have the dimensions of the  $7/4$  power of a length. The simplest assumption for the function which determines the influence of the section parameters,  $\rho_x$  and  $\rho_y$ , is that it depends on only the geometrical mean value  $\sqrt{\rho_x \rho_y}$ . The parameter therefore appears in the form:

$$\sqrt{\frac{bd}{\rho_x \rho_y}} \left( \frac{R}{\sqrt{\rho_x \rho_y}} \right)^{3/4}$$

In checking the validity of this parameter, it is necessary to evaluate the amount of sheet acting with the frames and longitudinals in order to calculate  $\rho_x$  and  $\rho_y$ . It is quite difficult to evaluate by analytic means the amount of sheet acting with the reinforcing members; trial calculations indicated that the best results were obtained if the total width of sheet was used. For this reason  $\rho_x$  and  $\rho_y$  were calculated with the entire width of sheet assumed to be effective. The variation of  $\rho_x$  and  $\rho_y$ , with flat sheet assumed, as a function of the effective width of sheet  $w_e$  is shown in figures 59 to 63.

Specimens were also tested in which both the sheet thickness and sectional properties of the longitudinals were varied. The results of all tests are shown plotted in figure 64. It is seen that up to values of 10,000 pounds per square inch all test values scatter closely about a straight line. For higher values of  $\tau_{\max}$  there is a sudden shift in the experimental values. However, the majority of tests again follow a straight line having the same slope as the line corresponding to the lower values of  $\tau_{\max}$ . Since the observed diagonal-tension field varied between about  $30^\circ$  to  $50^\circ$ , it is seen from equation (3) (see appendix) that for a shear stress of 10,000 pounds per square inch the corresponding tensile stress would be between 20,000 and 23,000 pounds per square

inch. It was thought that this tensile stress might be sufficiently close to the proportional limit of the sheet covering to explain the sudden shift in the experimental values. However, an examination of the stress-strain curves (figs. 9 to 12) indicates that the tensile stress at a shear stress of 10,000 pounds per square inch is well below the proportional limit.

A more desirable presentation of the test data would be to plot

$\frac{\tau_{\max}}{G_E}$  against  $\sqrt{\frac{\rho_x \rho_y}{bd}} \left( \frac{\sqrt{\rho_x \rho_y}}{R} \right)^{3/4}$ , since  $\tau_{\max}/G_E$  corresponds to the

shearing strain  $\gamma$ . Such a presentation would be more general and would allow for materials of different physical properties or for changes in the physical properties above the proportional limit. It had not been realized at the beginning of the test program that it would be desirable to obtain a measure of  $\tau/G_E$  at failure. For this reason angular deformations were measured on only a number of specimens. Not enough measurements are available to make such a plot. A plot of  $\tau_{\max}/E$  as a func-

tion of  $\sqrt{\frac{\rho_x \rho_y}{bd}} \left( \frac{\sqrt{\rho_x \rho_y}}{R} \right)^{3/4}$  is given in figure 65. The value of  $E$

in this figure corresponds to that of the sheet covering and was taken as  $10^7$  pounds per square inch, since this is very close to the actual test values obtained for the sheet.

It should be noted that the curve of figure 65 as presented is strictly applicable to the aluminum alloys tested. However, an estimate of the failing stress of a reinforced cylinder of different material can be obtained by calculating the numerical value of the parameter and ascertaining the value of  $\tau_{\max}/E$  from the curves of figure 65.

#### CONCLUSIONS

The over-all general-instability test program was undertaken to furnish the designer with sufficient information to enable him to make an estimate of the allowable general-instability stress of a reinforced metal cylinder. With the completion of the pure-torsion-loading program sufficient information is available to estimate the general-instability stress for a variety of loading conditions, that is, pure bending; pure torsion; combined bending and torsion; and combined bending, transverse shear, and torsion.

The quantities involved in the parameter were all varied through a sufficient range to verify the generality of the parameter. The sudden break which occurs in the summary curve of general-instability failure has not been adequately explained. However, it is thought that it is connected with a variation in the physical properties of the various structural elements of the reinforced cylinder rather than a breakdown of the parameter. The reason for this statement is that of the eight specimens which failed above a shear stress of 10,000 pounds per square inch, one specimen falls on the original curve and the other seven on a curve which is parallel to the original curve. The parameter as derived does not itself give the numerical value of the ultimate stress, but defines essentially the slope of the ultimate-stress curve. If the shearing stress at failure  $\tau_{max}$  were replaced by a measured shear-strain deformation the experimental results might fall on a single curve. If, for example, in the pure-bending parameter of reference 5 the measured unit strain were replaced by a calculated stress corresponding to the ultimate bending moment the experimental results would not fall on a single curve.

California Institute of Technology,  
Pasadena, Calif., March 5, 1946.

APPENDIX

INDUCED LONGITUDINAL STRAIN

In considering a sheet panel bounded by two longitudinal stringers and the end mounting rings as shown in figure 4(a), it can be seen that, upon buckling, the diagonal-tension field produces horizontal components of force on the two end rings. The end plate to which one mounting ring is bolted is fixed to the base of the testing machine; whereas the other end plate is mounted on rollers and is free to move. Therefore, the horizontal force components must be resisted by the longitudinal stiffeners.

By considering an element of sheet of unit width (fig. 4(b)), the following relations can be derived:

$$P = t \sigma_t \cos \alpha$$

$$P_V = P \sin \alpha = t \sigma_t \sin \alpha \cos \alpha = t \tau$$

from which

$$\sigma_t = \tau / \sin \alpha \cos \alpha = 2\tau / \sin 2\alpha \quad (3)$$

$$P_H = P \cos \alpha = t \sigma_t \cos^2 \alpha = t \tau \cot \alpha$$

Since the diagonal-tension field exists only beyond the buckling stress  $\tau_{cr}$  it follows that

$$P_H = t(\tau - \tau_{cr}) \cot \alpha$$

The total horizontal component of force around the circumference is

$$P_{H\text{tot.}} = 2\pi R t(\tau - \tau_{cr}) \cot \alpha$$

And the unit strain in the longitudinals is given by:

$$\epsilon_{st} = \frac{2\pi t (\tau - \tau_{cr}) \cot \alpha}{n A_{st} E} \quad (4)$$

where

$n$  number of longitudinals

$A_{st}$  area of a longitudinal

By using the relation of equation (1), equation (4) can be written in the form,

$$\epsilon_{st} = \frac{(M_T - M_{Tcr}) \cot \alpha}{n R A_{st} E} \quad (5)$$

In order to compare the values of unit strain given by equation (5) with experimental values, it is necessary to know the value of  $M_{Tcr}$ . For purposes of comparison, the value of the moment at which a sharp change occurs in the slope of the moment-strain curve was considered to be  $M_{Tcr}$ . A comparison of measured and calculated unit strains is presented in figures 66 and 67. For the calculated strains, the value of  $\alpha$  was assumed to be  $45^\circ$ . It is seen that for the particular stiffeners of figure 67 the agreement is quite good; whereas for the two stiffeners of figure 66 the agreement is rather poor. A check of available photographs indicated that  $\alpha$  varied between  $30^\circ$  and  $50^\circ$  depending on the reinforcement spacing. By using the appropriate value of  $\alpha$ , therefore, a closer agreement may be obtained. For example, the value of  $\alpha$  for specimen 208 appears from the photographs to be slightly greater than

45° and for specimen 209 slightly less than 45°. In both cases, these angles tend to improve the agreement between calculated and measured values. For specimens 196 and 200, photographs are not available.

It should also be noted that there is considerable variation in the measured unit strain between longitudinals for a given test specimen. It is thought that, in general, equation (5) will give values sufficiently accurate for design purposes provided the correct value of  $\alpha$  is used.

## REFERENCES

1. Guggenheim Aeronautical Laboratory, California Institute of Technology: Some Investigations of the General Instability of Stiffened Metal Cylinders. I - Review of Theory and Bibliography. NACA TN No. 905, 1943.
2. Guggenheim Aeronautical Laboratory, California Institute of Technology: Some Investigations of the General Instability of Stiffened Metal Cylinders. II - Preliminary Tests of Wire-Braced Specimens and Theoretical Studies. NACA TN No. 906, 1943.
3. Guggenheim Aeronautical Laboratory, California Institute of Technology: Some Investigations of the General Instability of Stiffened Metal Cylinders. III - Continuation of Tests of Wire-Braced Specimens and Preliminary Tests of Sheet-Covered Specimens. NACA TN No. 907, 1943.
4. Guggenheim Aeronautical Laboratory, California Institute of Technology: Some Investigations of the General Instability of Stiffened Metal Cylinders. IV - Continuation of Tests of Sheet-Covered Specimens and Studies of the Buckling Phenomena of Unstiffened Circular Cylinders. NACA TN No. 908, 1943.
5. Guggenheim Aeronautical Laboratory, California Institute of Technology: Some Investigations of the General Instability of Stiffened Metal Cylinders. V - Stiffened Metal Cylinders Subjected to Pure Bending. NACA TN No. 909, 1943.
6. Guggenheim Aeronautical Laboratory, California Institute of Technology: Some Investigations of the General Instability of Stiffened Metal Cylinders. VI - Stiffened Metal Cylinders Subjected to Combined Bending and Transverse Shear. NACA TN No. 910, 1943.
7. Guggenheim Aeronautical Laboratory, California Institute of Technology: Some Investigations of the General Instability of Stiffened Metal Cylinders. VII - Stiffened Metal Cylinders Subjected to Combined Bending and Torsion. NACA TN No. 911, 1943.
8. von Kármán, Th., Dunn, Louis G., and Tsien, Hsue-Shen: The Influence of Curvature on the Buckling Characteristics of Structures. Jour. of Aero. Sci., vol. 7, no. 7, May 1940, pp. 276-289.
9. Donnell, L. H.: Stability of Thin-Walled Tubes under Torsion. NACA Rep. No. 479, 1933.

TABLE I

Specimen	Stiffener	Frame	b	d	$\sqrt{bd}$	R	$R^{3/4}$	$\sqrt{bd} R^{3/4}$	$\rho_x$	$\rho_y$	$(\rho_x \rho_y)^{7/8}$	$\sqrt{\frac{\rho_x \rho_y}{bd}} \left[ \sqrt{\frac{\rho_x \rho_y}{R}} \right]^{3/4}$	t	$M_{T_{max}}$	$\tau_{max}$
149	S <sub>2</sub>	F <sub>5</sub>	5.12	4	4.52	16	8.0	36.1	0.1061	0.0269	0.00594	$16.45 \times 10^5$	0.010	$10.70 \times 10^{-4}$	6,600
162	S <sub>2</sub>		2.56	4	3.20	16	8.0	25.6	.1169	.0269	.00648	25.3	.010	13.00	8,100
171	S <sub>1</sub>		2.56	4	3.20	16	8.0	25.6	.1145	.0269	.00636	24.82	.010	11.85	7,380
175	S <sub>1</sub>		2.56	8	4.52	16	8.0	36.1	.1145	.0234	.00563	15.6	.010	8.00	4,970
176	S <sub>1</sub>		2.56	2	2.26	16	8.0	18.075	.1145	.0285	.00670	37.05	.010	15.80	9,840
177	S <sub>1</sub>		5.12	16	8.98	16	8.0	71.9	.0967	.01732	.00373	5.19	.015	5.00	2,070
178	S <sub>1</sub>		5.12	8	6.36	16	8.0	50.9	.0967	.0218	.00455	8.94	.015	7.50	3,110
179	S <sub>1</sub>		5.12	4	4.52	16	8.0	36.1	.0967	.0262	.00536	14.8	.015	10.90	4,510
180	S <sub>1</sub>		5.12	2	3.20	16	8.0	25.6	.0967	.0289	.00584	22.8	.015	17.00	7,040
181	S <sub>1</sub>		5.12	16	8.98	16	8.0	71.9	.0915	.01525	.00318	4.42	.020	7.30	2,270
182	S <sub>1</sub>		5.12	8	6.36	16	8.0	50.9	.0915	.0202	.00406	7.97	.020	9.25	2,890
183	S <sub>1</sub>		5.12	4	4.52	16	8.0	36.1	.0915	.0251	.00491	13.6	.020	13.50	4,190
184	S <sub>1</sub>		5.12	2	3.20	16	8.0	25.6	.0915	.0289	.00556	21.7	.020	23.35	7,010
185	S <sub>1</sub>		5.24	8	6.48	10	5.62	37.4	.0961	.0218	.00453	12.1	.015	3.80	4,025
186	S <sub>1</sub>		5.24	4	4.58	10	5.62	25.8	.0961	.0262	.00533	20.6	.015	6.30	6,670
187	S <sub>1</sub>		5.24	2	3.24	10	5.62	18.2	.0961	.0289	.00581	31.9	.015	8.90	9,500
189	S <sub>1</sub>		10.24	32	18.1	16	8.0	144.9	.0895	.0143	.00296	2.04	.010	1.30	810
190	S <sub>1</sub>		10.24	16	12.8	16	8.0	102.5	.0899	.0188	.00376	3.67	.010	2.50	1,560
191	S <sub>1</sub>		10.24	8	8.98	16	8.0	71.9	.0899	.0234	.00455	6.33	.010	4.10	2,550
192	S <sub>1</sub>		10.24	4	6.36	16	8.0	50.9	.0899	.0269	.00514	10.1	.010	6.76	4,210
193	S <sub>1</sub>		2.56	2	2.26	16	8.0	18.075	.1145	.0285	.0067	37.05	.010	16.00	9,940
194	S <sub>3</sub>		5.24	8	6.48	10	5.62	37.4	.0947	.0228	.00466	12.45	.0115	2.90	4,010

TABLE I - Concluded.

Speci- men	Stiff- ener	Frame	b	d	$\sqrt{bd}$	R	$R^{3/4}$	$\sqrt{bd} R^{3/4}$	$\rho_x$	$\rho_y$	$(\rho_x \rho_y)^{7/8}$	$\sqrt{\frac{\rho_x \rho_y}{bd}} \left[ \frac{\sqrt{\rho_x \rho_y}}{R} \right]^{3/4}$	t	$M_{T_{max}}$	$T_{max}$
195	$S_3$		5.24	4	4.58	10	5.62	25.8	0.0947	0.0266	0.00533	$20.65 \times 10^5$	.0115	$4.95 \times 10^4$	6,780
196	$S_3$		5.24	2	3.24	10	5.62	18.2	.0947	.0287	.00571	31.30	.0115	6.70	9,270
197	$S_2$		2.62	8	4.58	10	5.62	25.8	.1166	.0228	.00558	21.60	.0115	5.10	7,050
198	$S_2$		2.62	4	3.24	10	5.62	18.2	.1166	.0266	.00641	35.20	.0115	7.40	10,250
199	$S_2$	$F_5$	2.62	2	2.29	10	5.62	12.85	.1166	.0287	.00683	53.20	.0115	9.00	12,450
200	$S_2$		2.62	2	2.29	10	5.62	12.85	.1152	.0285	.00673	52.40	.010	7.90	12,560
201	$S_2$		2.62	1	1.62	10	5.62	9.05	.1152	.0281	.00665	73.50	.010	11.50	18,290
202	$S_2$		2.62	1	1.62	10	5.62	9.05	.1152	.0281	.006836	75.7	.020	24.00	19,100
203	$S_1$		2.62	8	4.58	10	5.62	25.8	.1136	.0385	.00866	33.6	.0115	7.00	9,690
204	$S_1$		2.62	4	3.24	10	5.62	18.2	.1136	.0428	.00950	52.2	.0115	10.50	14,540
205	$S_1$		2.62	2	2.29	10	5.62	12.85	.1136	.0436	.0966	75.2	.0115	13.90	19,200
206	$S_1$	$F_7$	2.62	8	4.58	10	5.62	25.8	.1110	.0316	.00708	27.5	.0200	10.50	8,350
207	$S_1$		2.62	4	3.24	10	5.62	18.2	.1110	.0415	.0092	50.5	.020	14.85	11,820
208	$S_1$		2.62	2	2.29	10	5.62	12.85	.1110	.0453	.0097	75.5	.020	22.00	17,500
209	$S_1$		2.62	3	2.8	10	5.62	15.72	.1110	.0435	.0965	61.5	.020	18.90	15,000

NATIONAL ADVISORY  
COMMITTEE FOR AERONAUTICS.

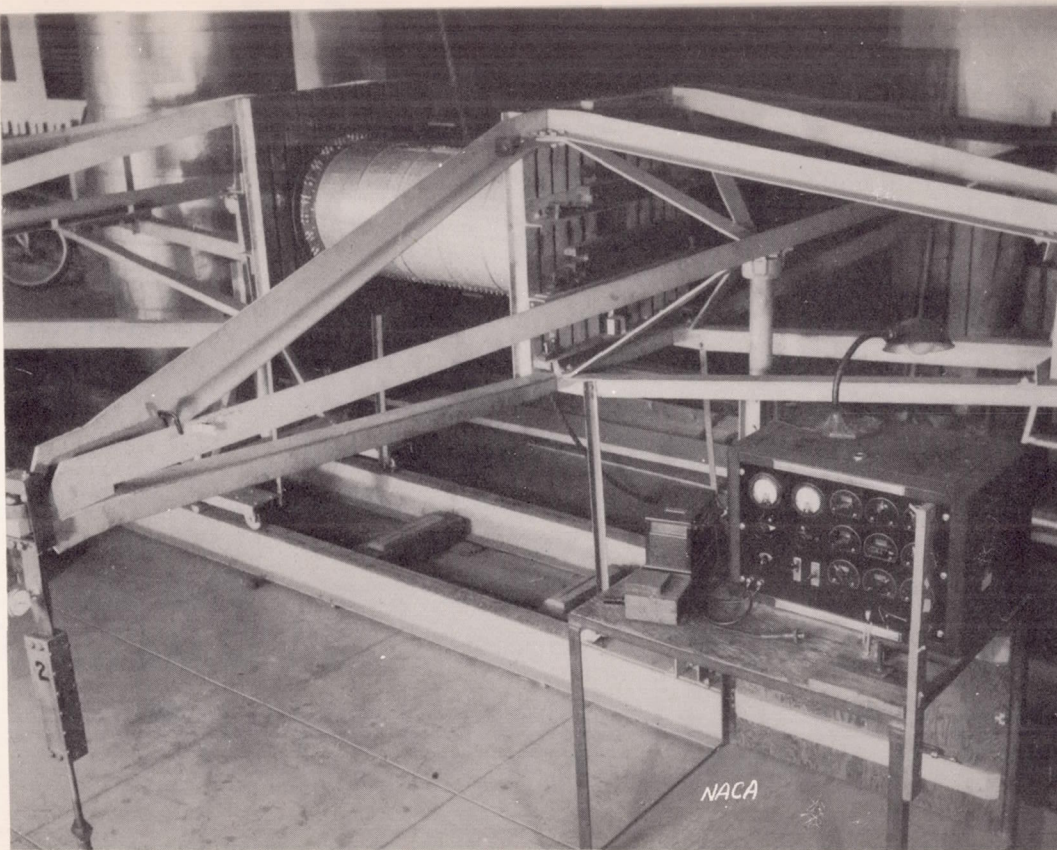


Figure 1.- Testing machine with test specimen in place.

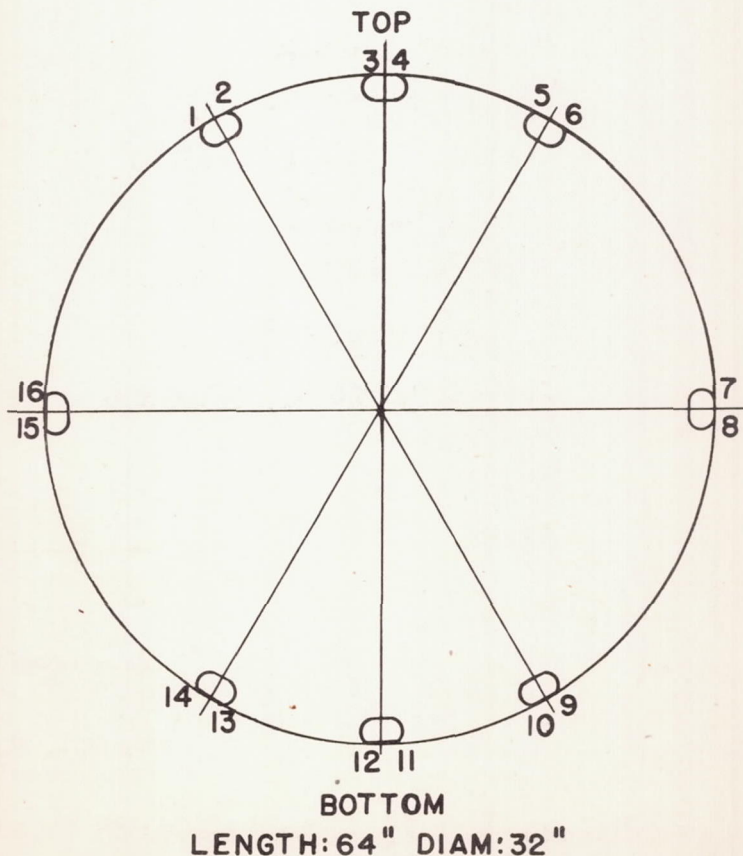
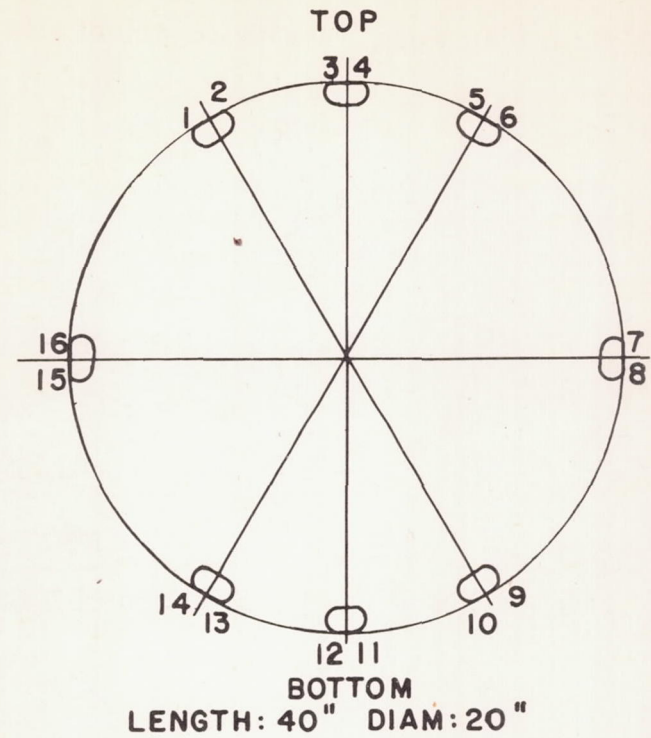


FIGURE 2.

Fig. 3

NACA TN No. 1197

NOTE: All drawings are twice actual size

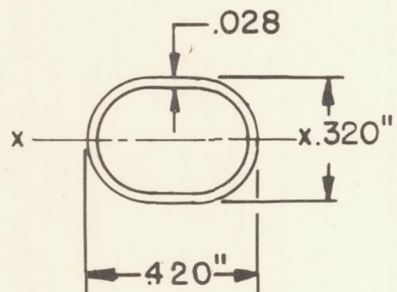
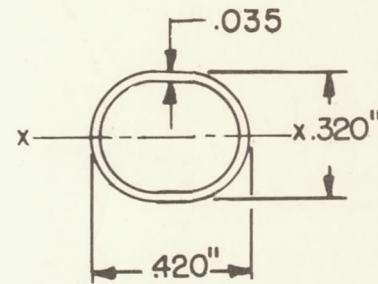
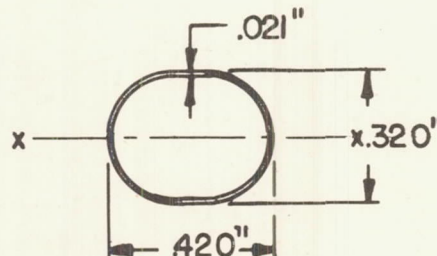
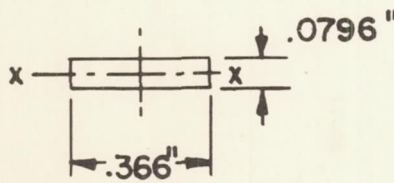
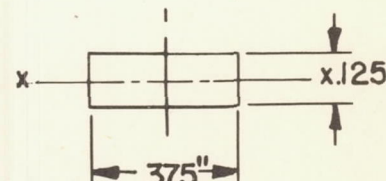
STIFFENER-S<sub>1</sub>Area = 0.0324  $I_{xx} = 0.000374$ STIFFENER-S<sub>2</sub>Area = 0.0368  $I_{xx} = 0.000407$ STIFFENER-S<sub>3</sub>Area = 0.02295  $I_{xx} = 0.000326$ FRAME-F<sub>5</sub>Area = 0.0291  $I_{xx} = 1.537 \times 10^{-5}$ FRAME-F<sub>7</sub>Area = 0.04688  $I_{xx} = 6.108 \times 10^{-5}$ 

FIGURE 3.

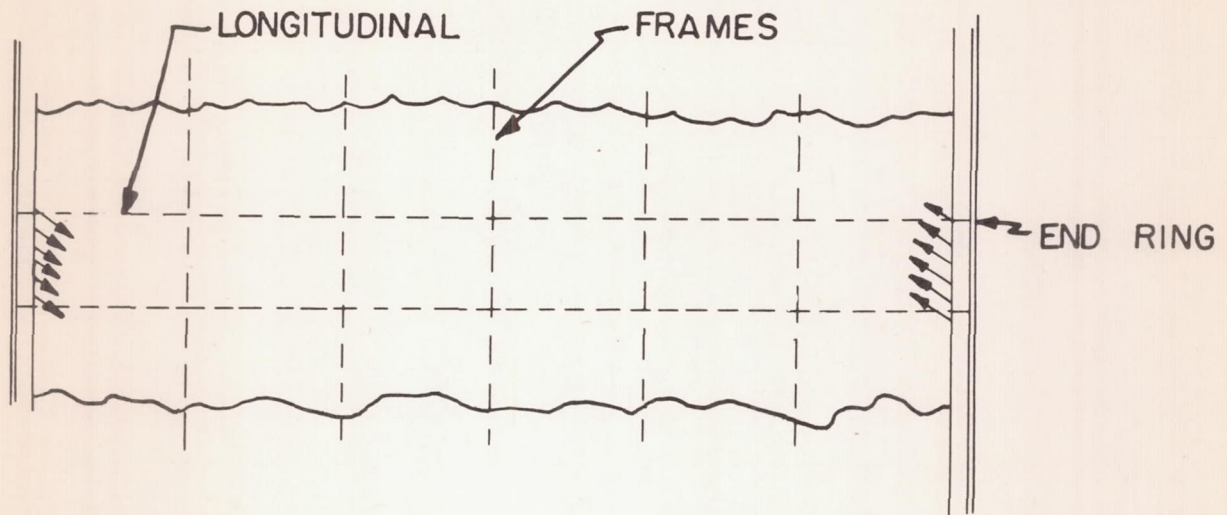


FIGURE 4a.

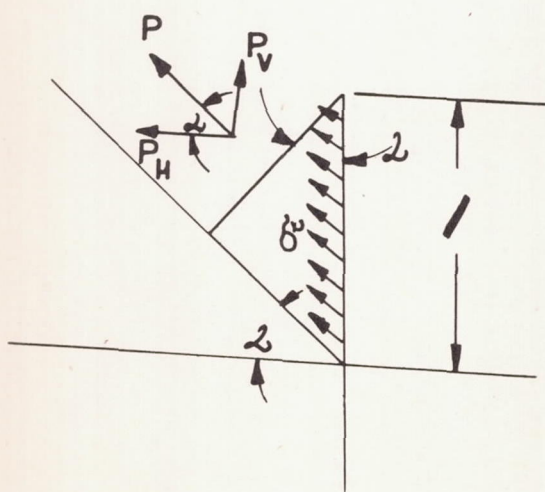
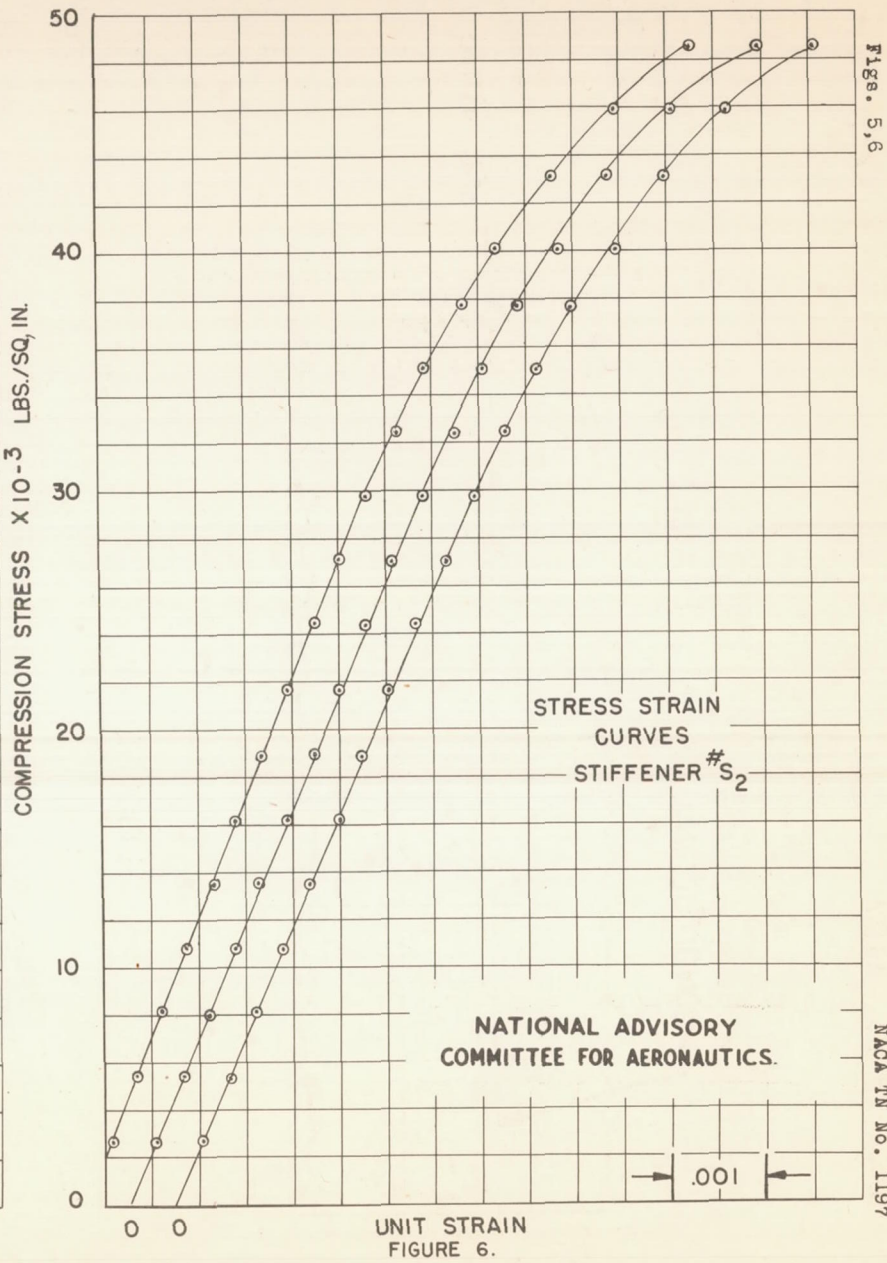
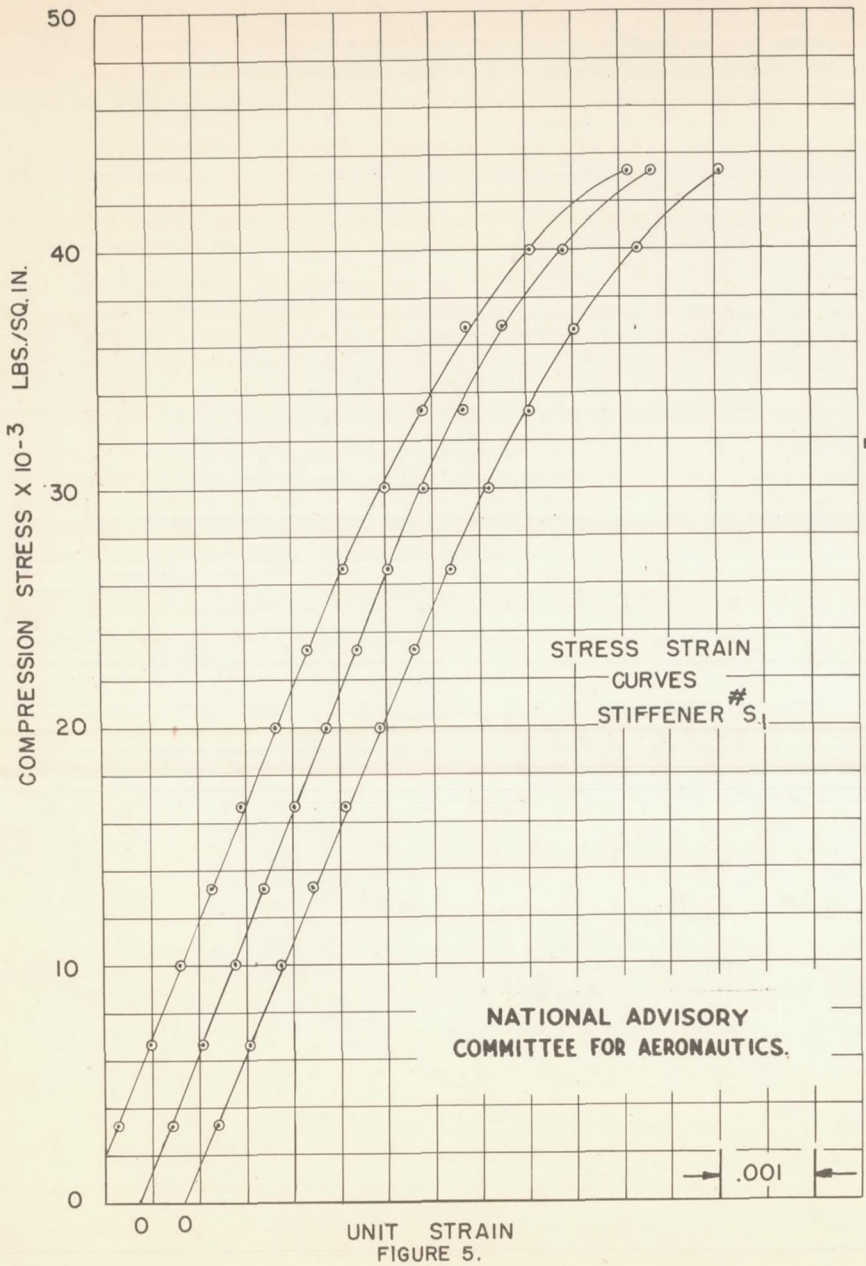
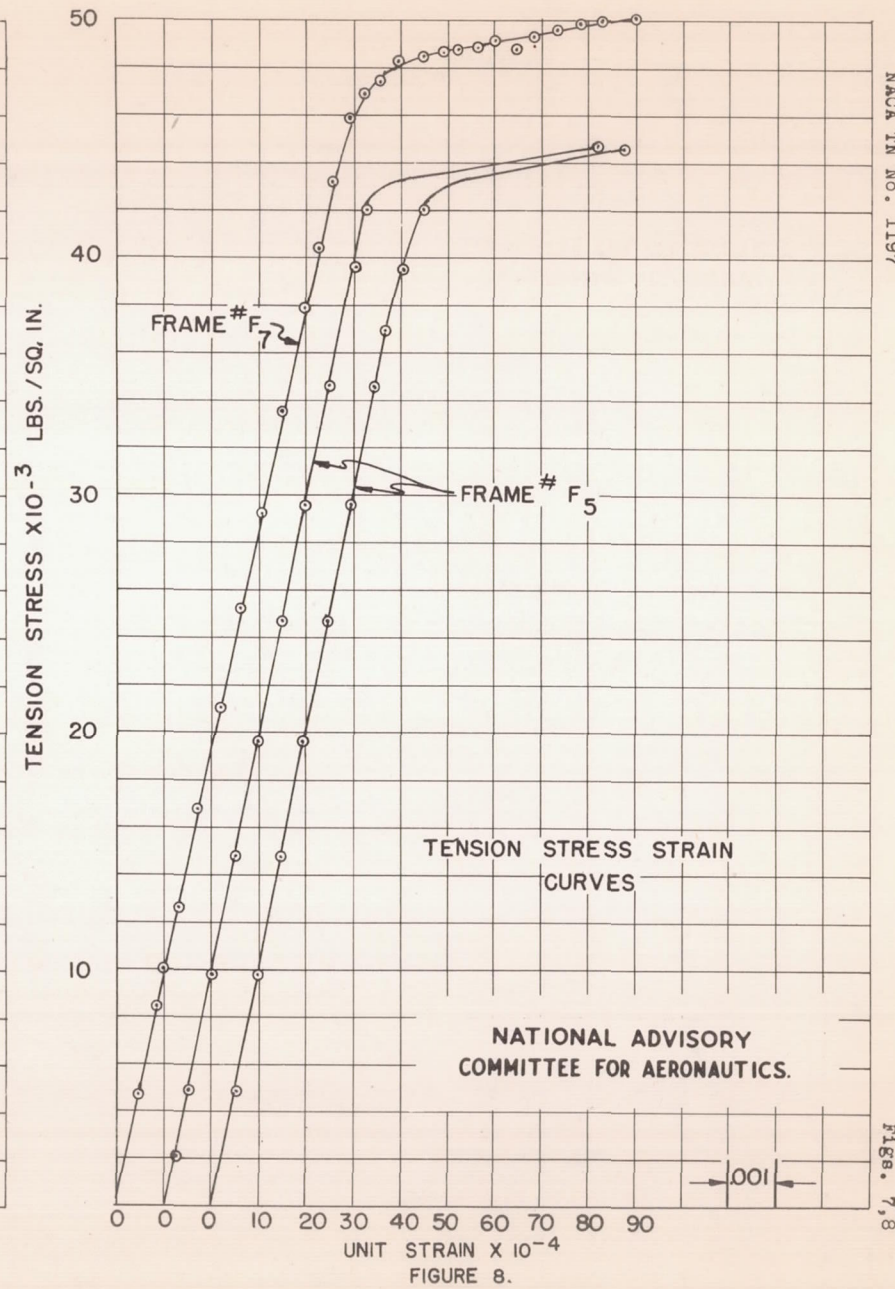
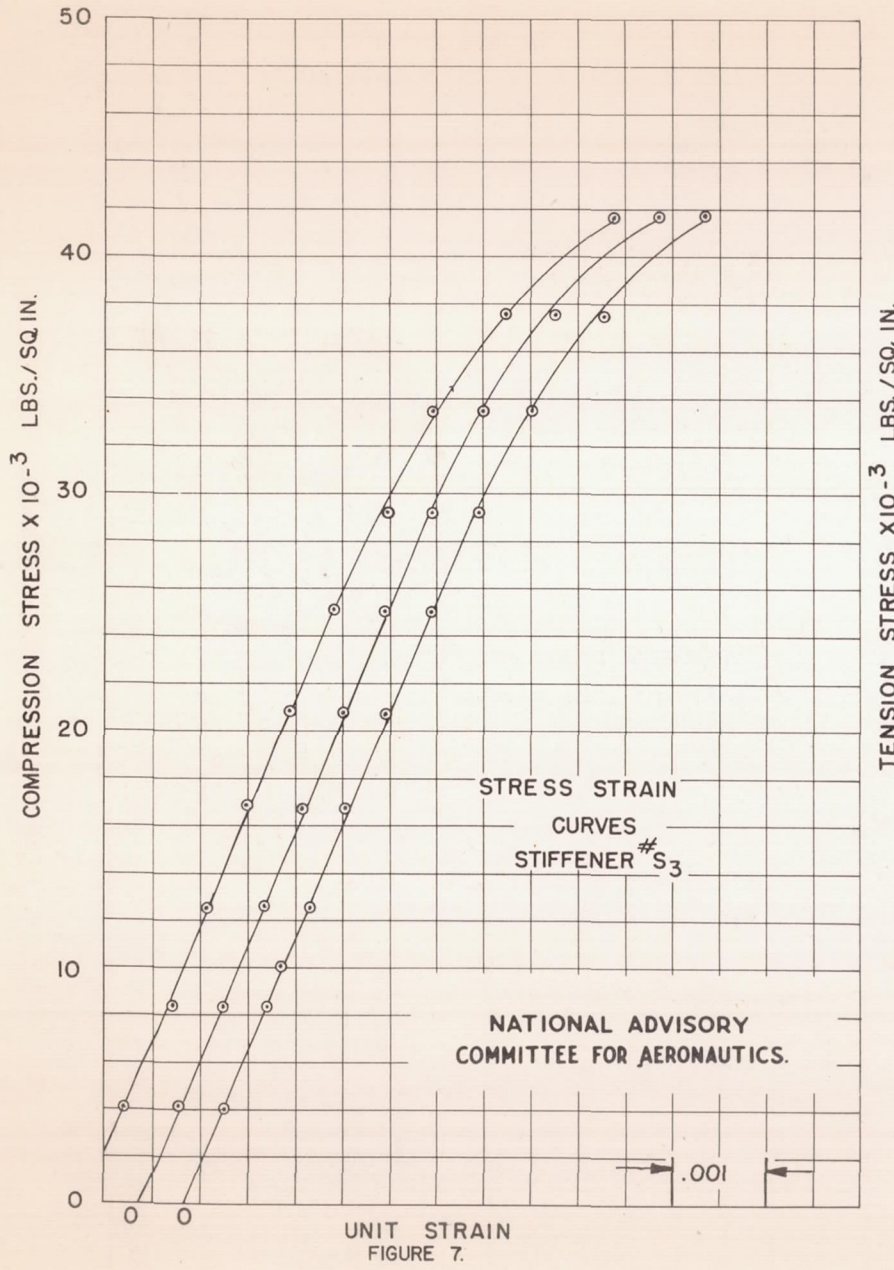


FIGURE 4b.





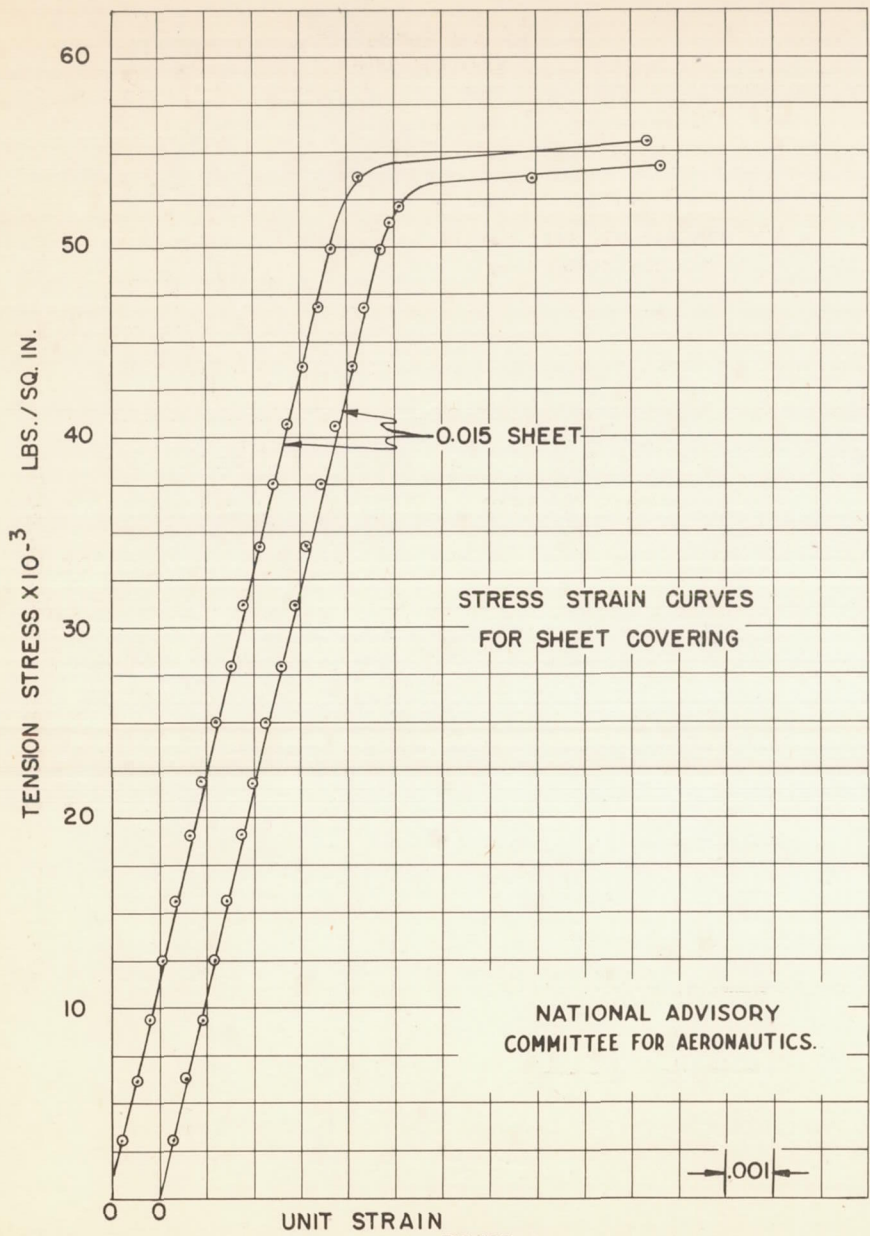
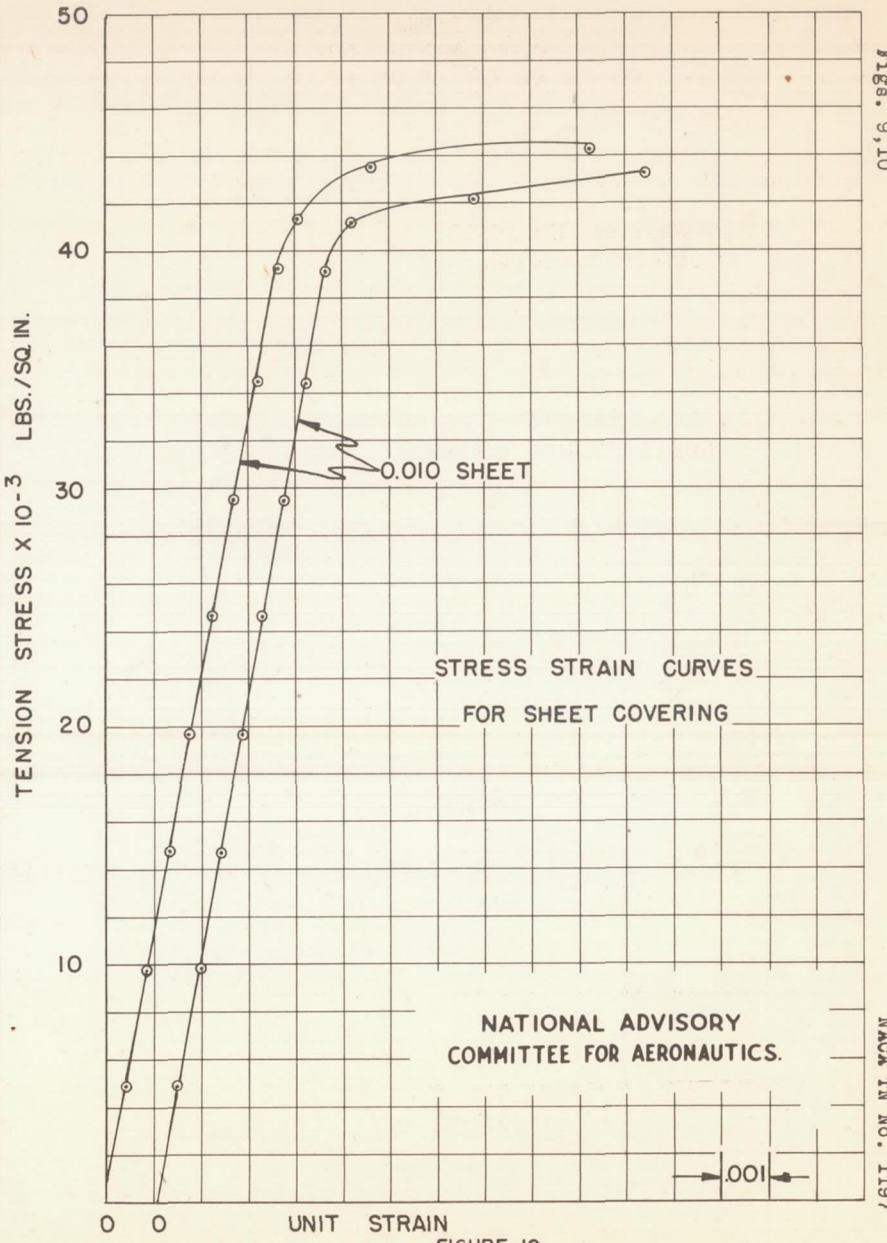
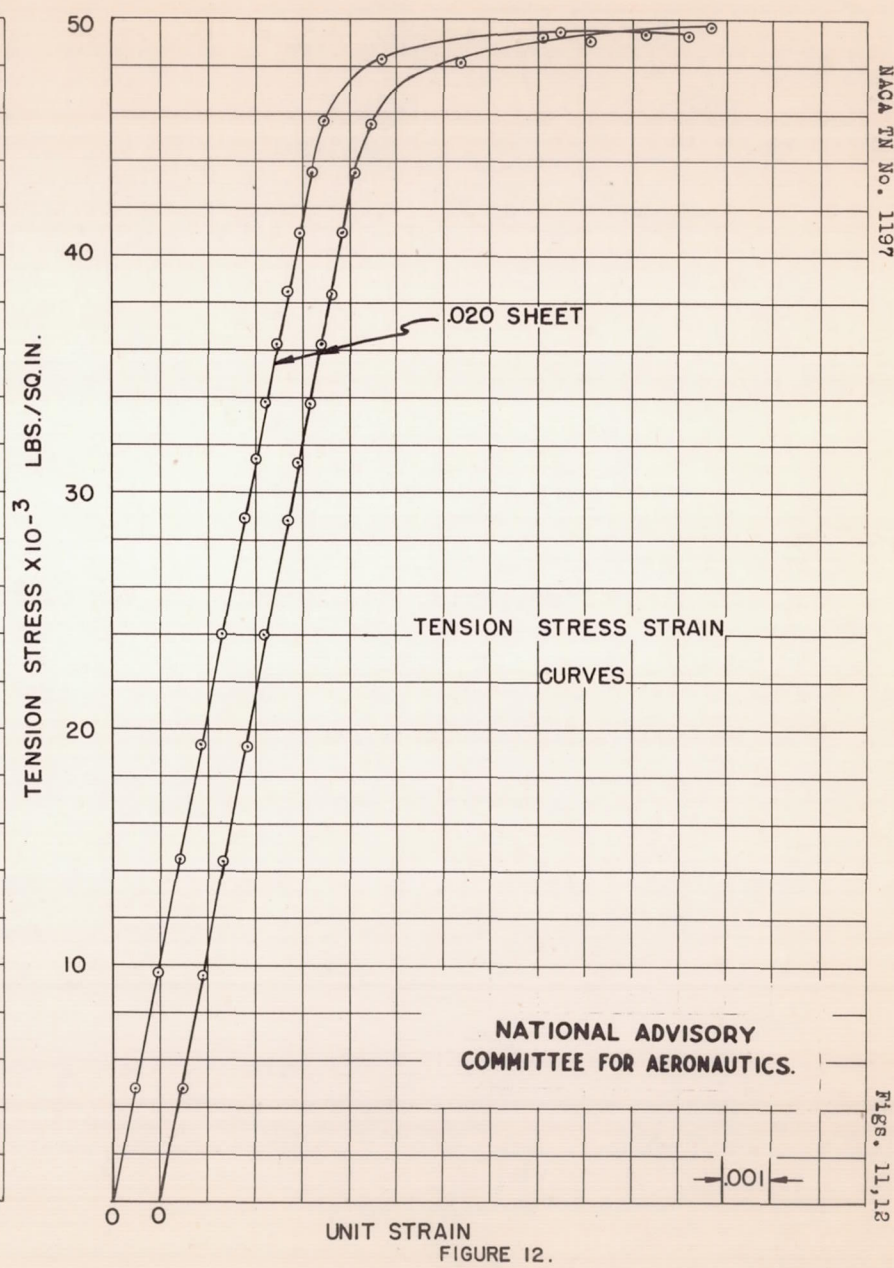
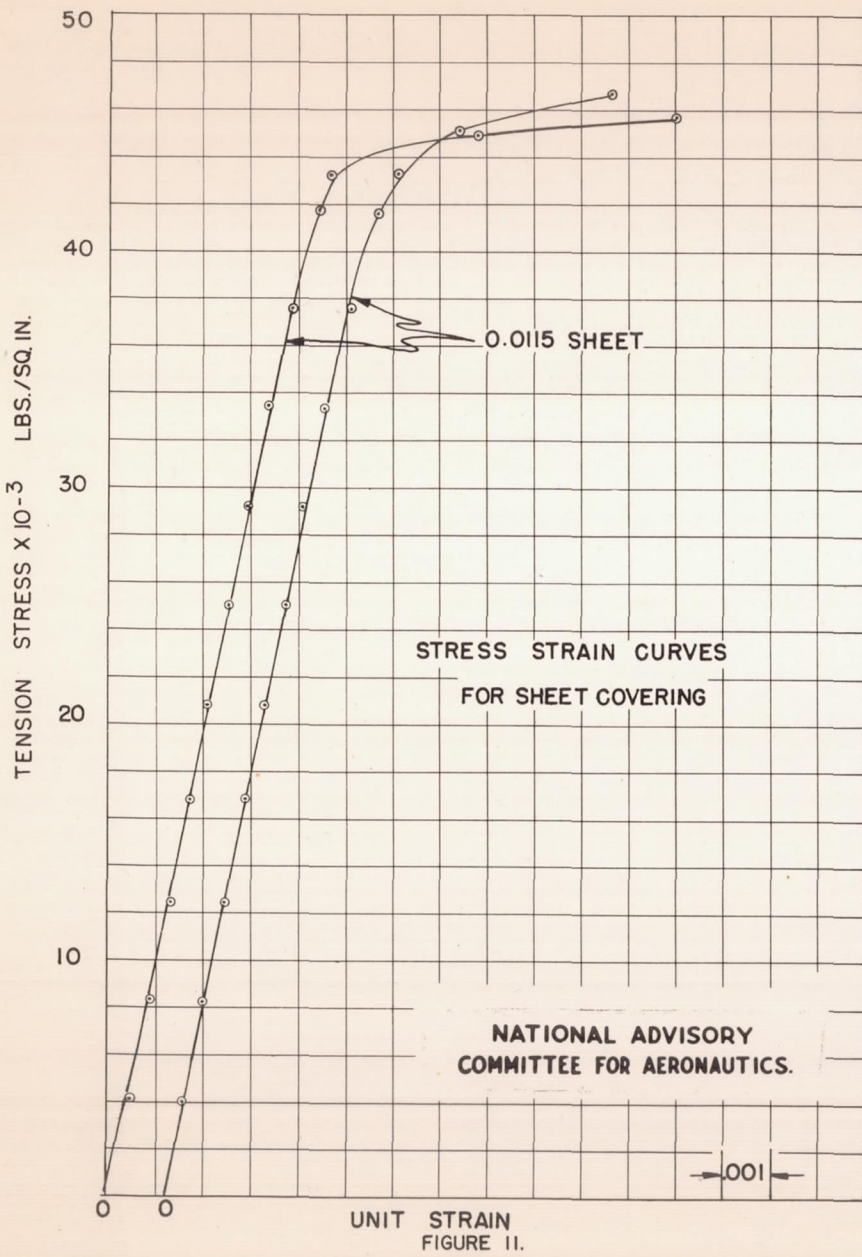


FIGURE 9.



NACA TN No. 1197

FIGS. 9, 10



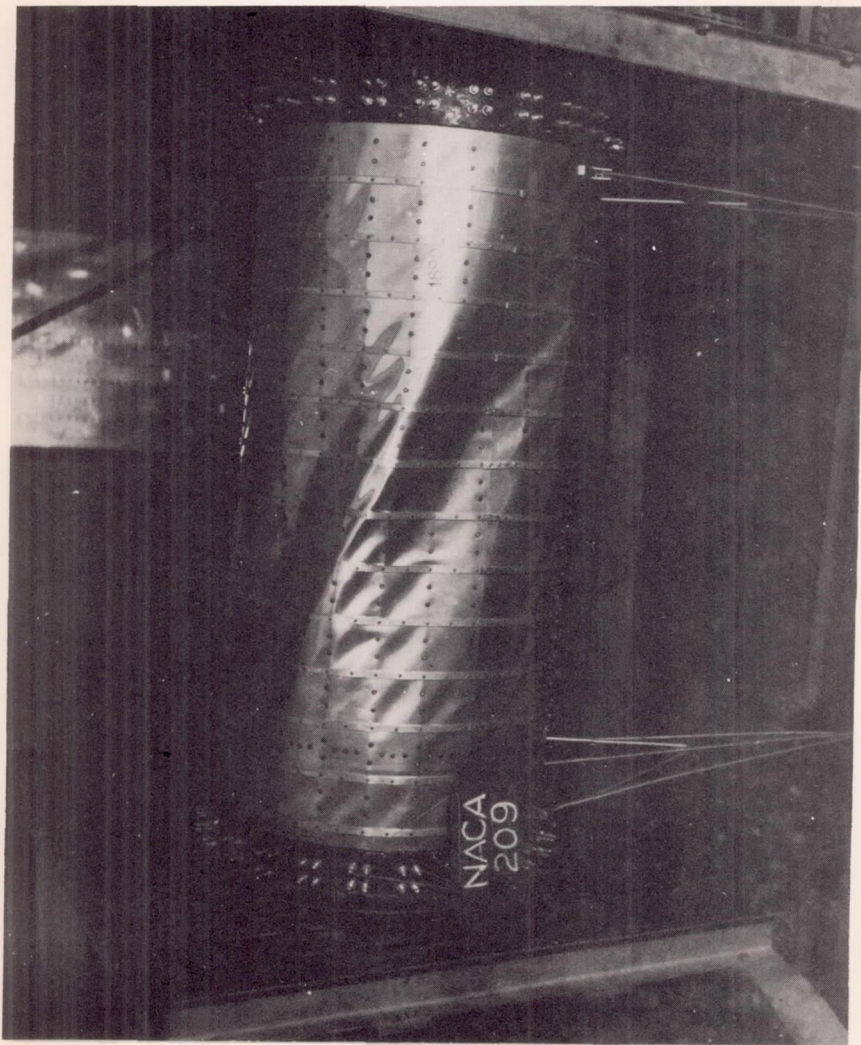


Figure 13.— Specimen with deflection pointers.

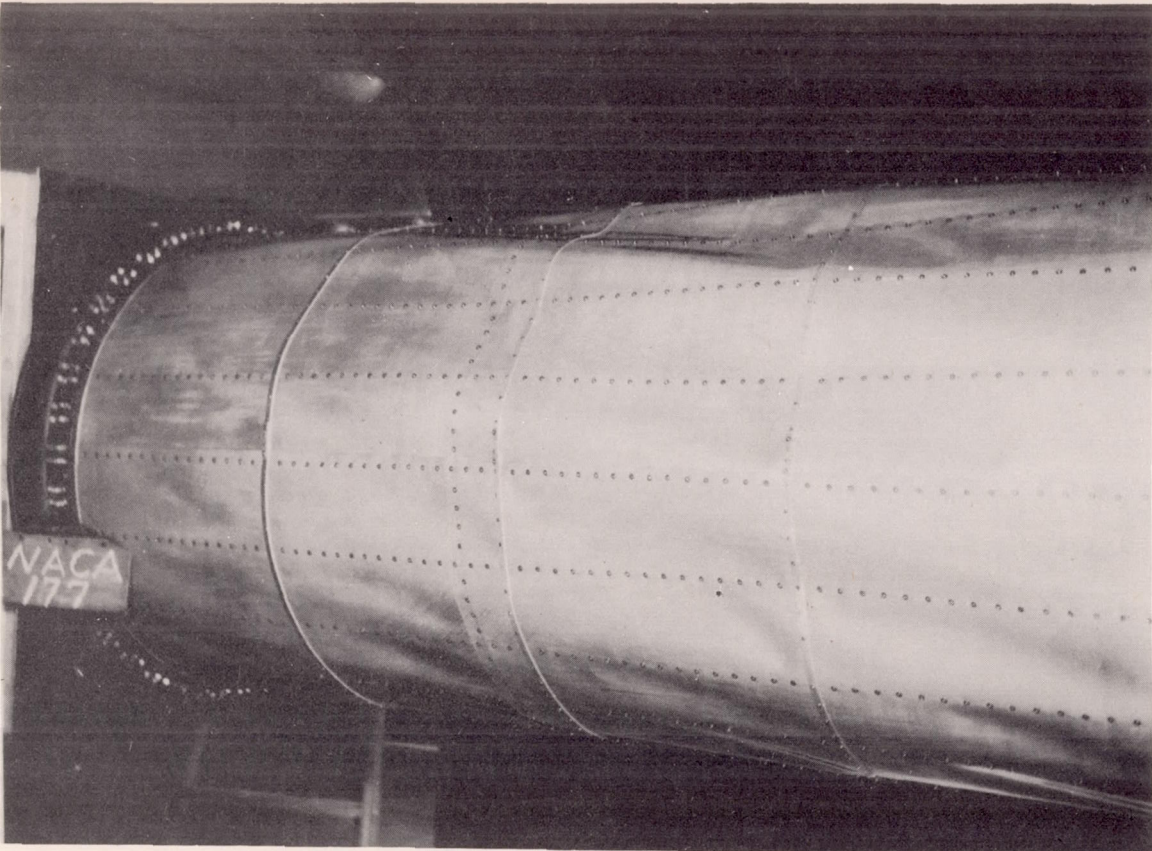


Figure 14.— Failure of a specimen with 16-inch frame spacing.

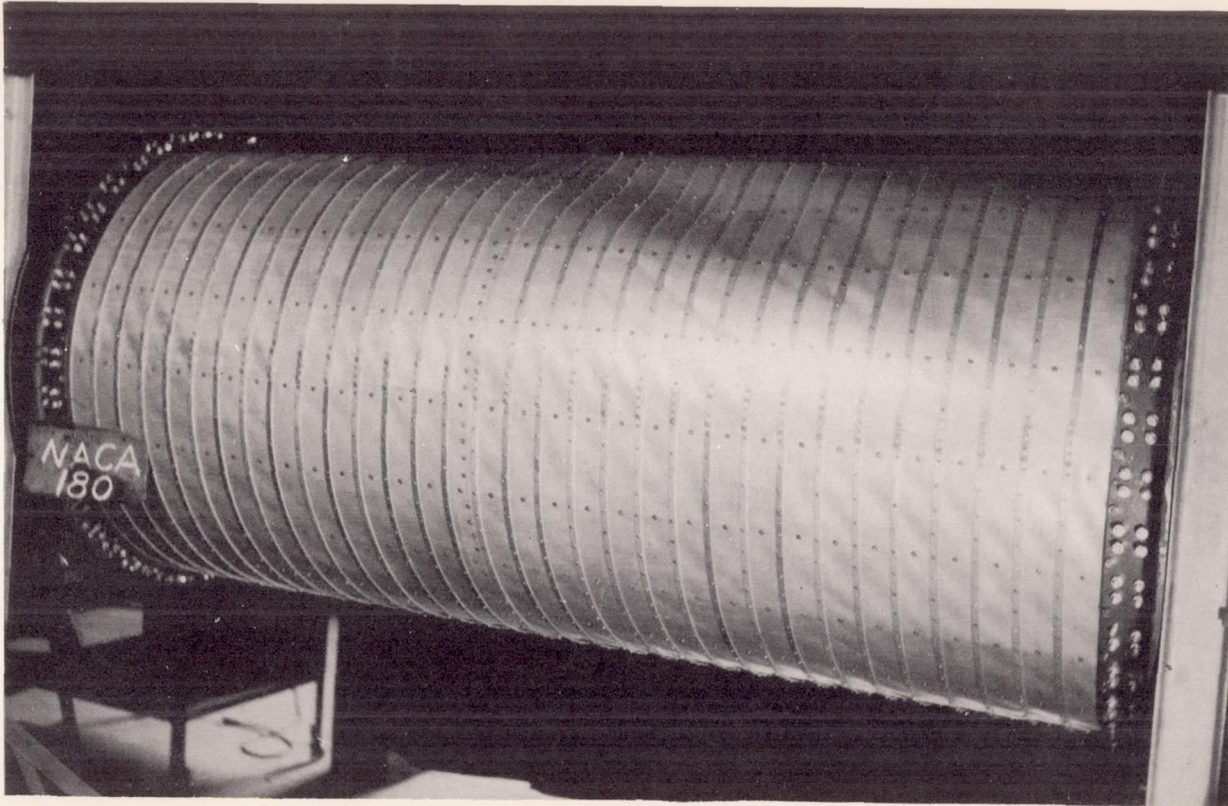


Figure 15.- Failure of a specimen with 2-inch frame spacing.

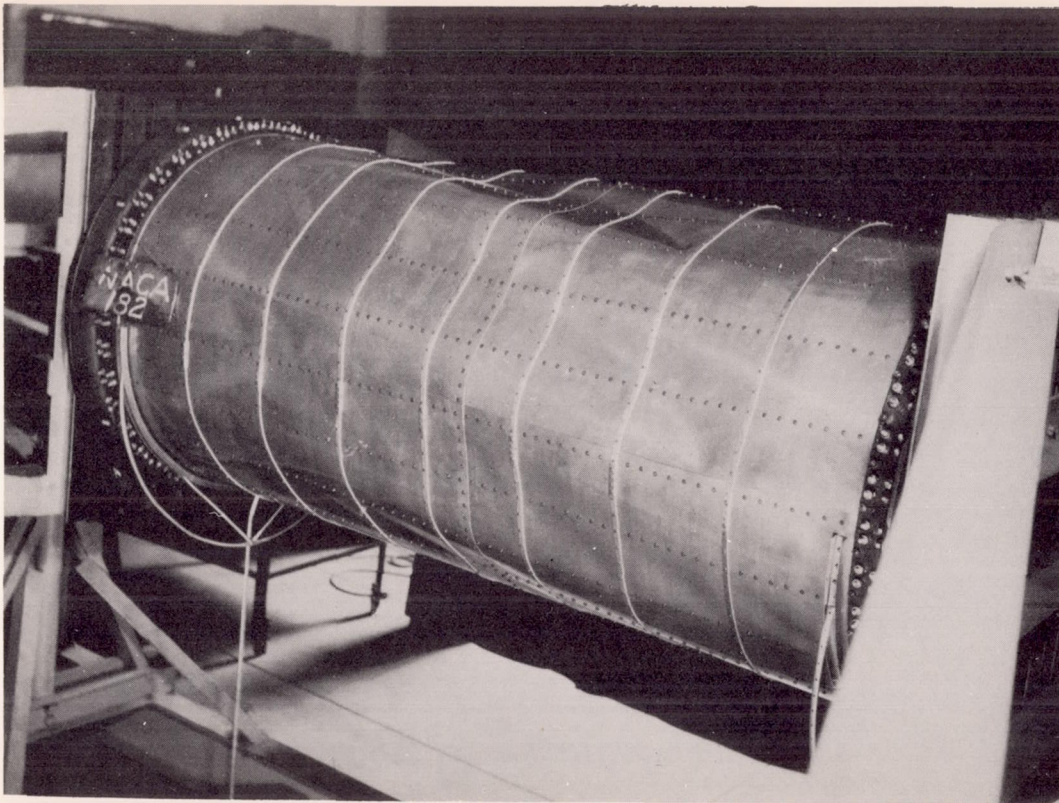


Figure 16.- Failure of a specimen with 8-inch frame spacing.

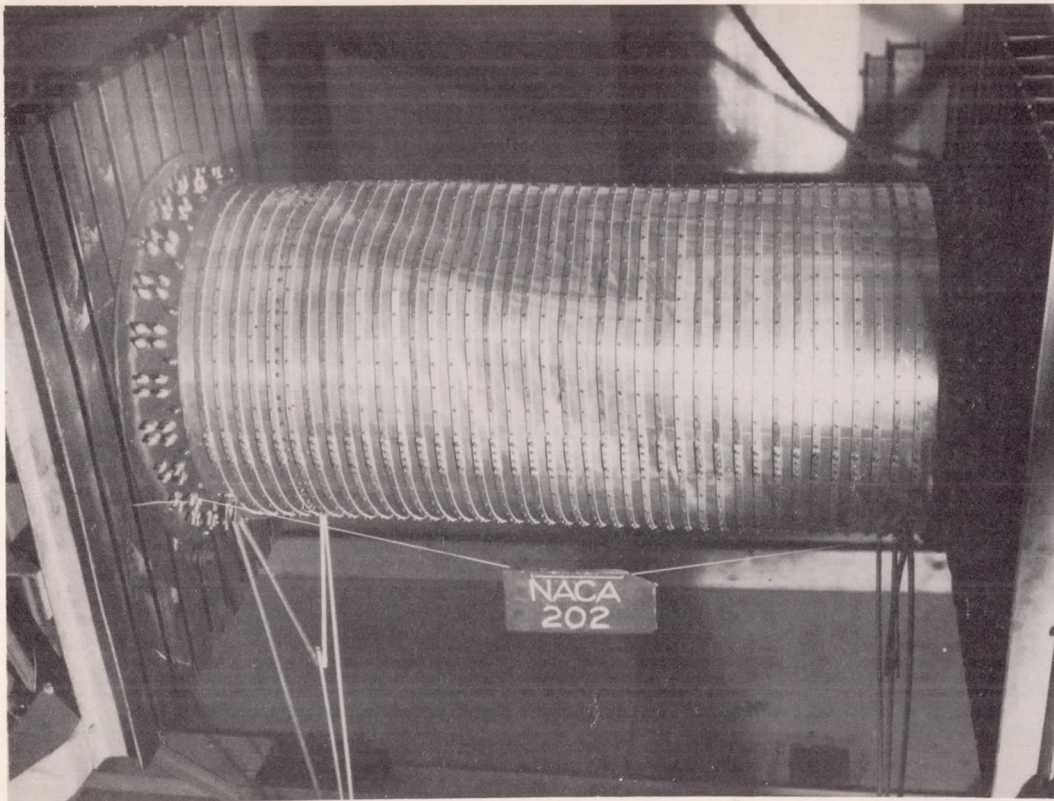
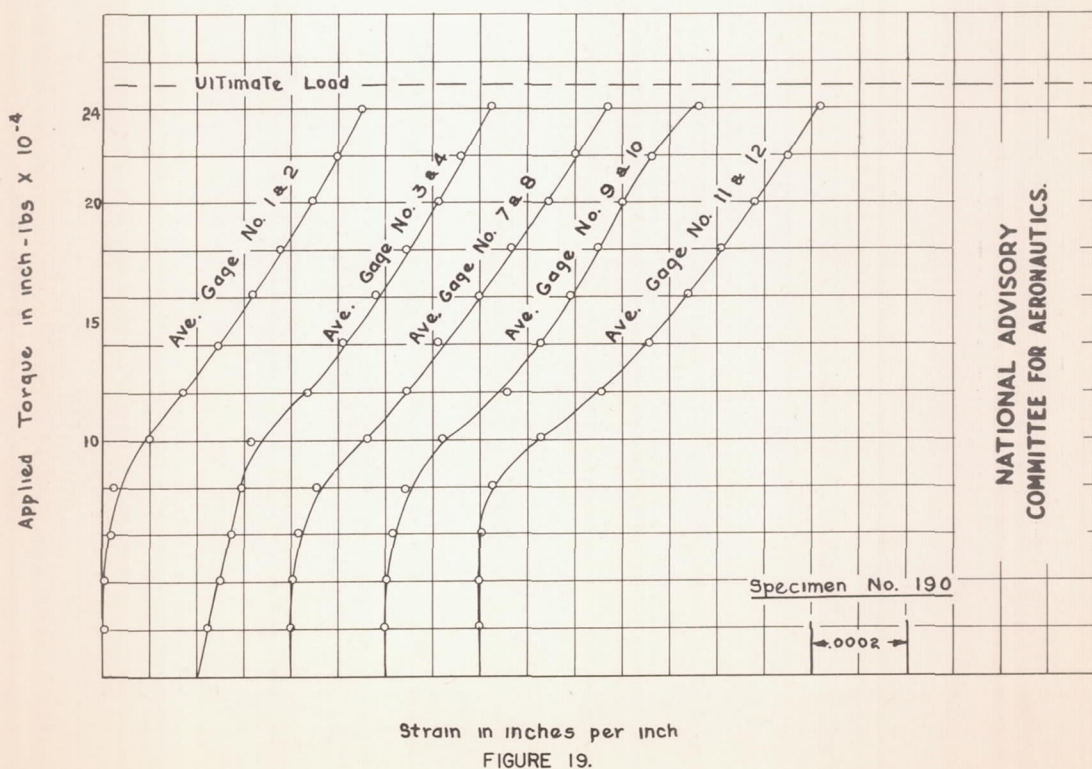
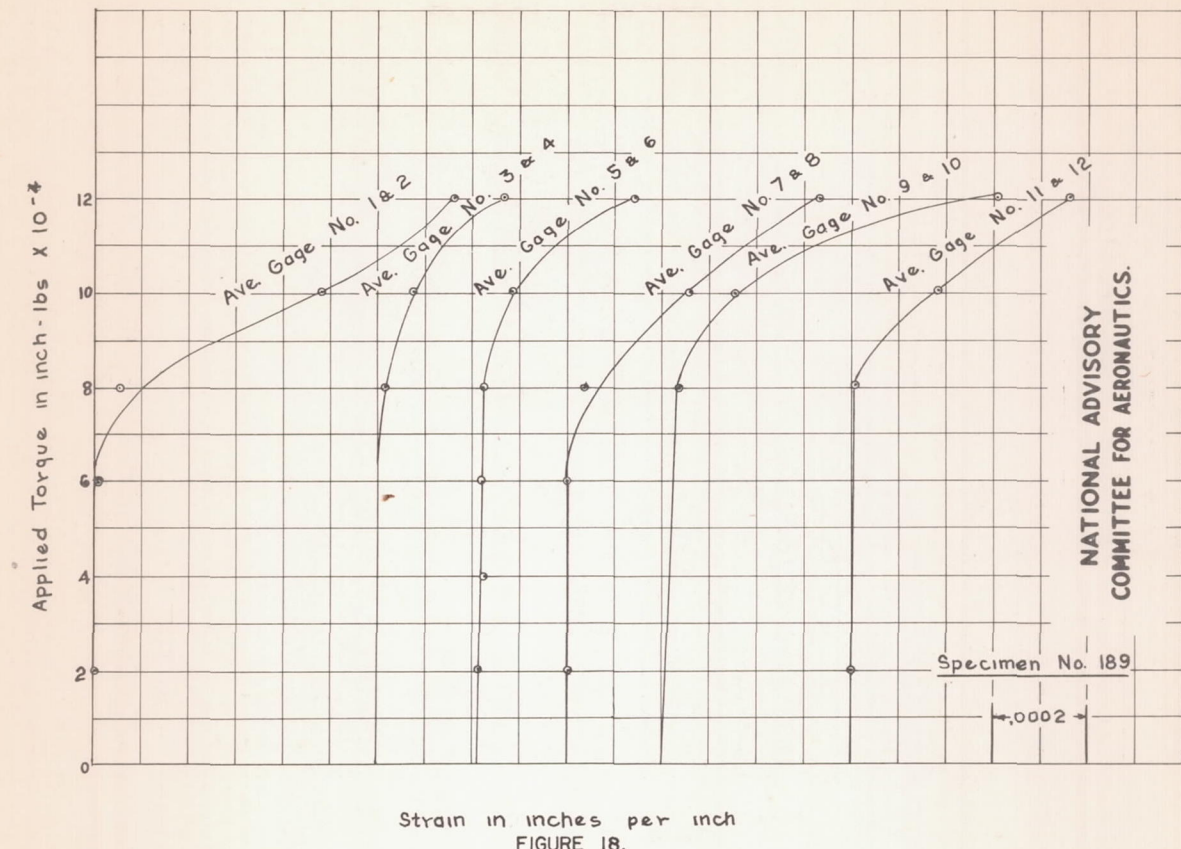
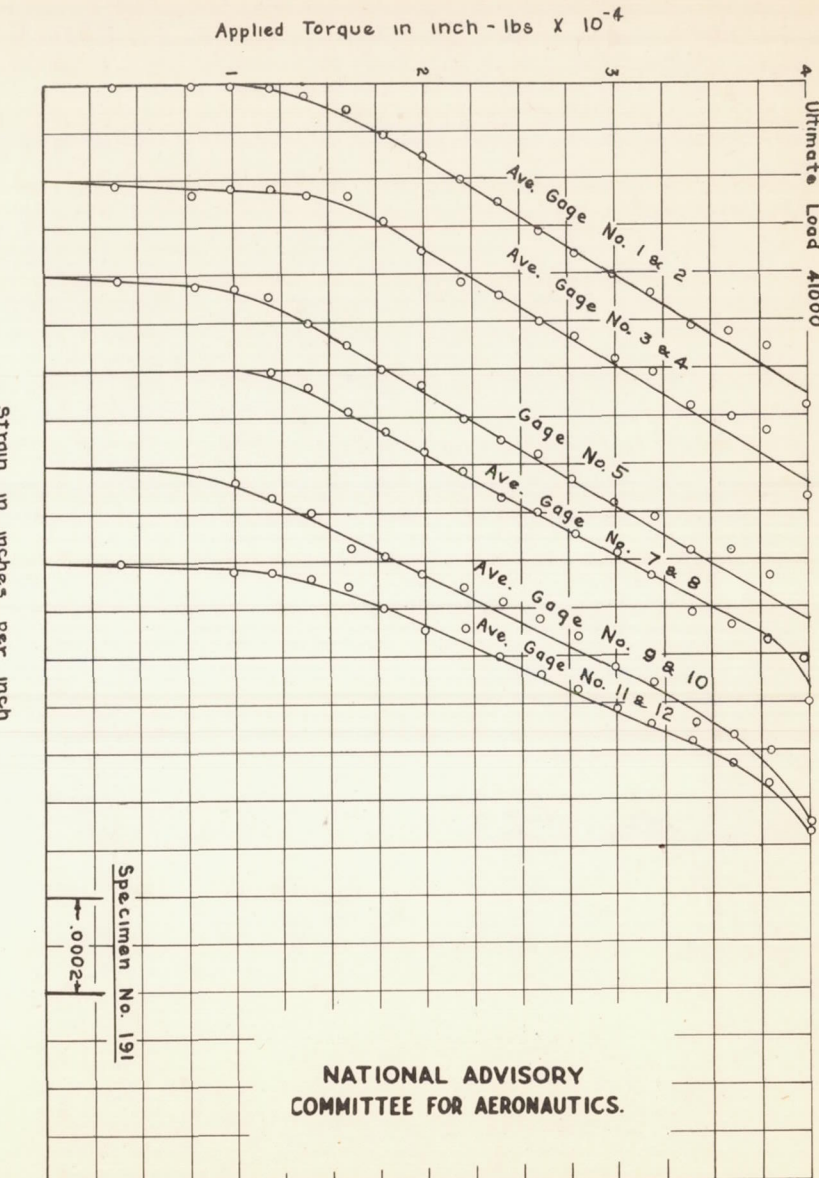


Figure 17.- Failure of a specimen with 1-inch frame spacing.

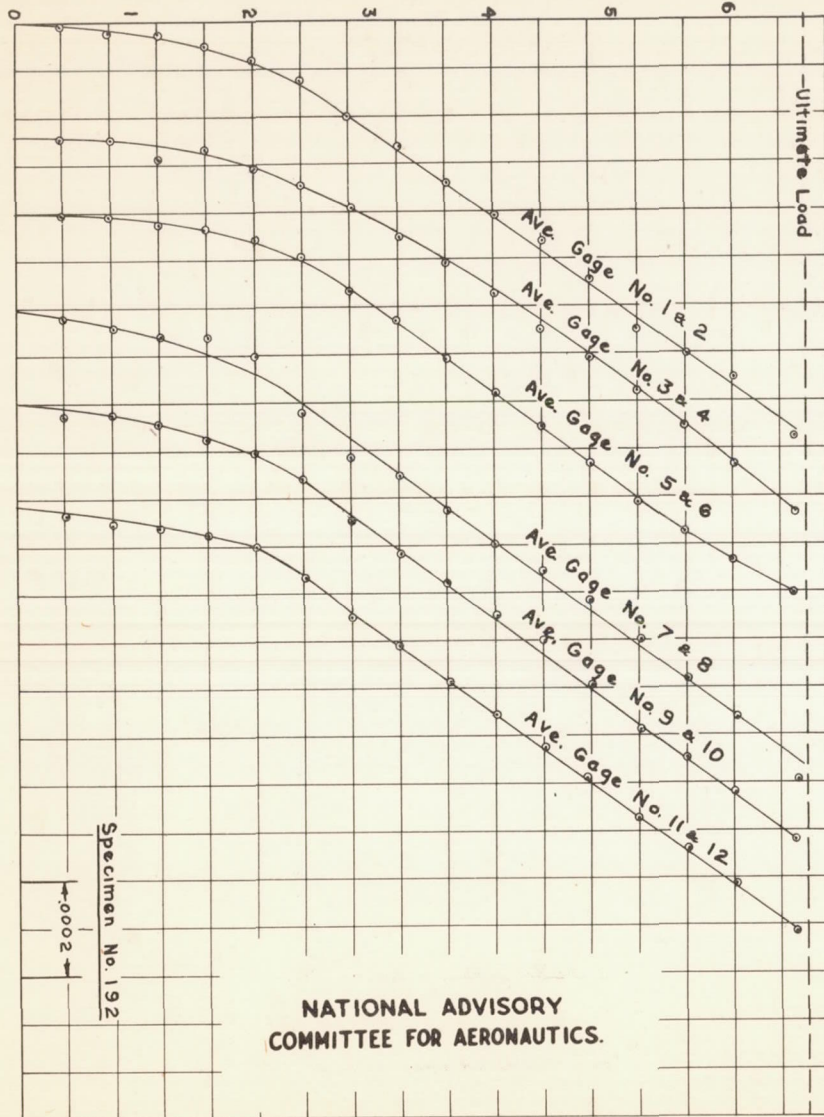


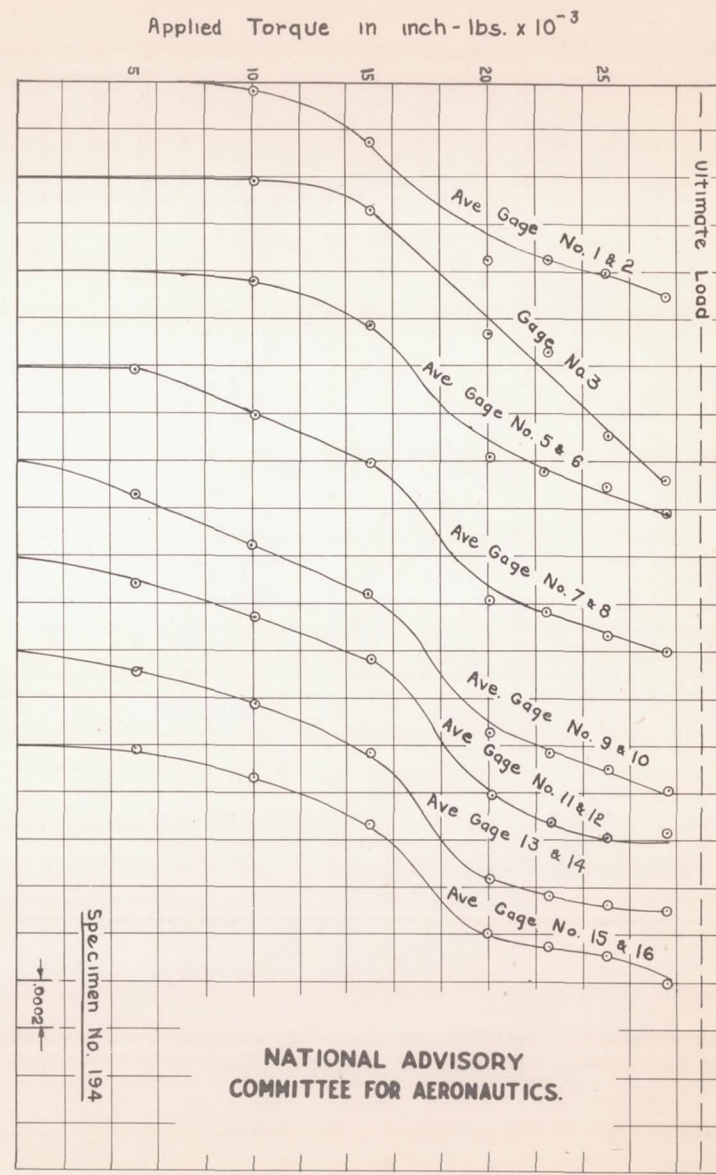
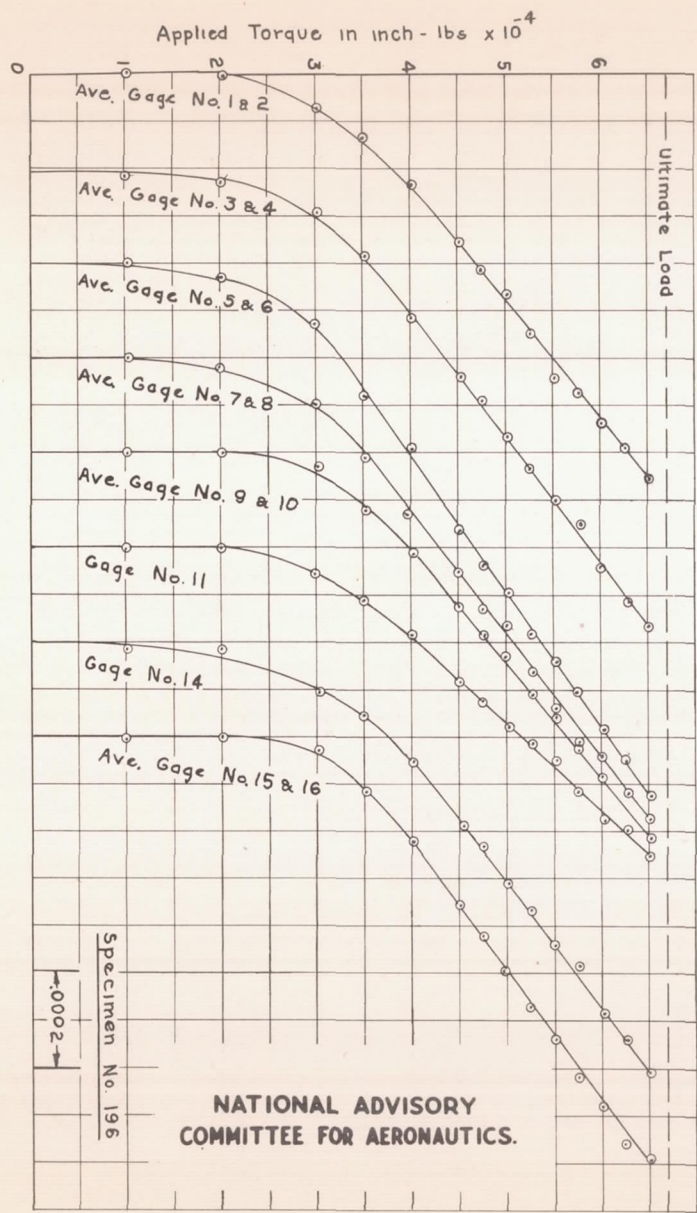


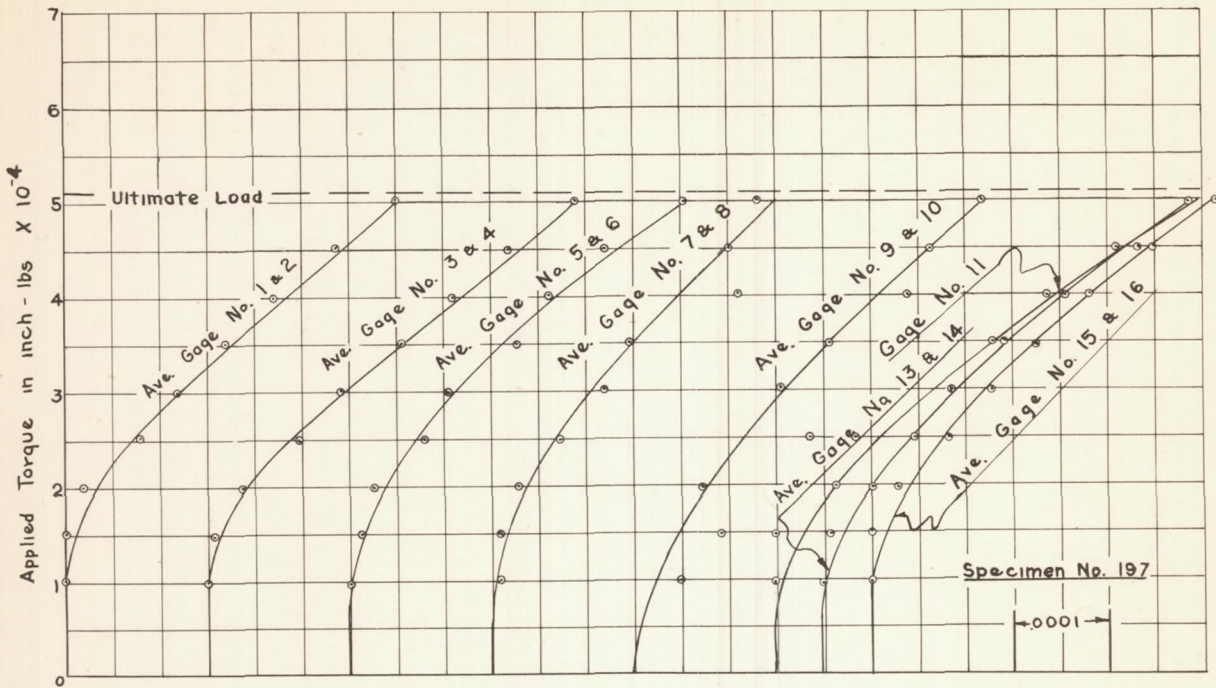
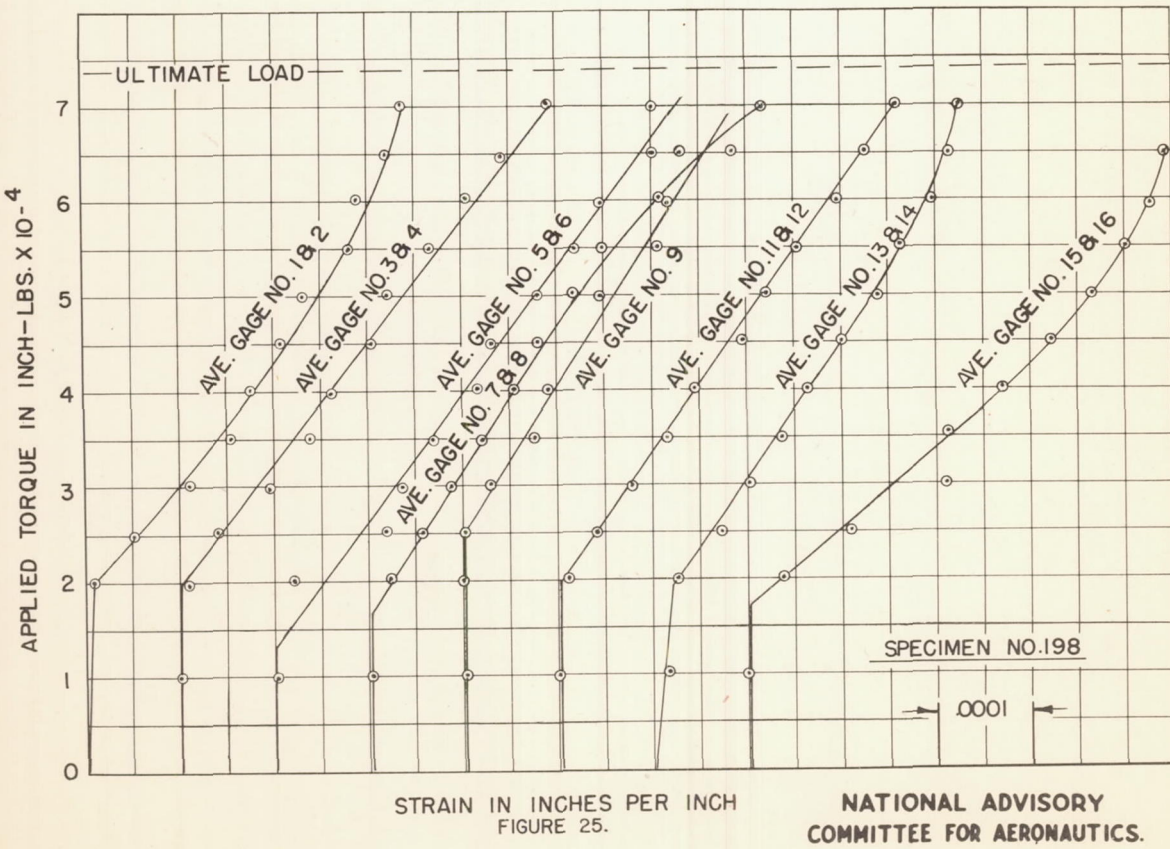
Strain in inches per inch

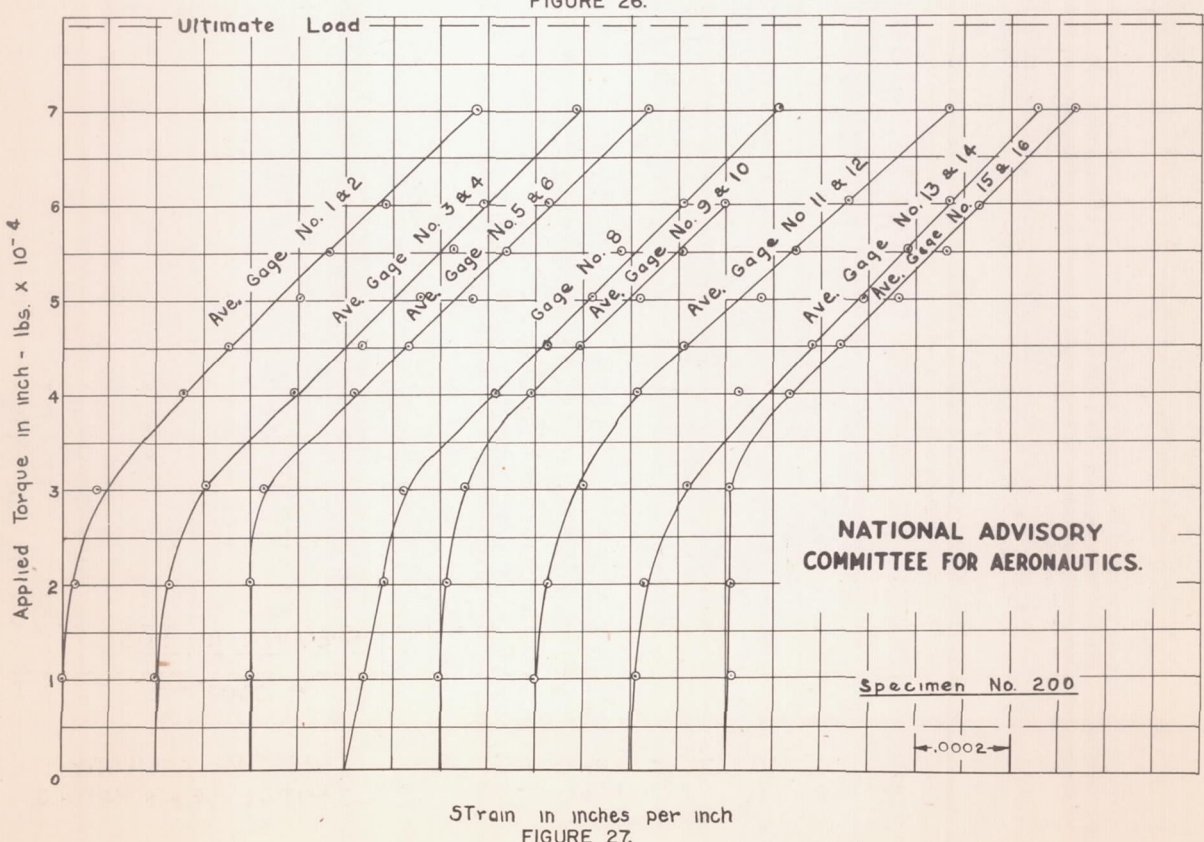
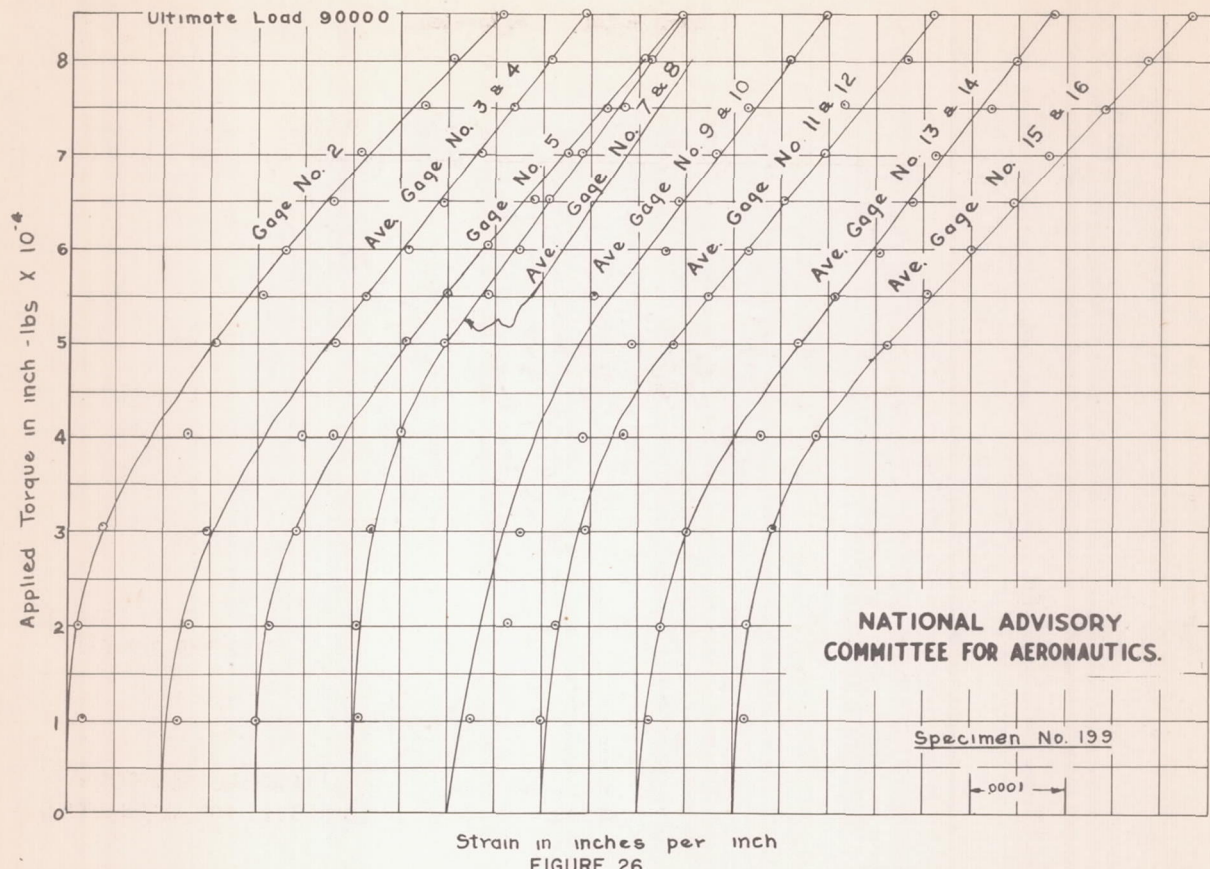
Specimen No. 192

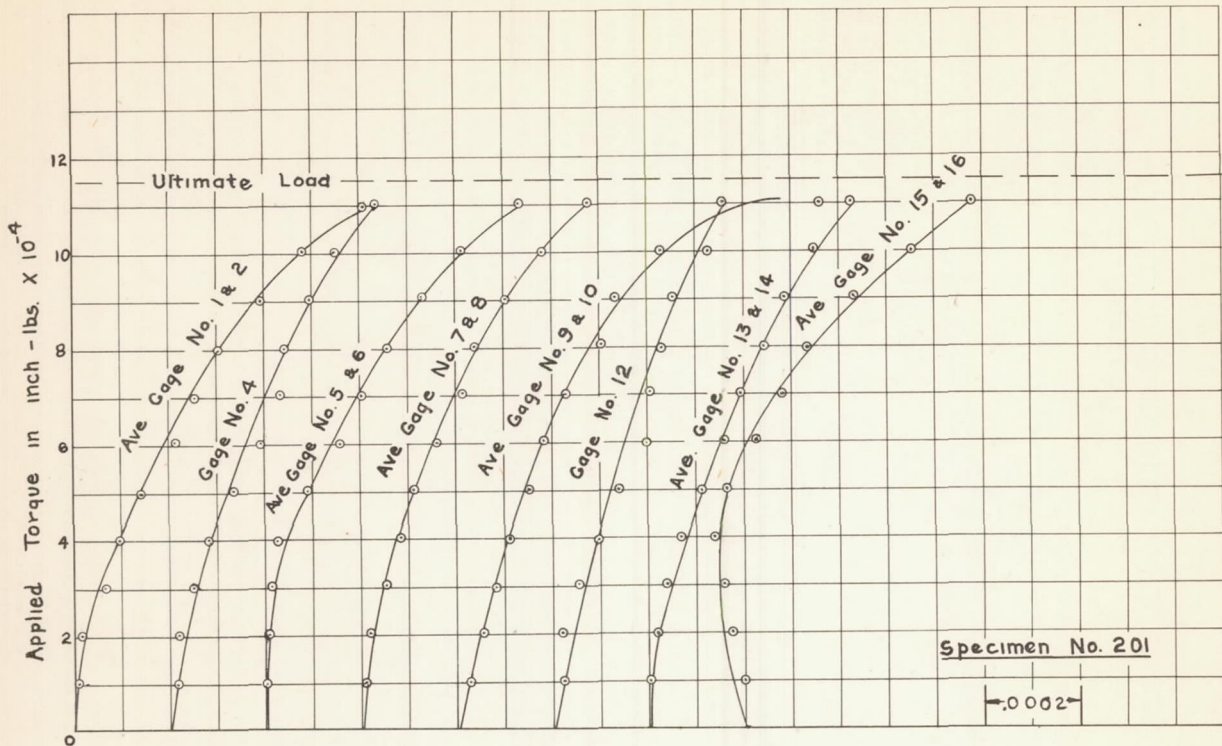
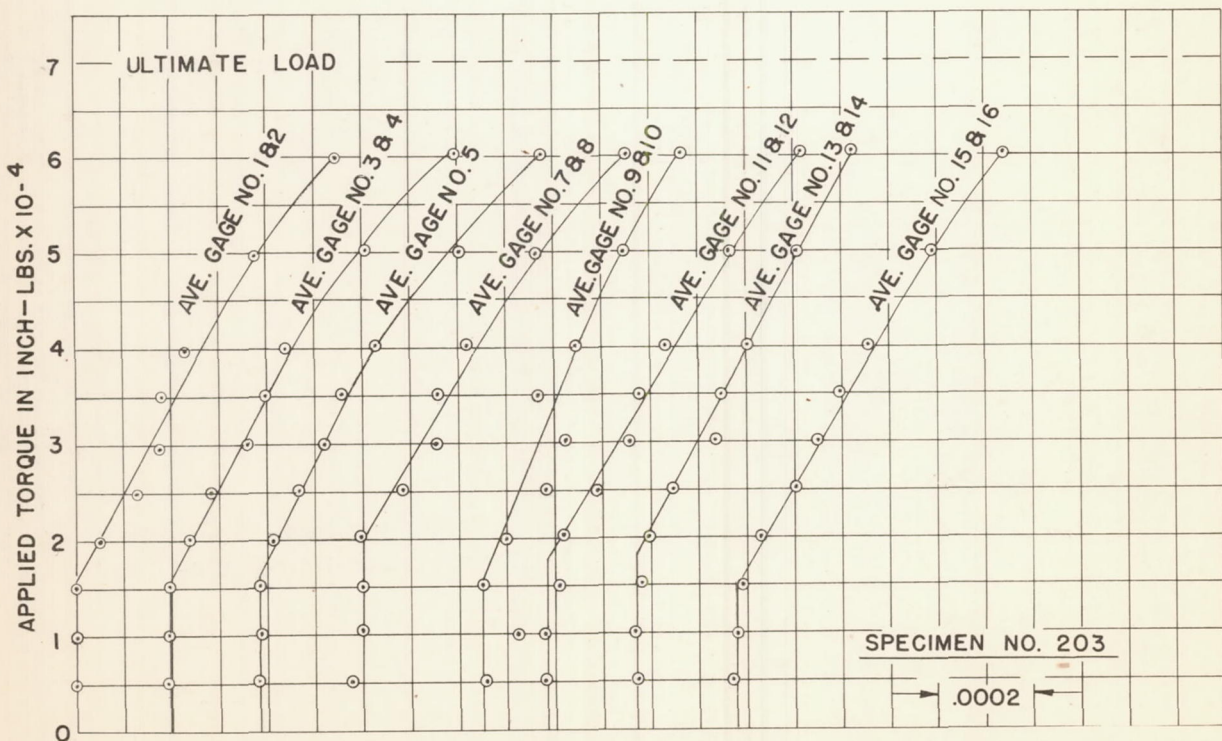
↓ .0002 ↓

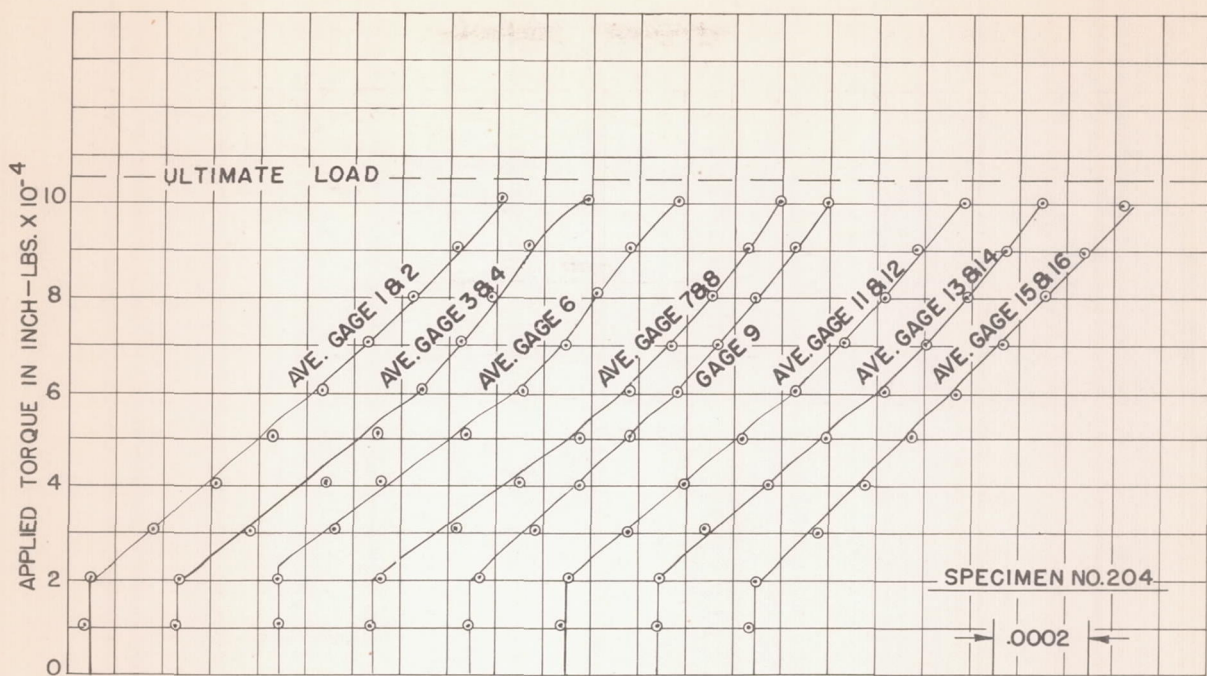
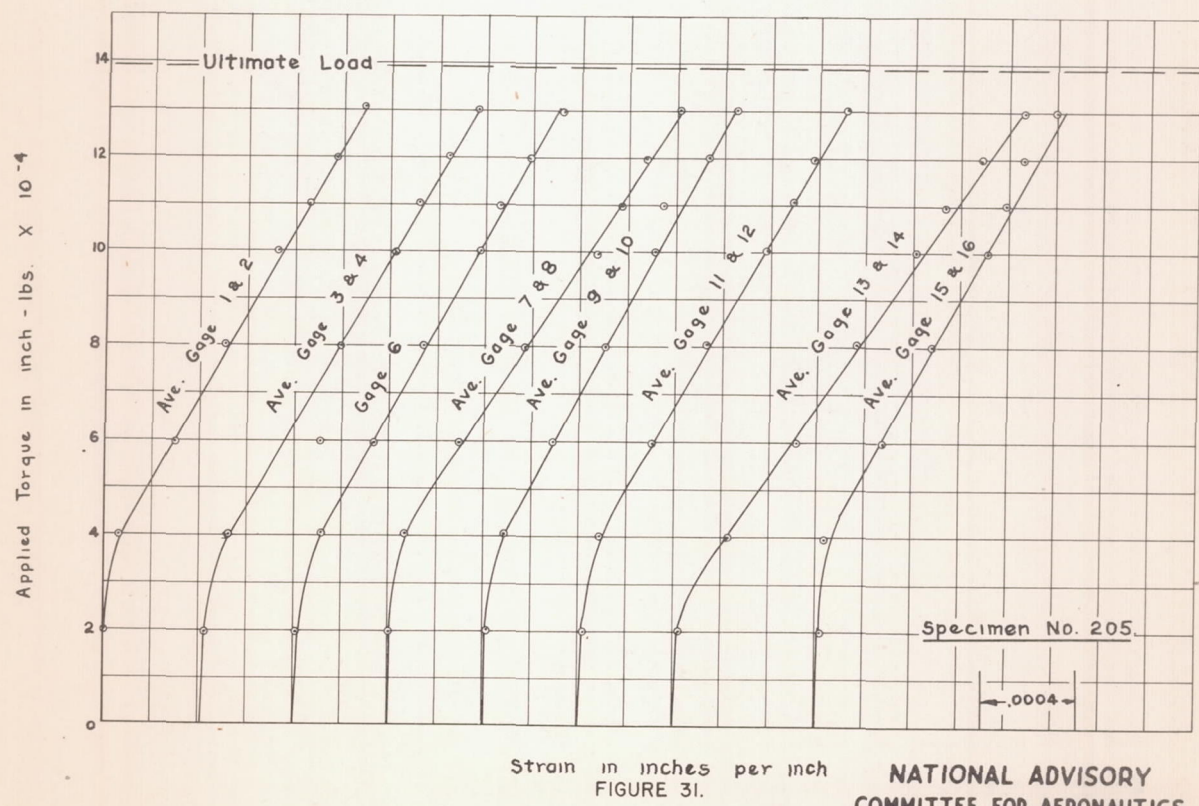
Applied Torque in inch-lbs  $\times 10^{-4}$ 

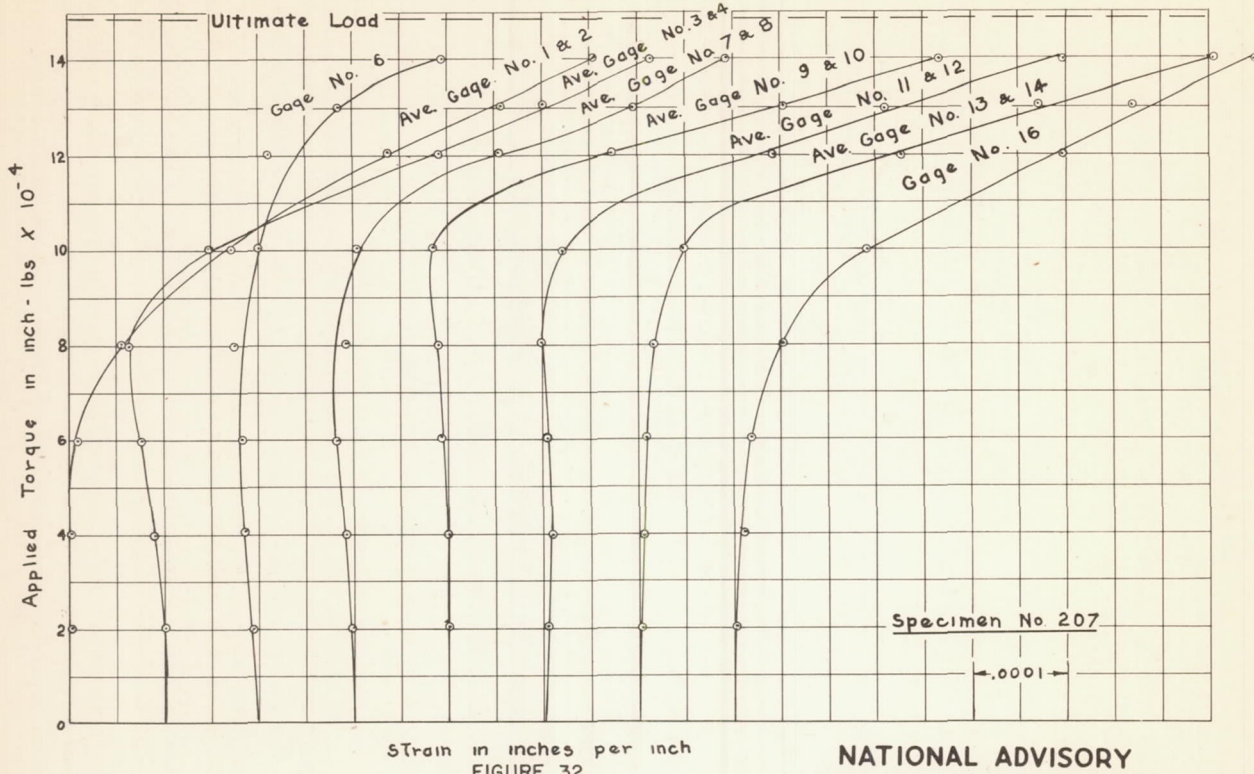
Strain in inches per inch  
FIGURE 22.Strain in inches per inch  
FIGURE 23.

Strain in inches per inch  
FIGURE 24.NATIONAL ADVISORY  
COMMITTEE FOR AERONAUTICS.Strain in inches per inch  
FIGURE 25.NATIONAL ADVISORY  
COMMITTEE FOR AERONAUTICS.

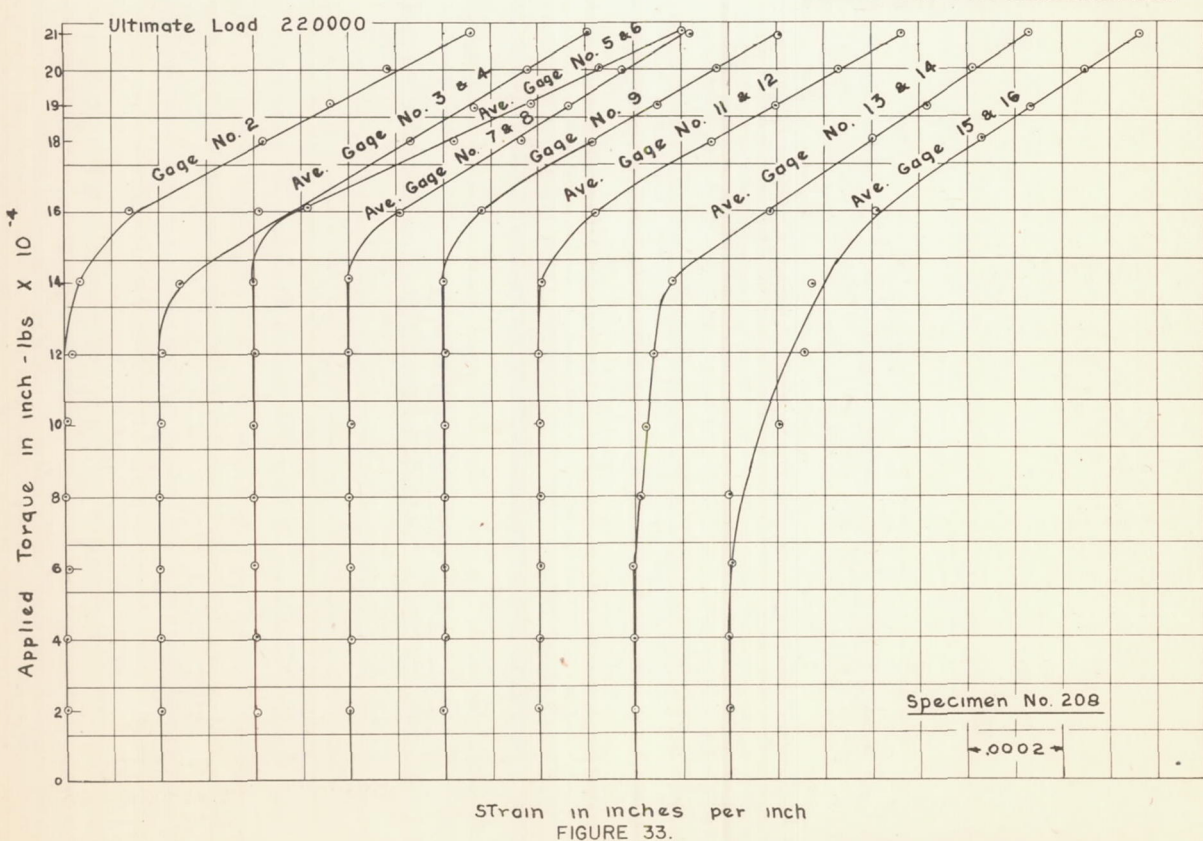


Strain in inches per inch  
FIGURE 28.NATIONAL ADVISORY  
COMMITTEE FOR AERONAUTICS.STRAIN IN INCHES PER INCH  
FIGURE 29.NATIONAL ADVISORY  
COMMITTEE FOR AERONAUTICS.

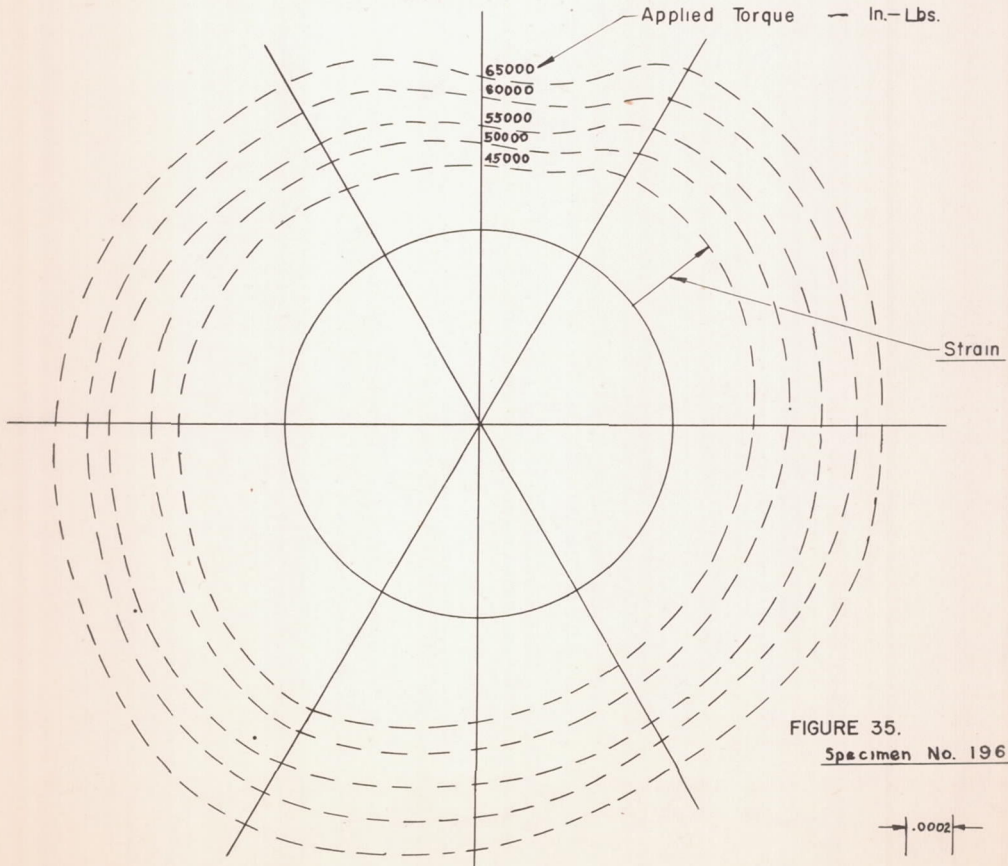
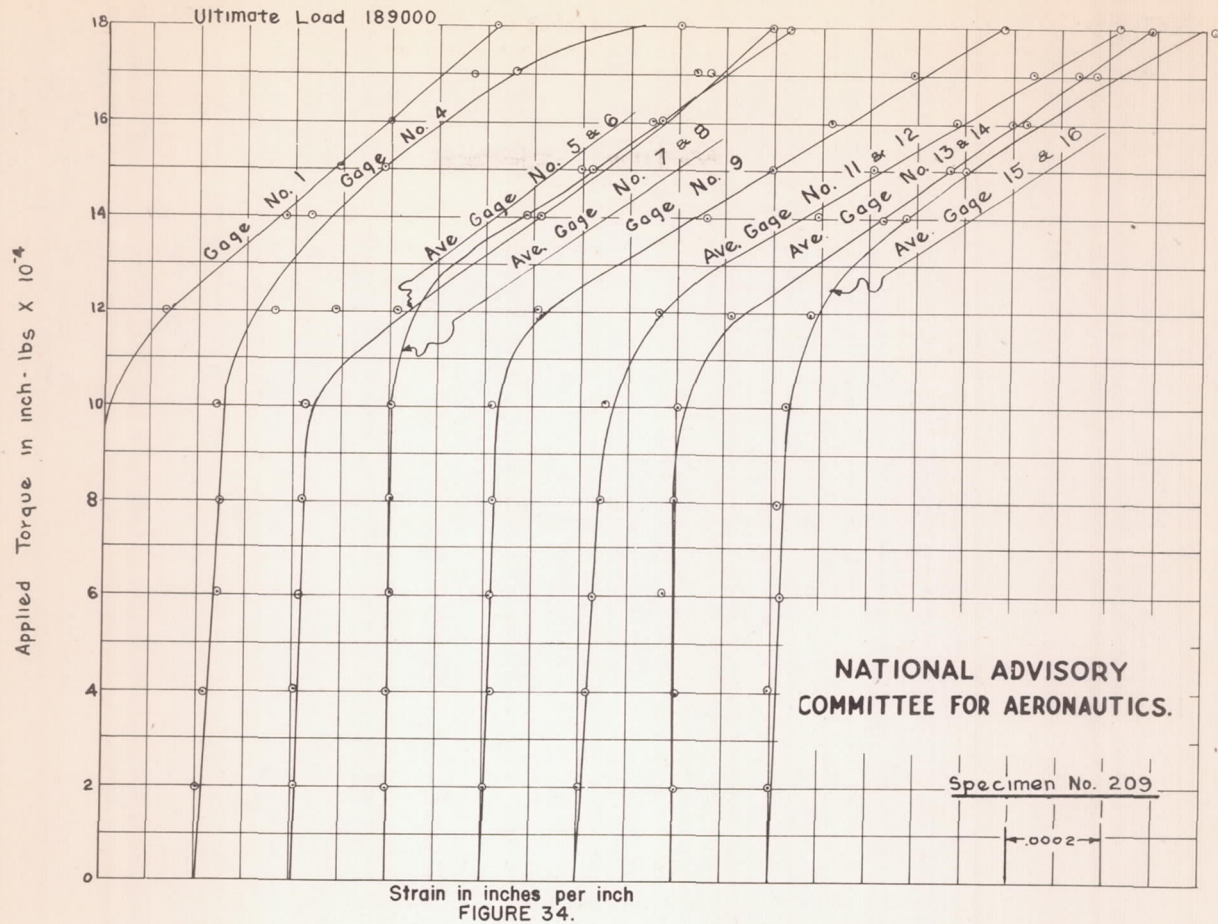
STRAIN IN INCHES PER INCH  
FIGURE 30.NATIONAL ADVISORY  
COMMITTEE FOR AERONAUTICSStrain in inches per inch  
FIGURE 31.NATIONAL ADVISORY  
COMMITTEE FOR AERONAUTICS.



NATIONAL ADVISORY  
COMMITTEE FOR AERONAUTICS.



NATIONAL ADVISORY  
COMMITTEE FOR AERONAUTICS.



NATIONAL ADVISORY COMMITTEE FOR AERONAUTICS.

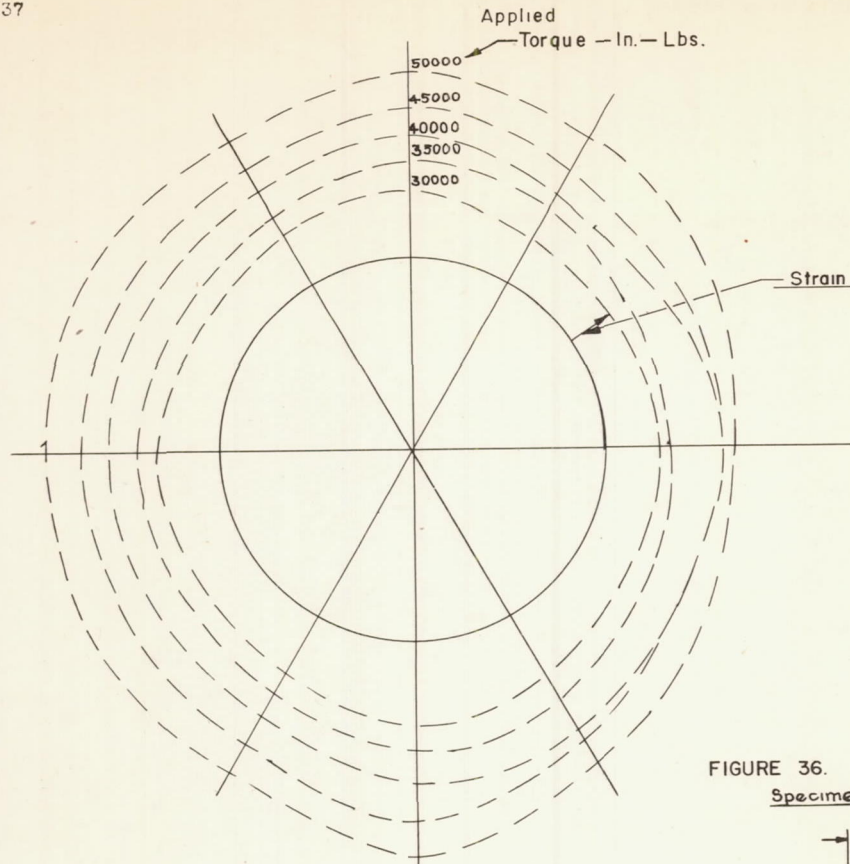


FIGURE 36.  
Specimen No. 197

.0001

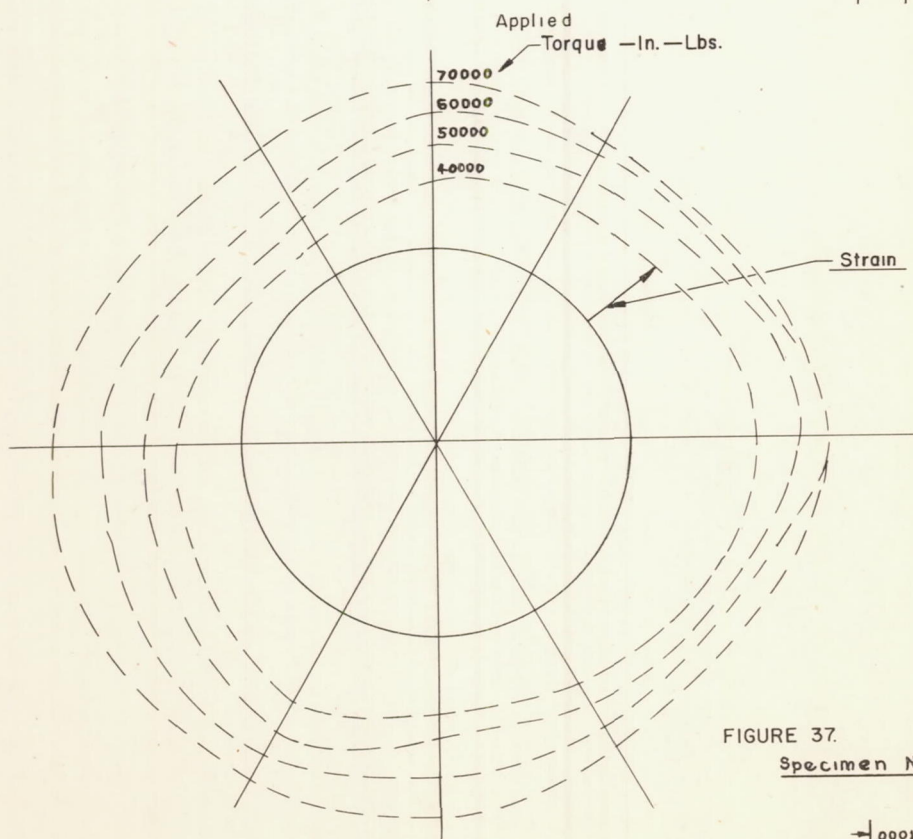
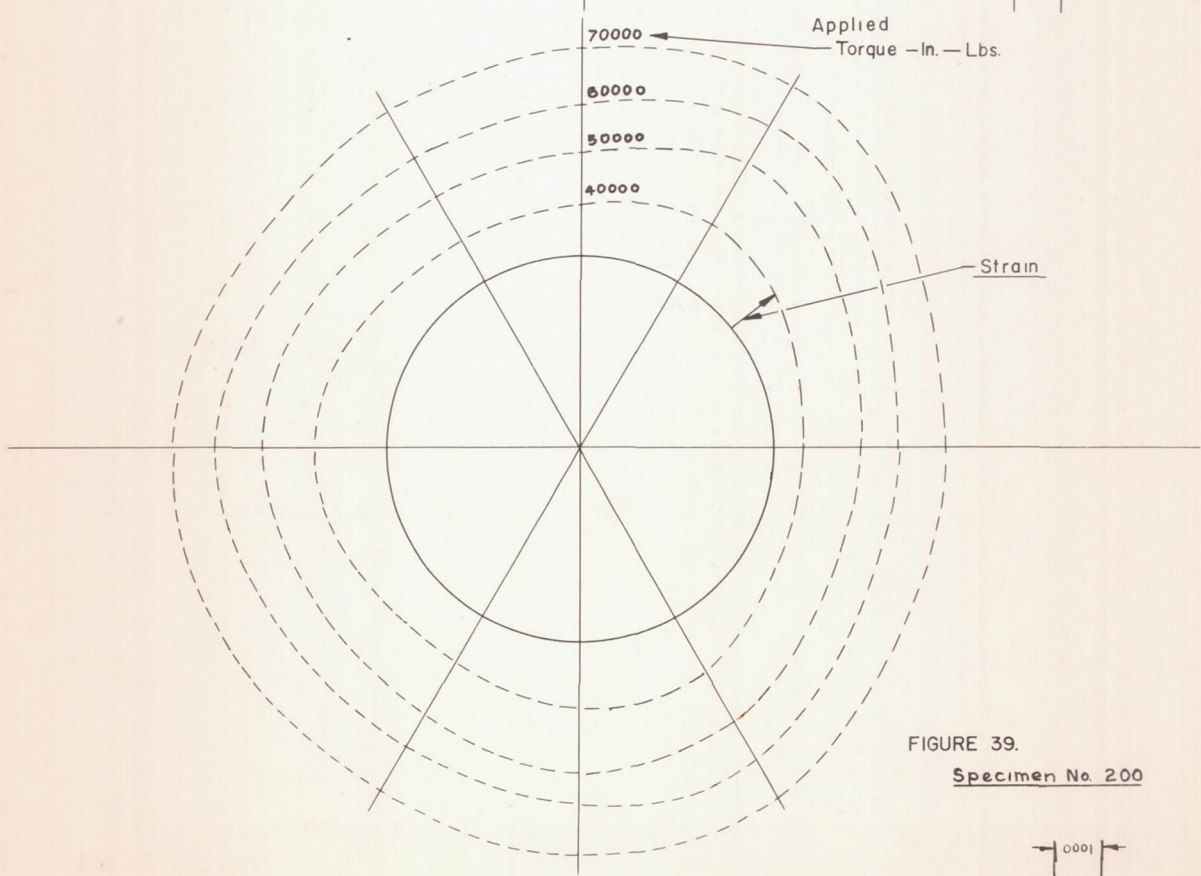
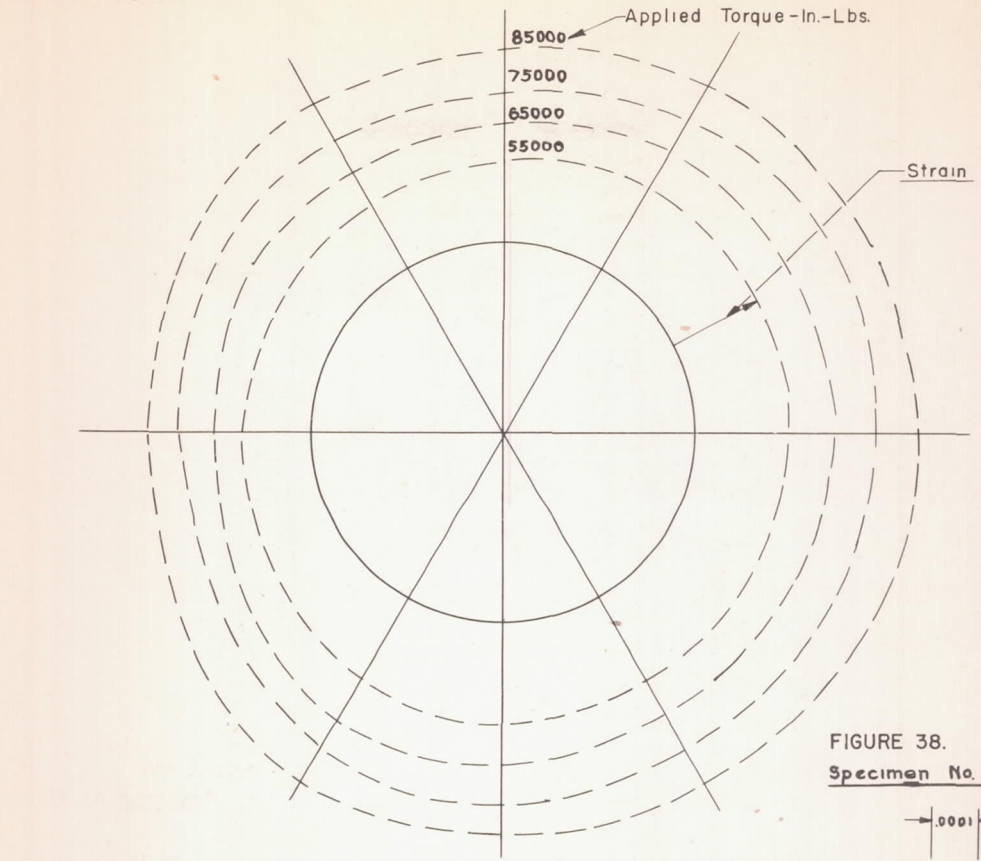


FIGURE 37.  
Specimen No. 198

.0001



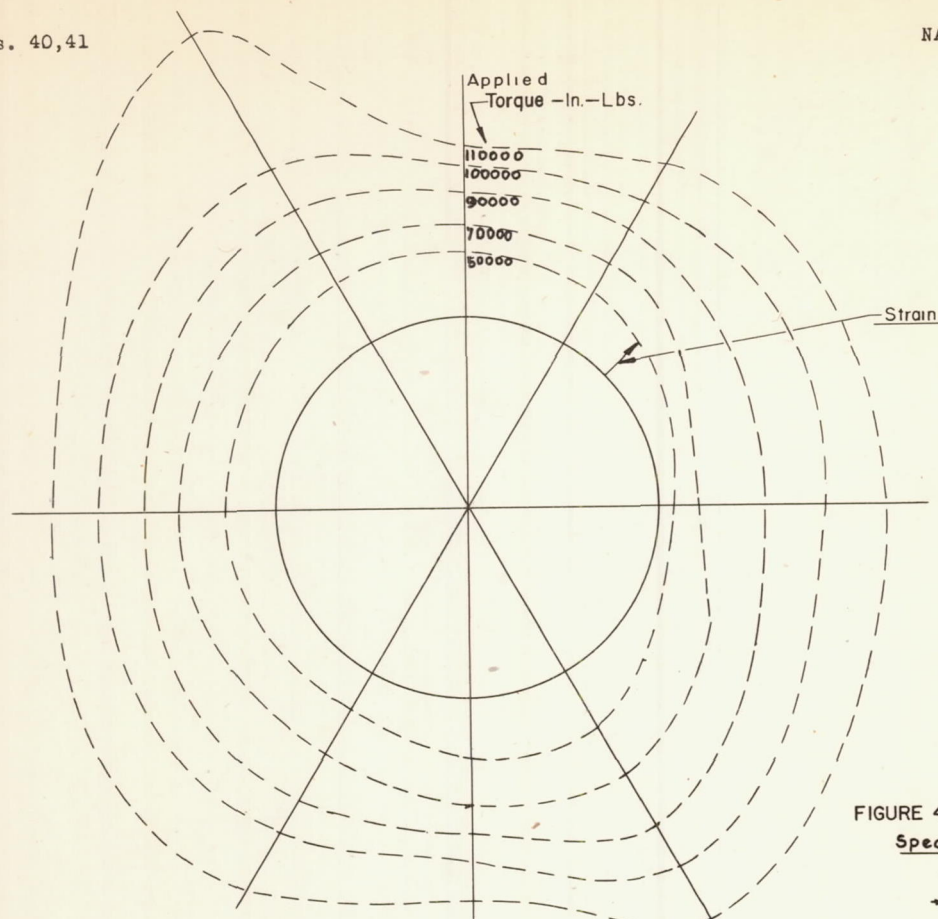


FIGURE 40.  
Specimen No. 201

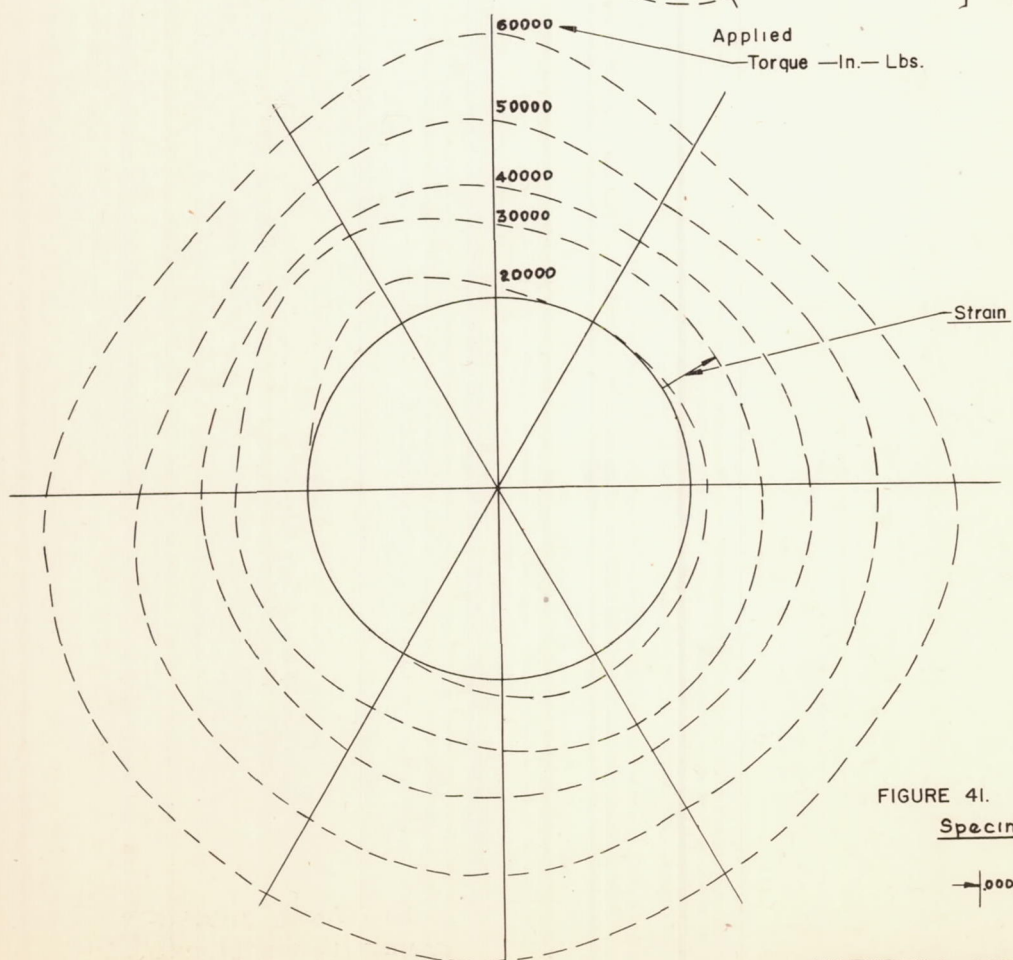


FIGURE 41.  
Specimen No. 203

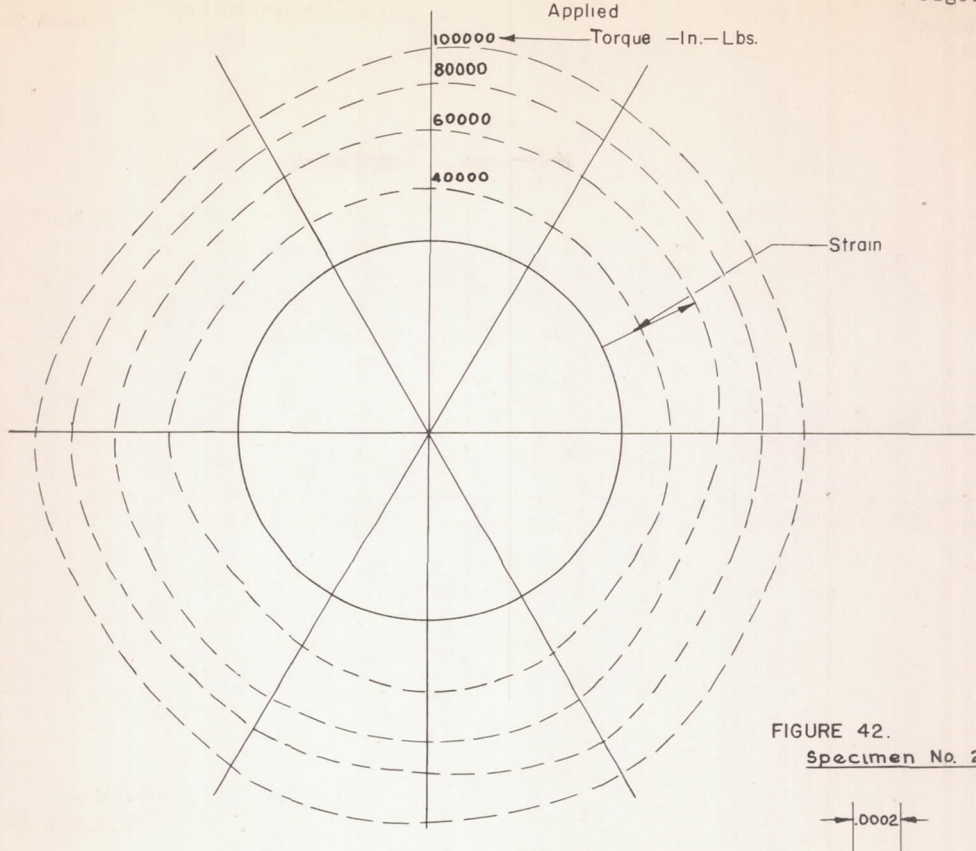


FIGURE 42.  
Specimen No. 204

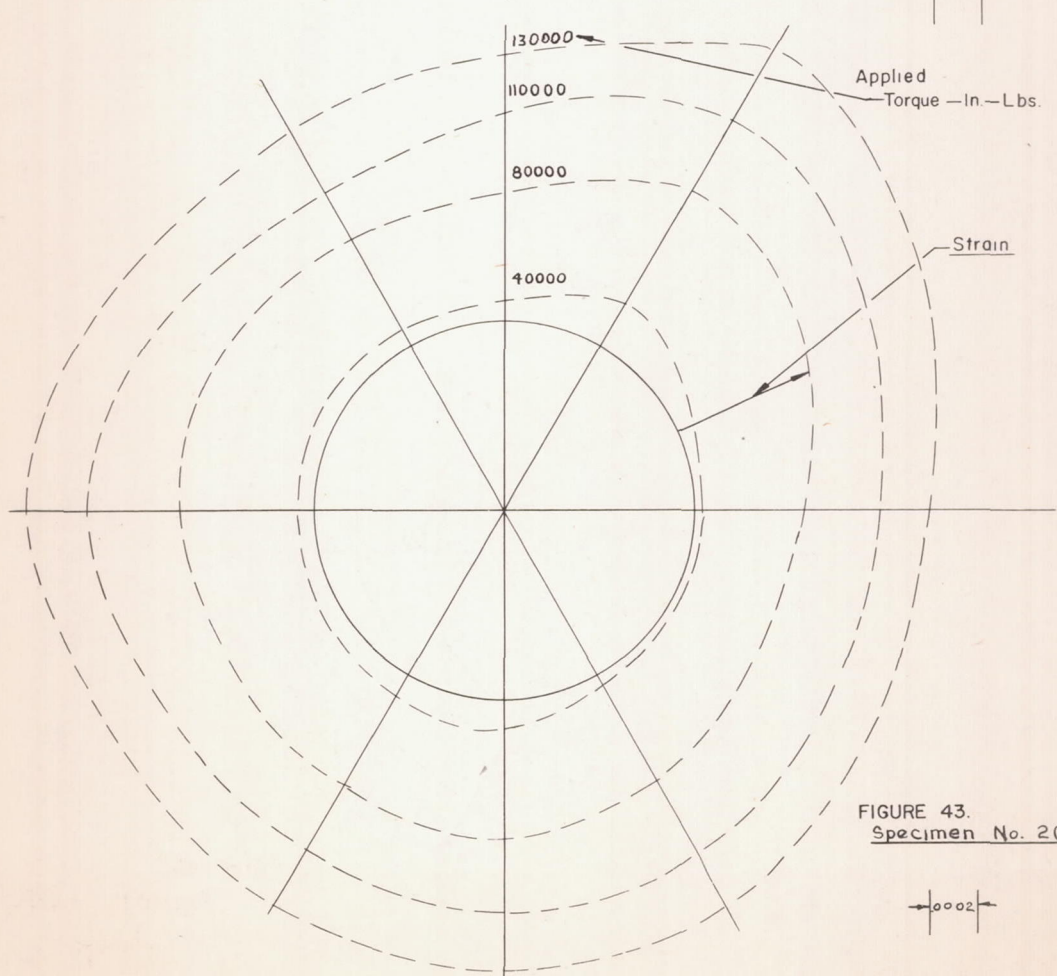
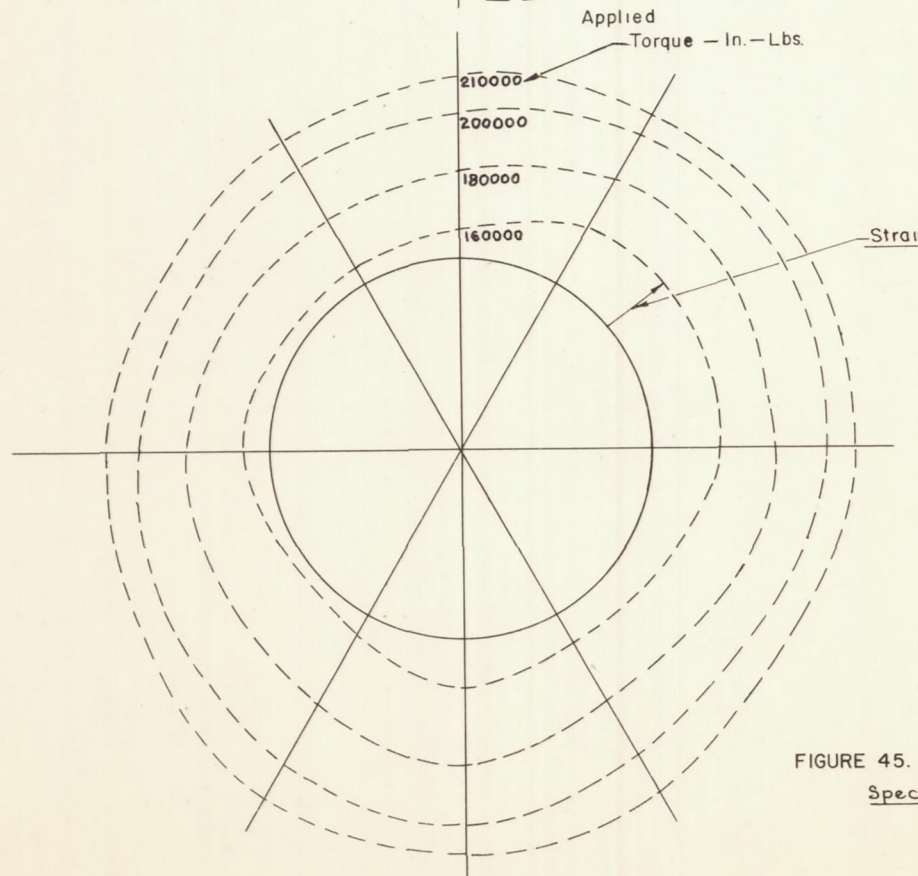
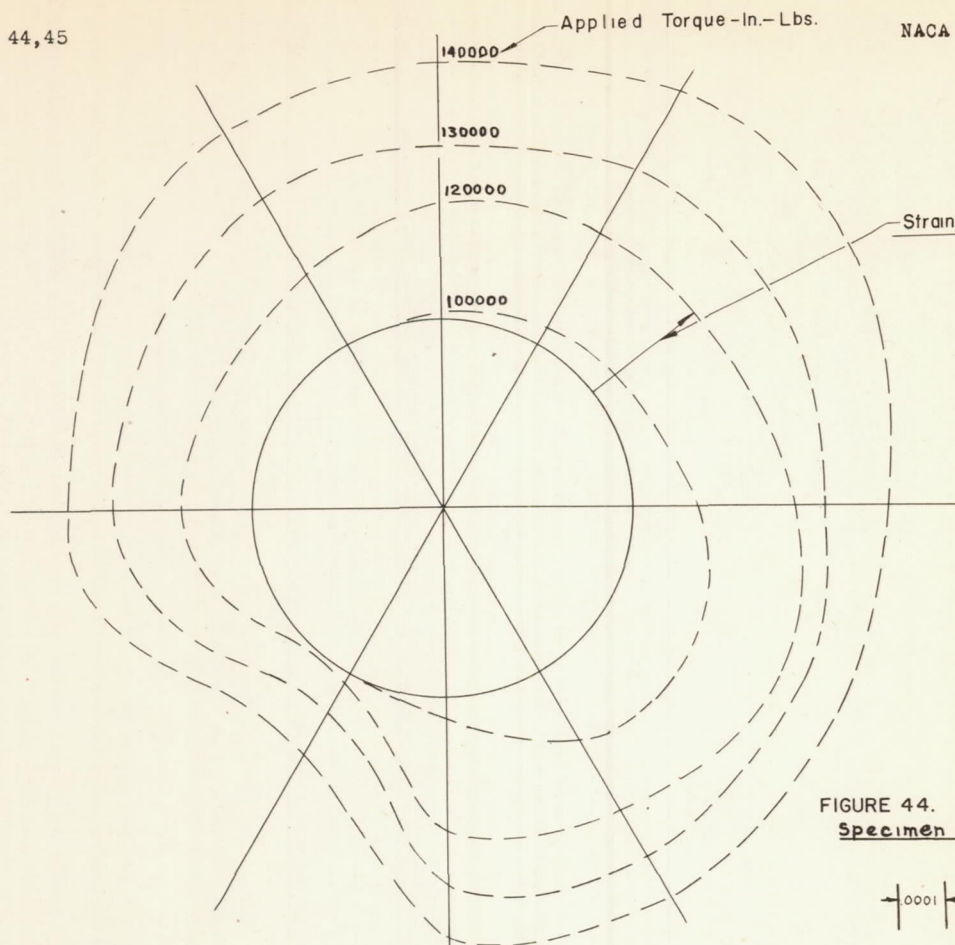
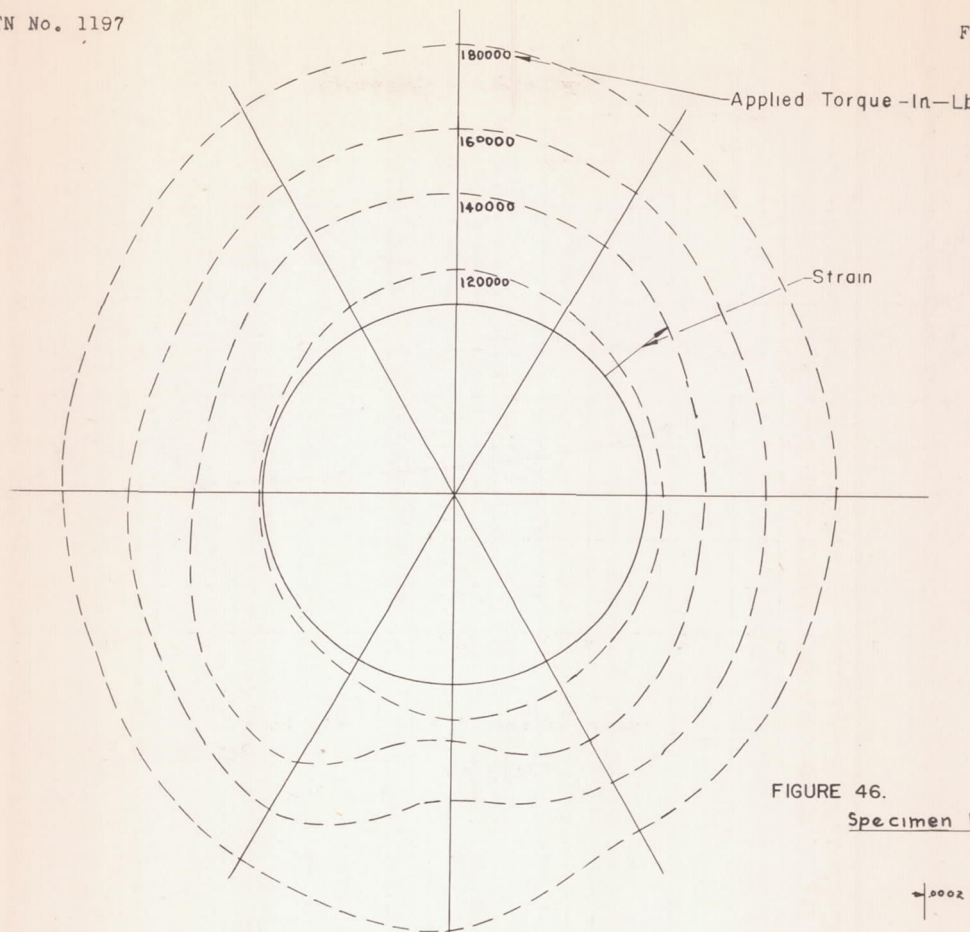


FIGURE 43.  
Specimen No. 205





0002

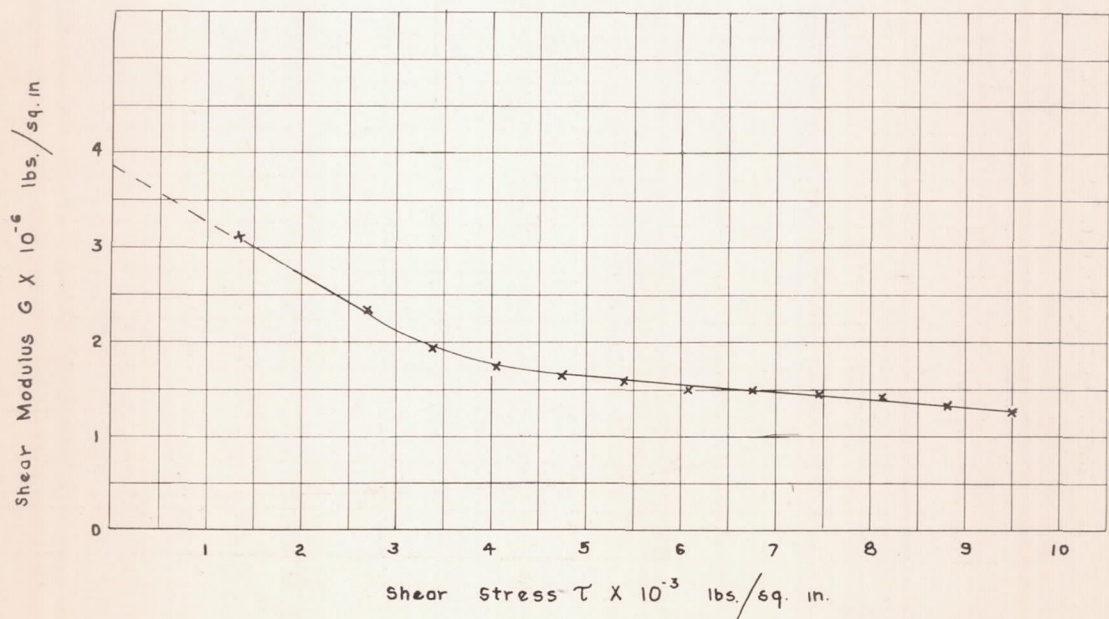
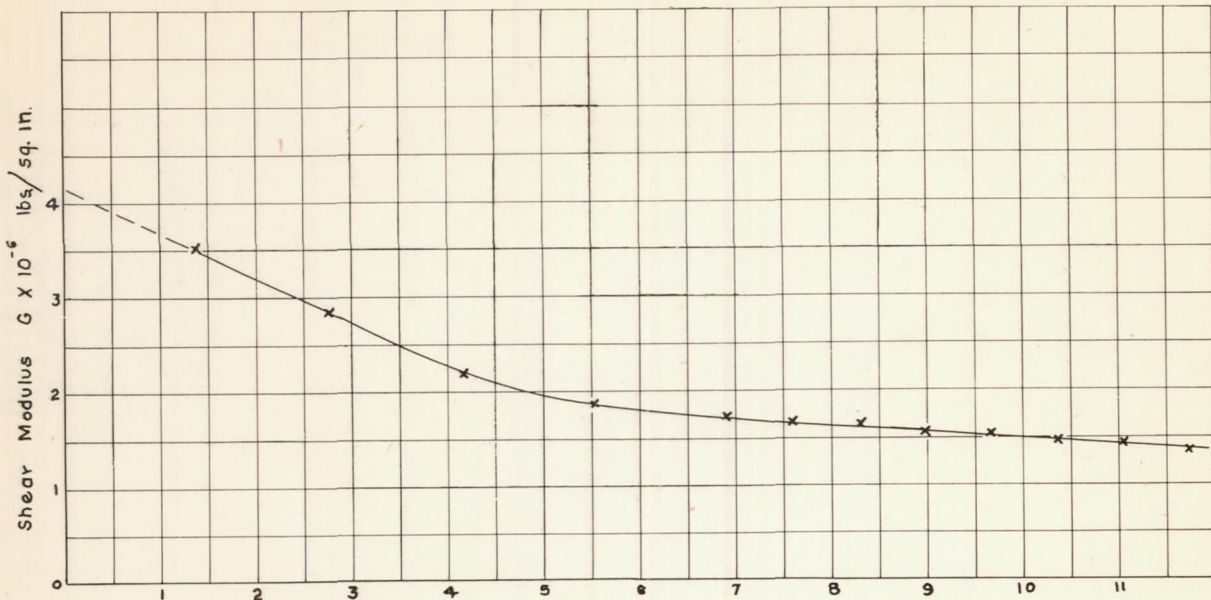


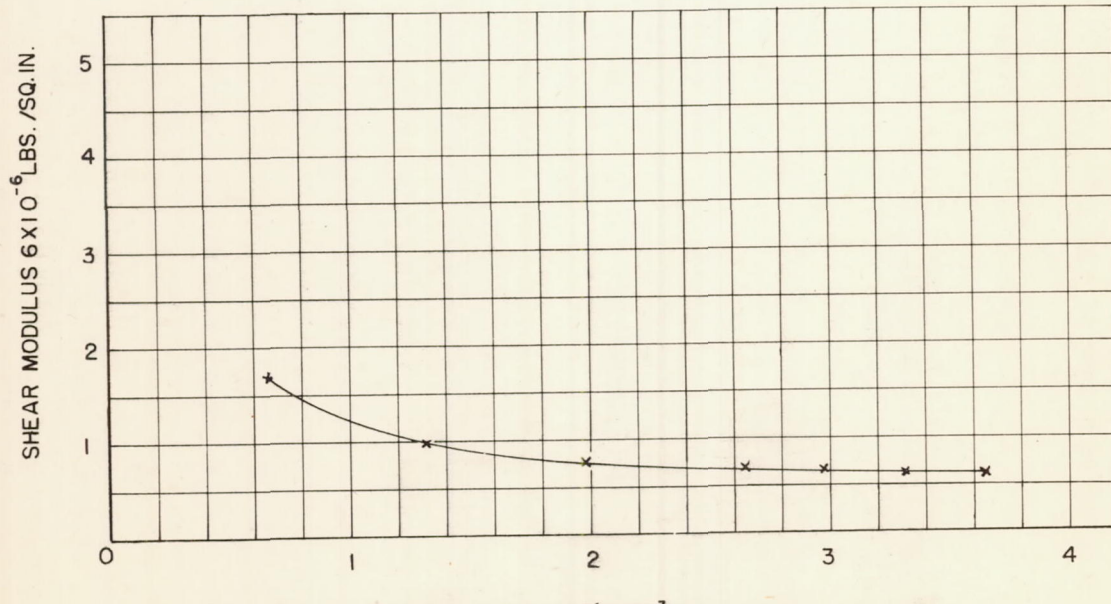
FIGURE 47.

NATIONAL ADVISORY  
COMMITTEE FOR AERONAUTICS.



Shear Stress  $\tau \times 10^3$  lbs./sq. in.  
Specimen No. 199

FIGURE 48.



SHEAR STRESS  $\tau \times 10^3$  LBS./SQ.IN.  
SPECIMEN NO. 194

FIGURE 49.

NATIONAL ADVISORY  
COMMITTEE FOR AERONAUTICS.

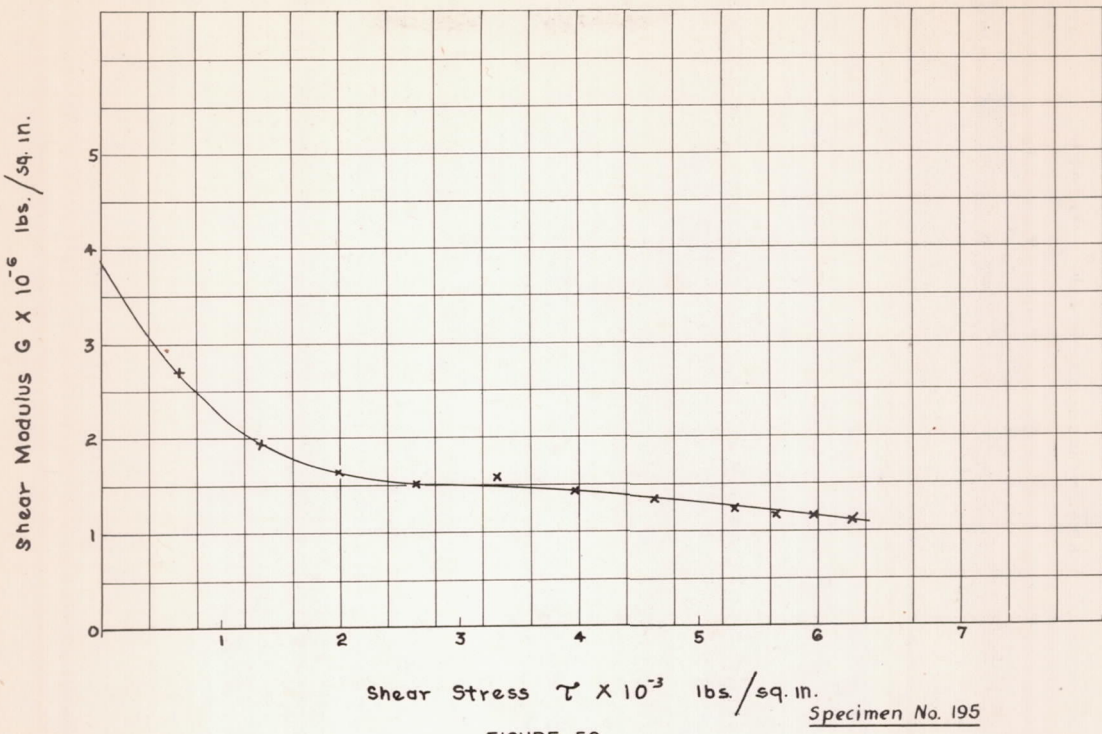


FIGURE 50.

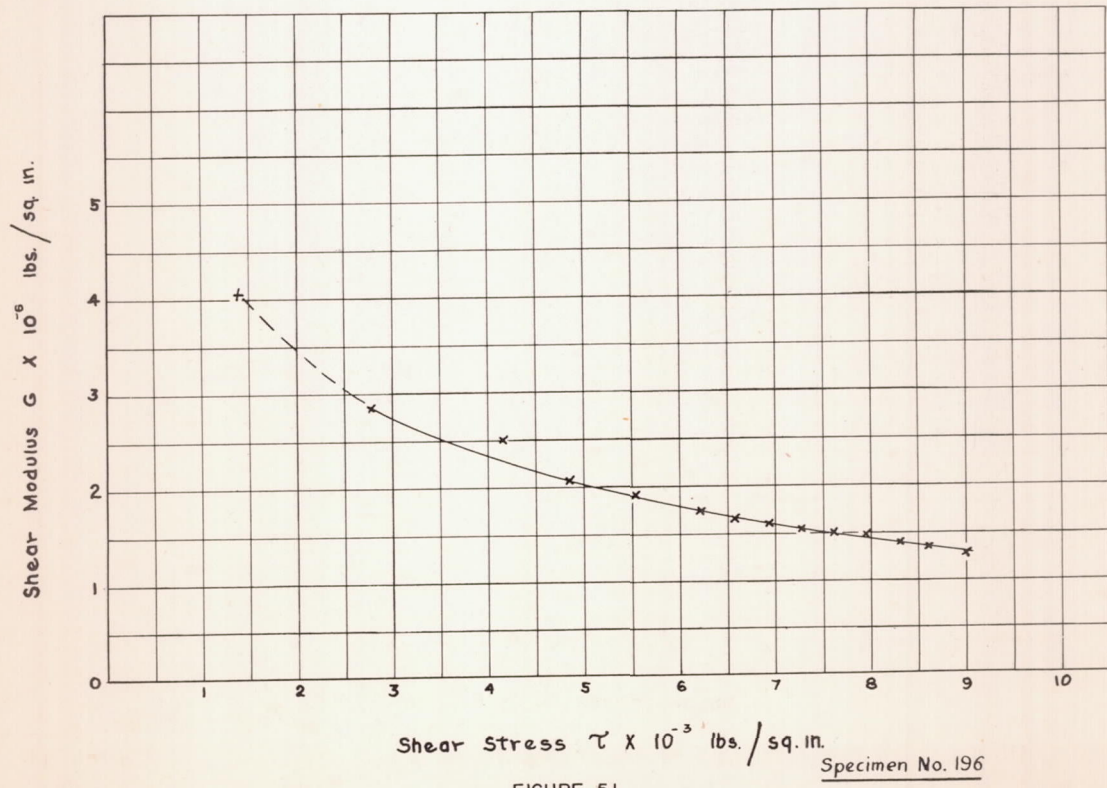


FIGURE 51.

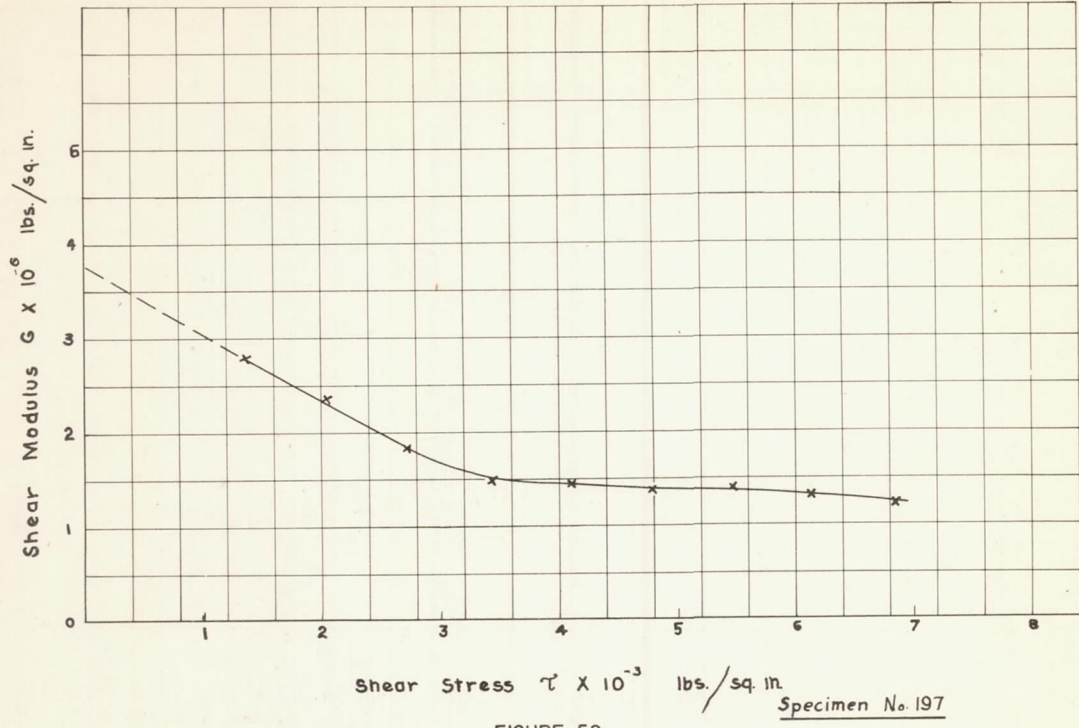


FIGURE 52.

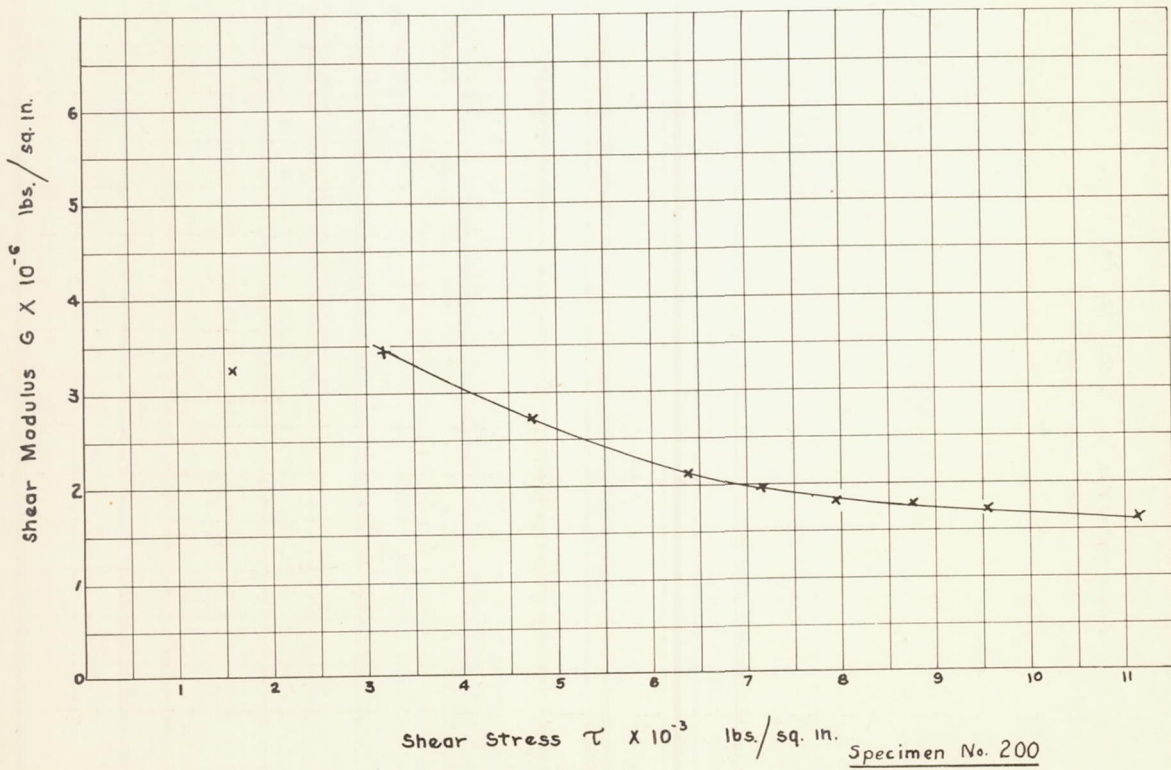
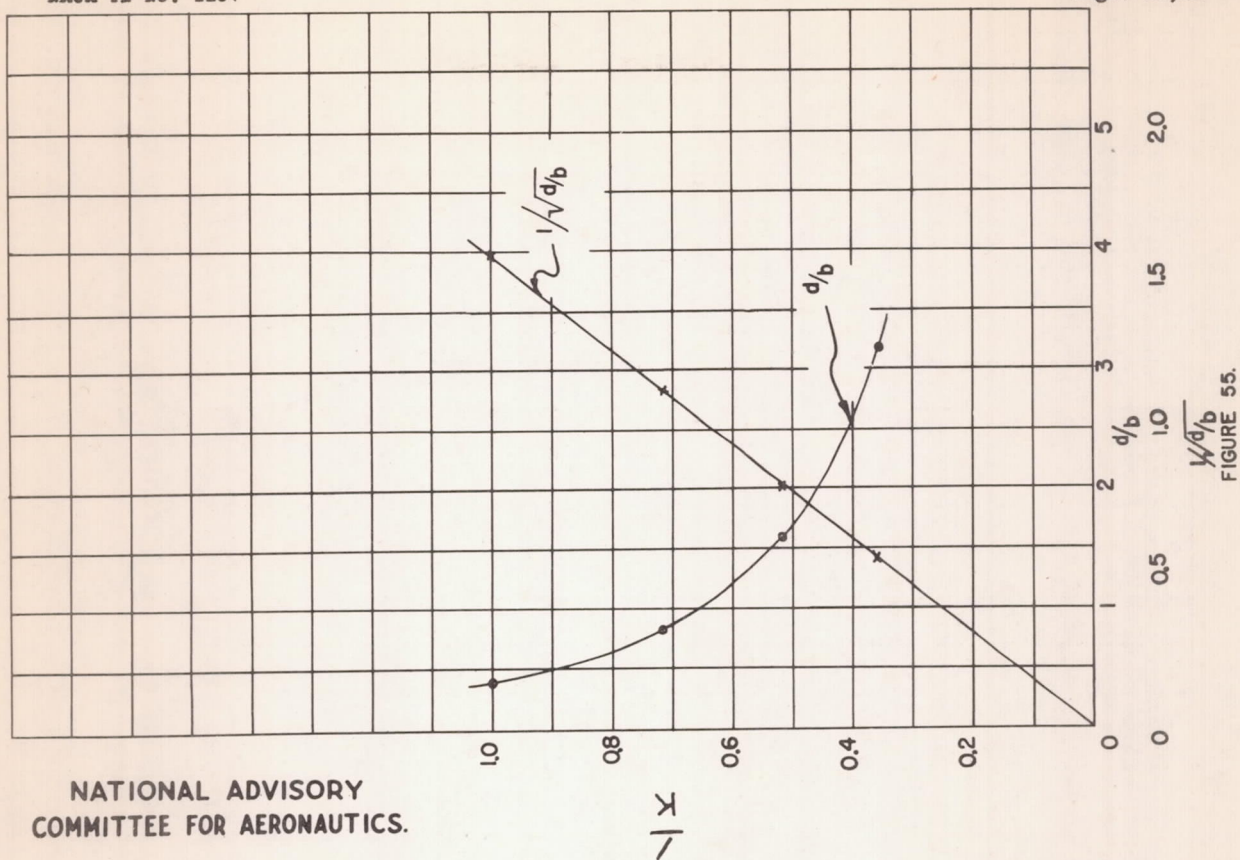
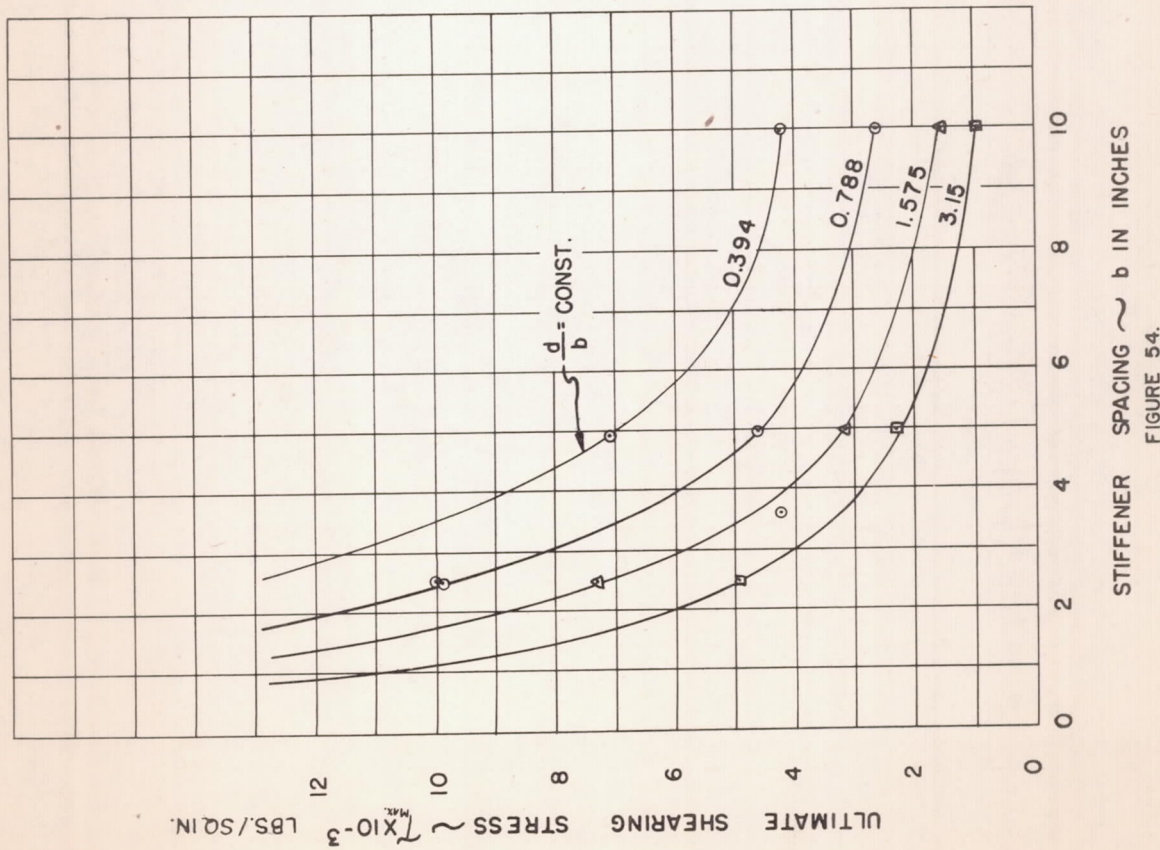


FIGURE 53.

NATIONAL ADVISORY  
COMMITTEE FOR AERONAUTICS.



NATIONAL ADVISORY  
COMMITTEE FOR AERONAUTICS.



ULTIMATE SHEARING STRESS  $\sim \frac{1}{\sqrt{d/b}}$   $\text{LBS./SQ. IN.}$

FIGURE 54.  
FIGURE 55.

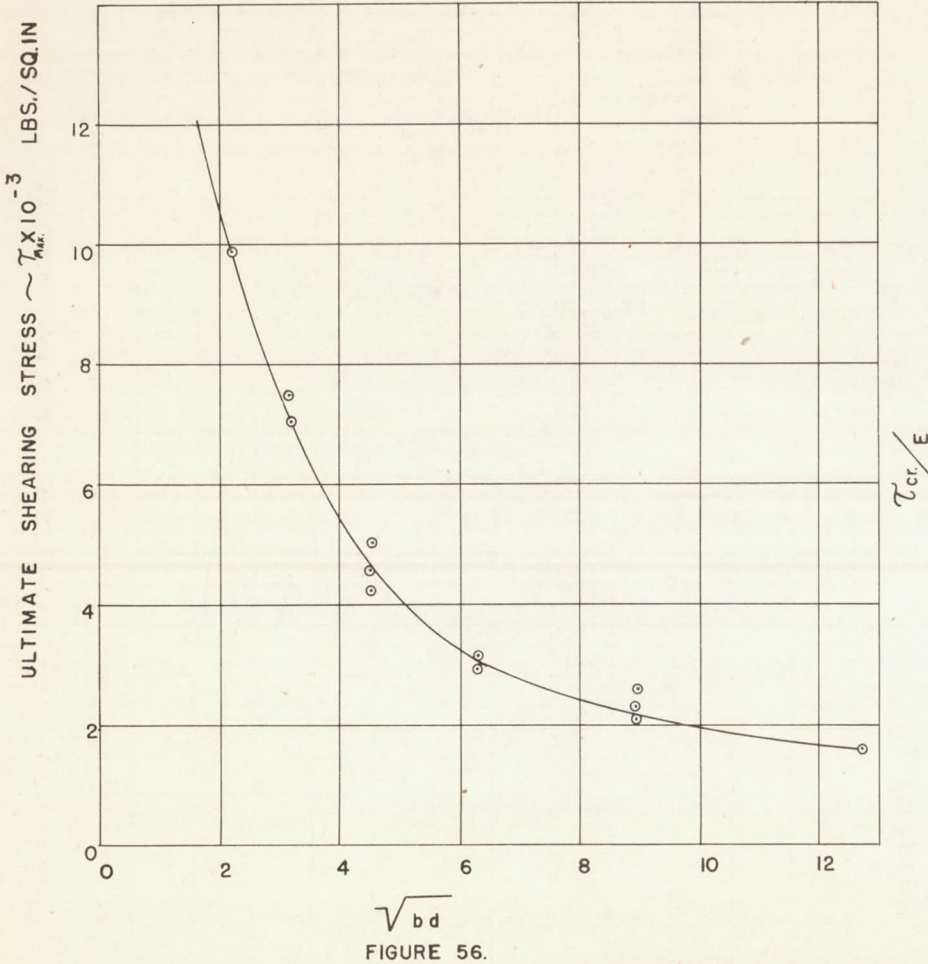
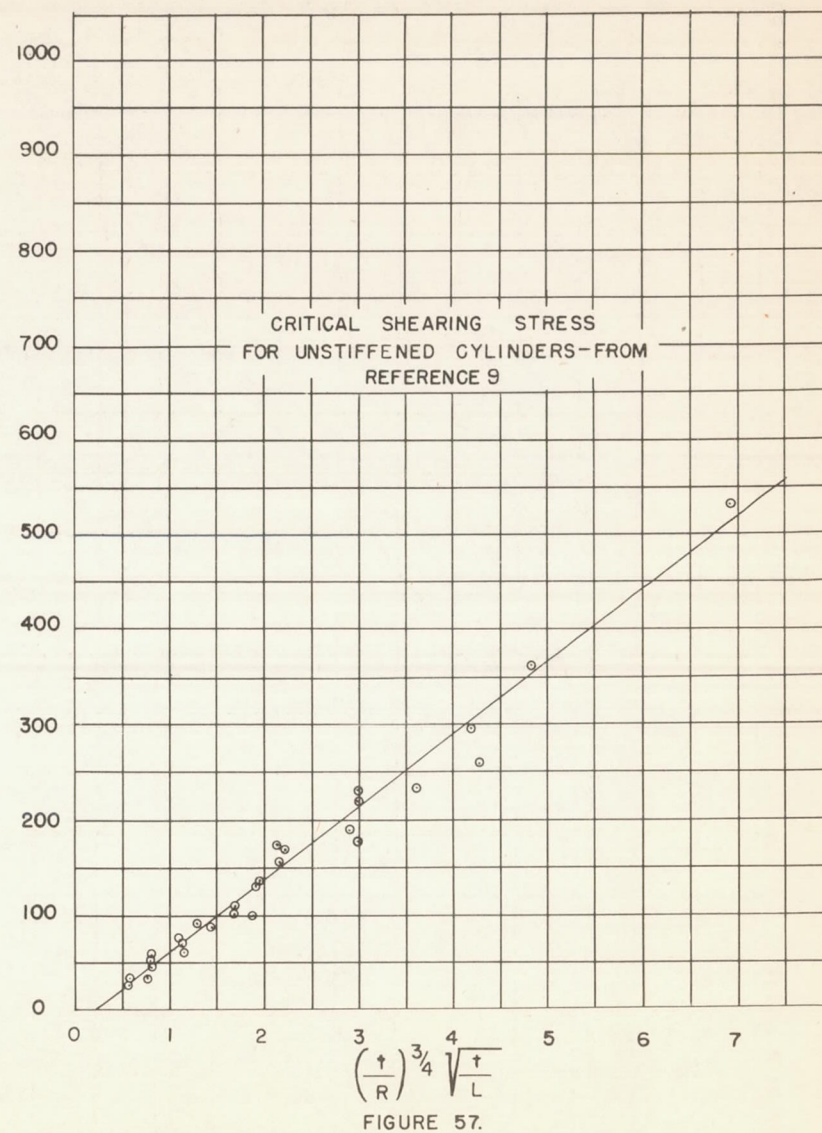


FIGURE 56.

NATIONAL ADVISORY  
COMMITTEE FOR AERONAUTICS.



FIGS. 56, 57

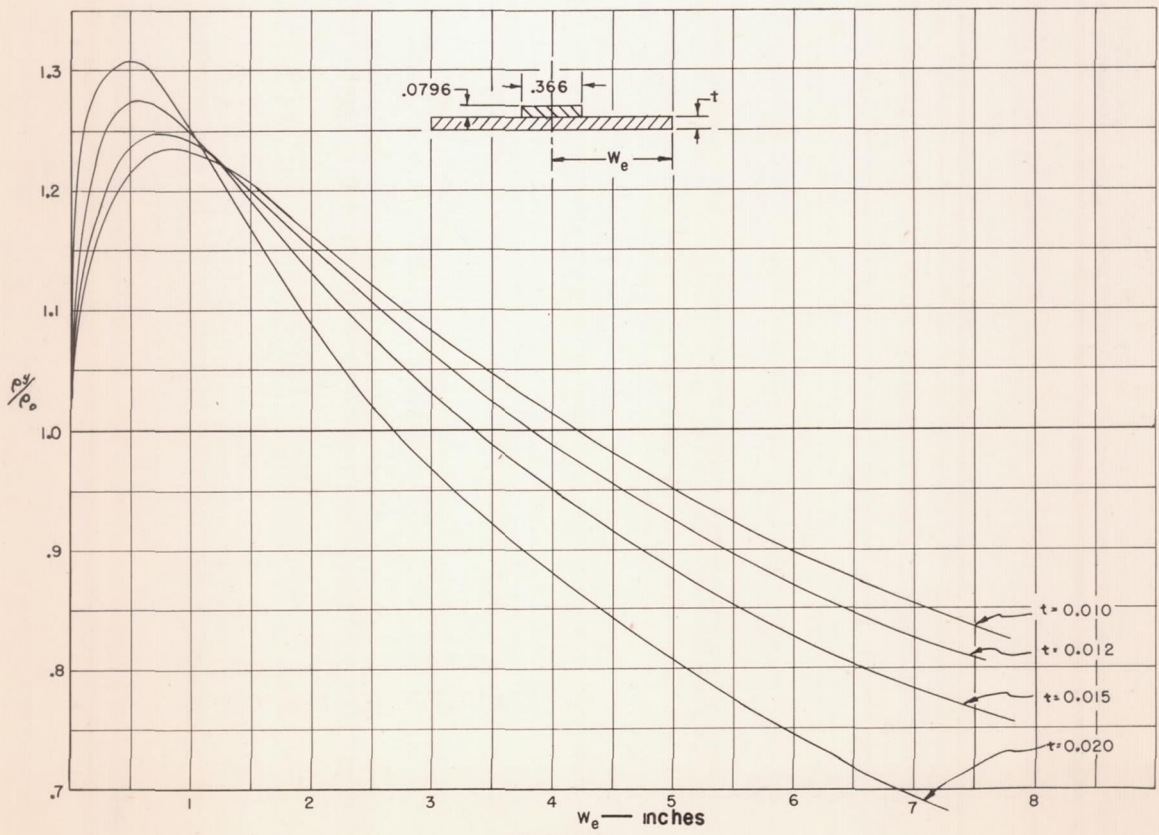
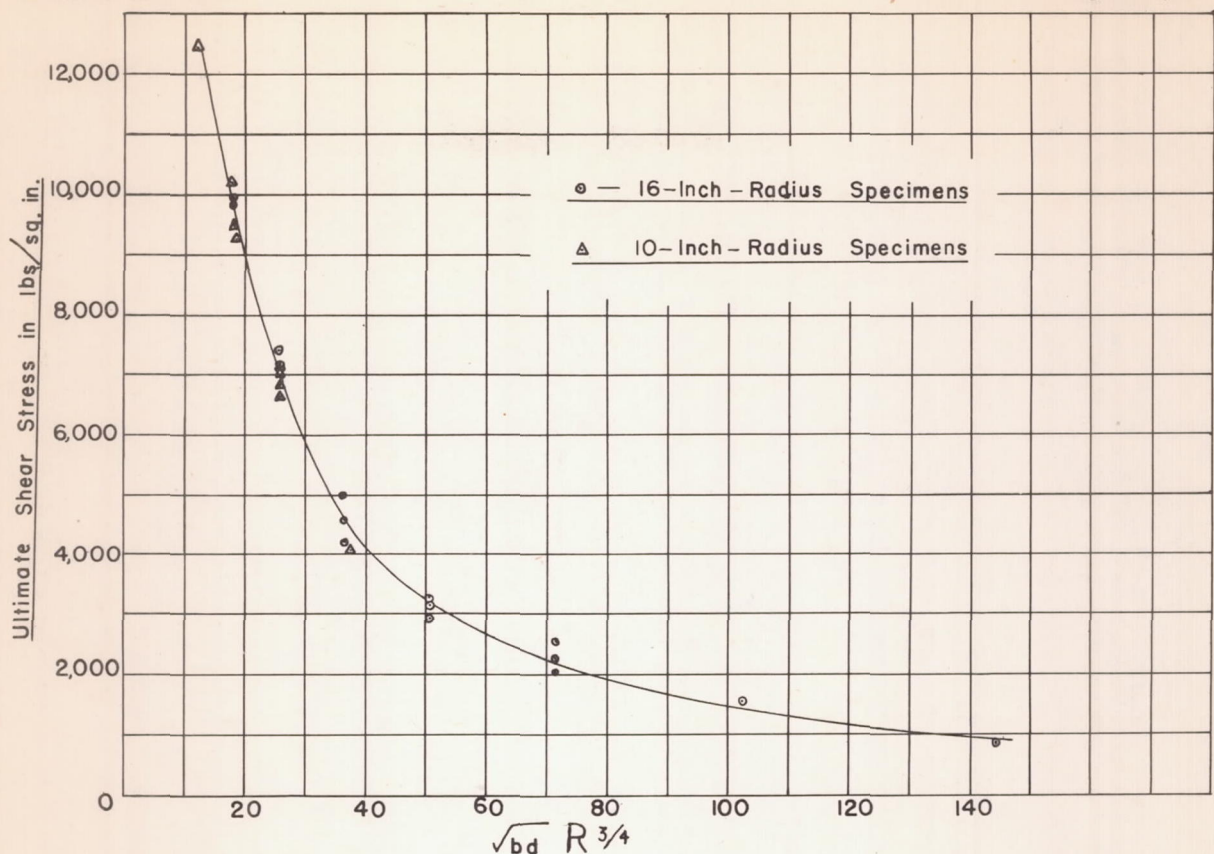


FIGURE 59.

NATIONAL ADVISORY  
COMMITTEE FOR AERONAUTICS.

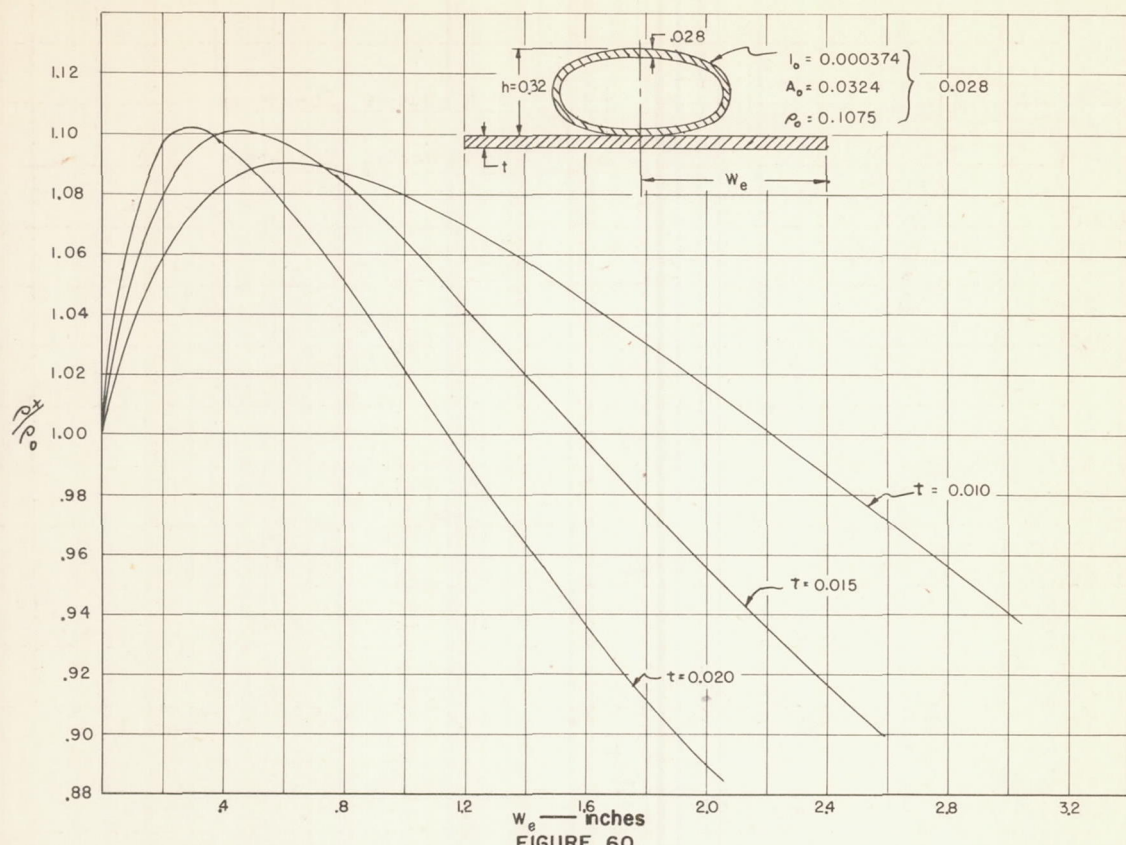
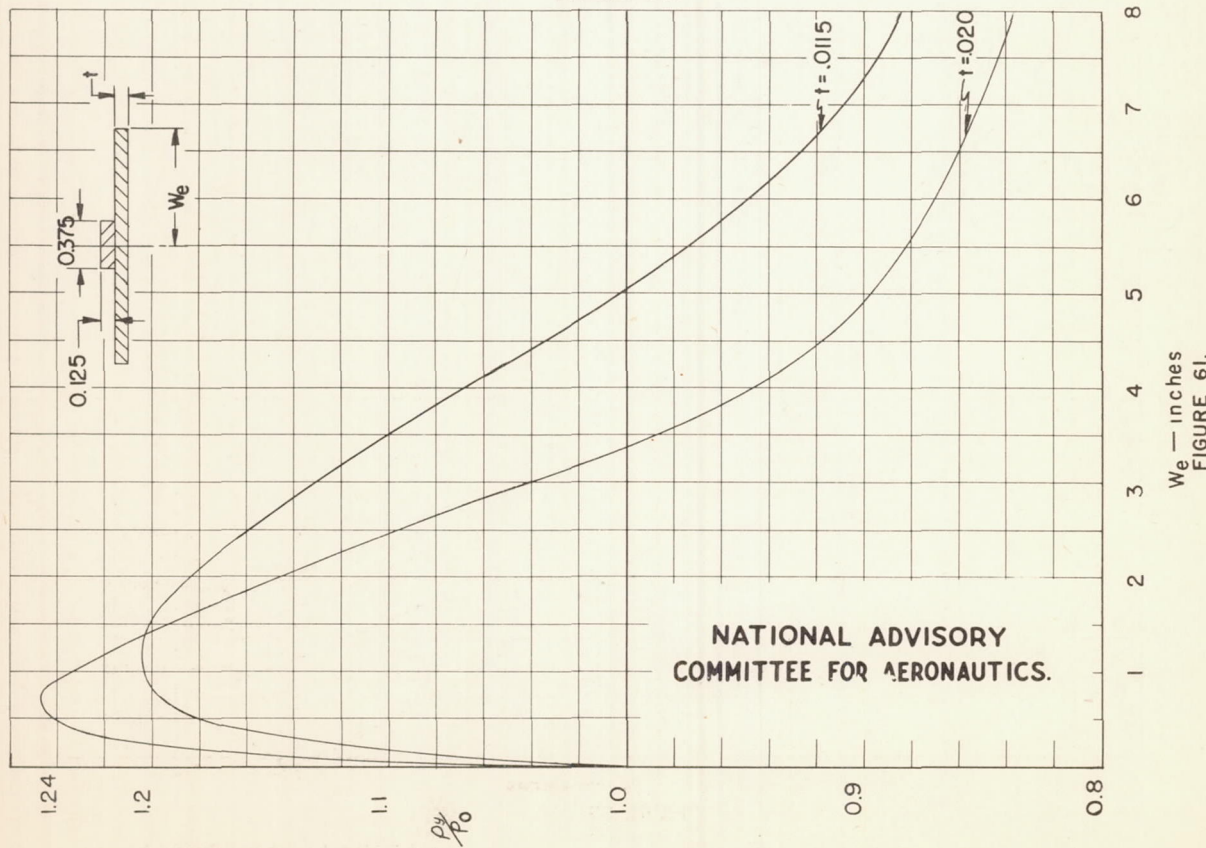
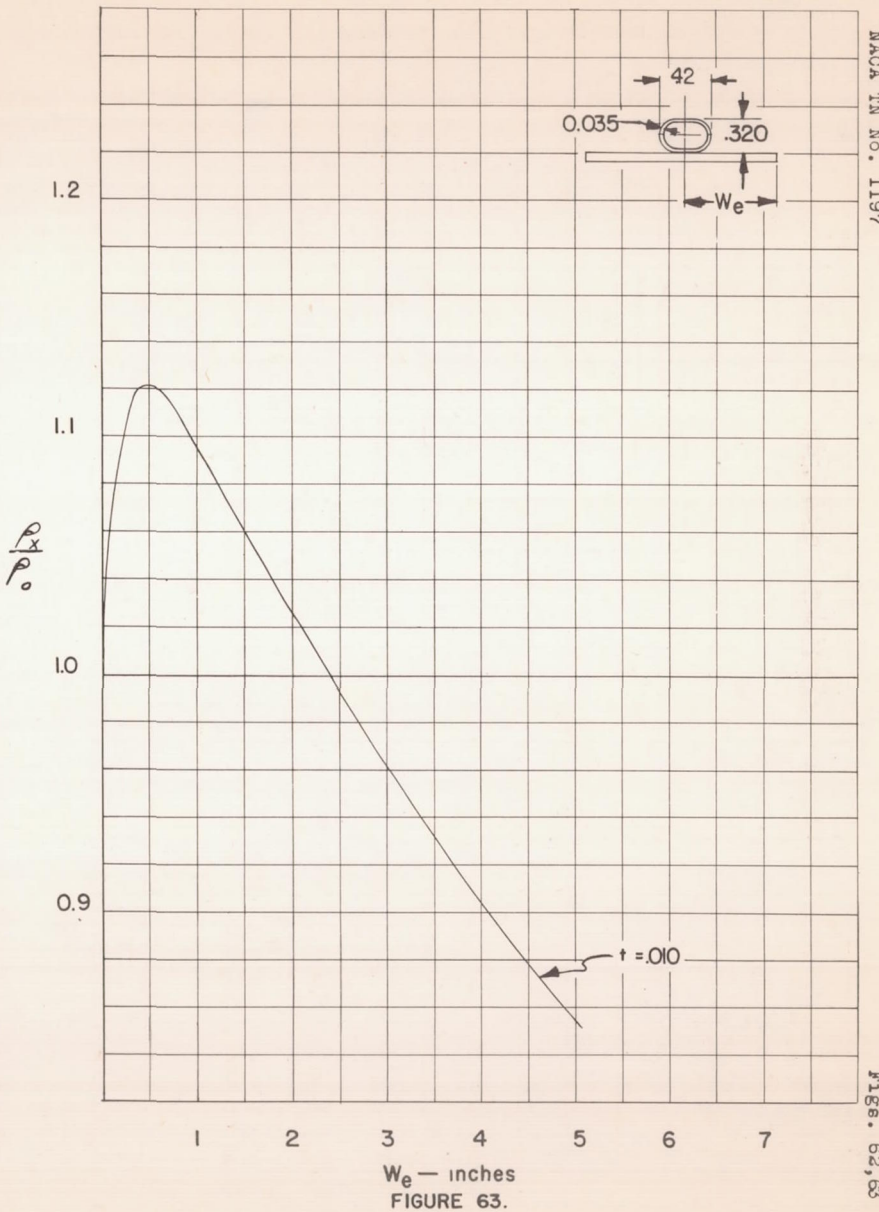
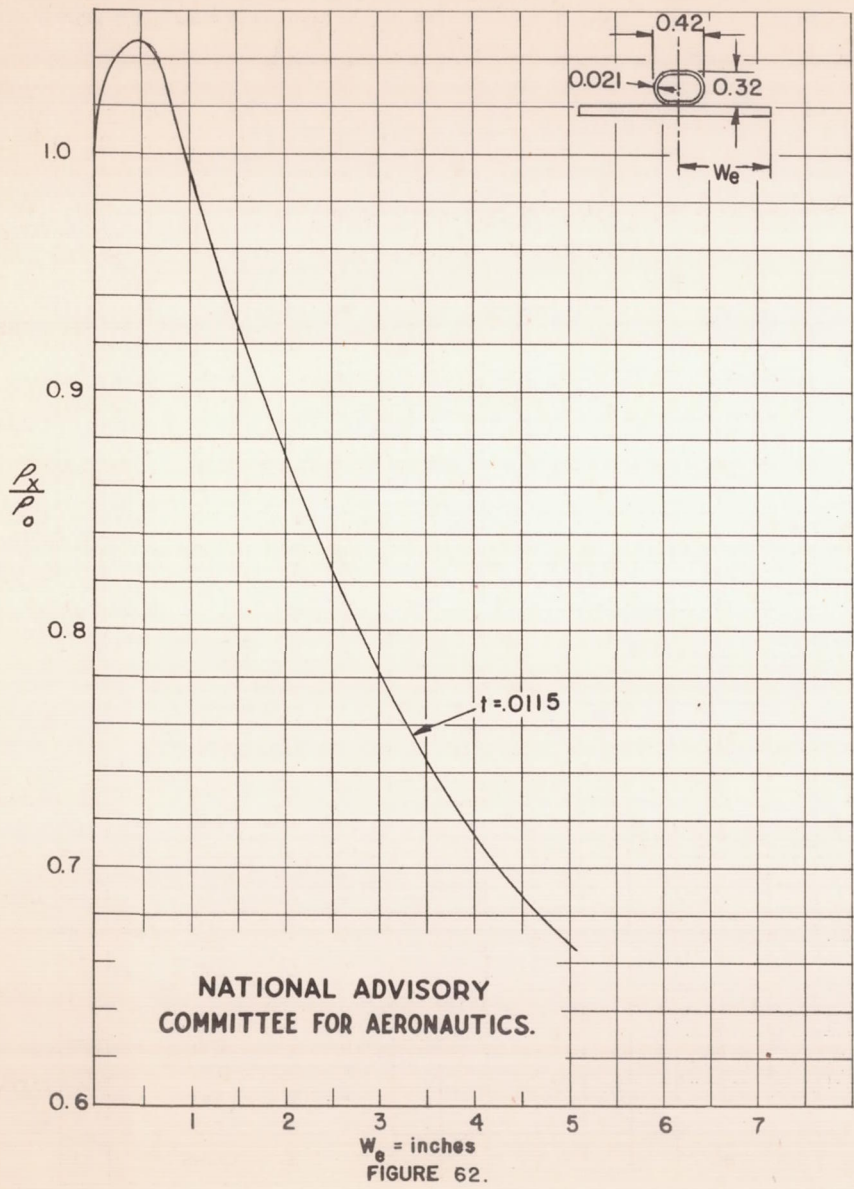


FIGURE 60.





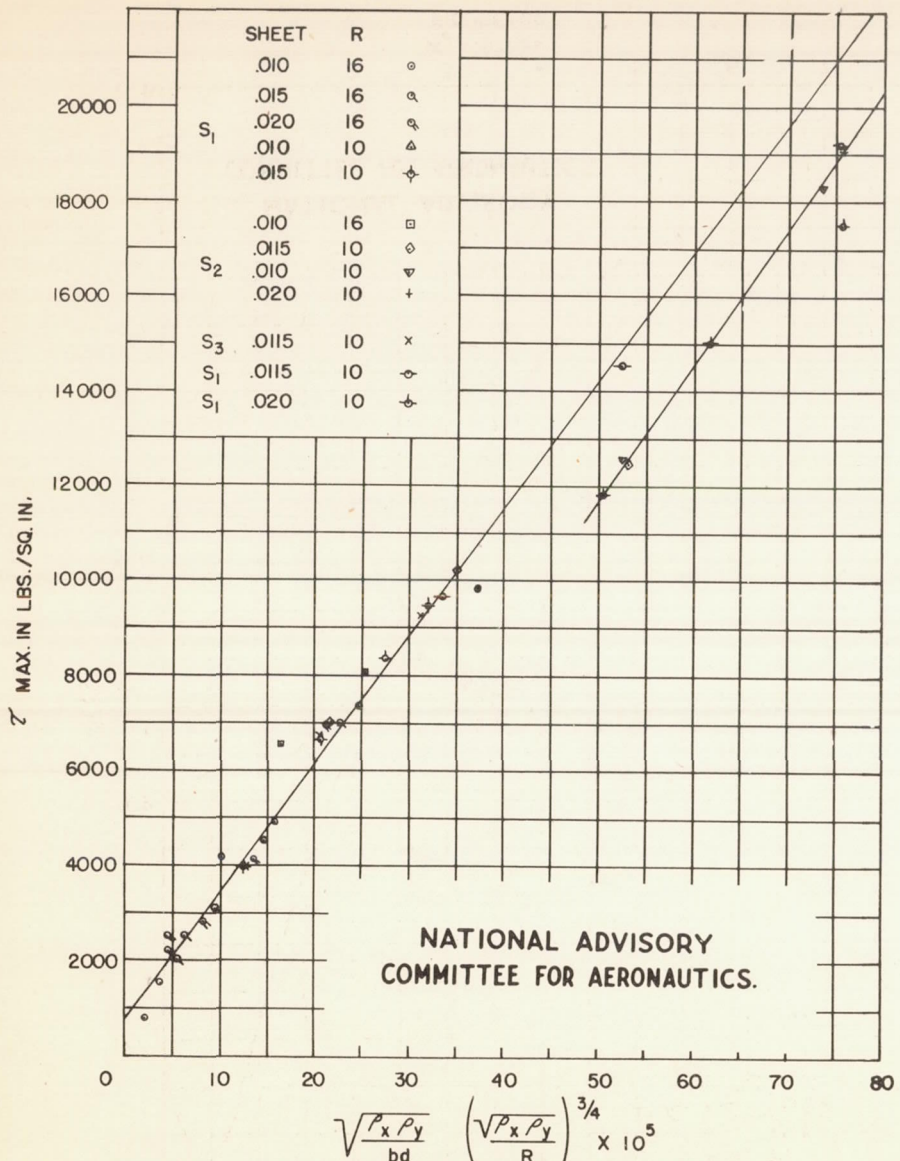


FIGURE 64.- GENERAL INSTABILITY FAILURE; PURE TORSION.

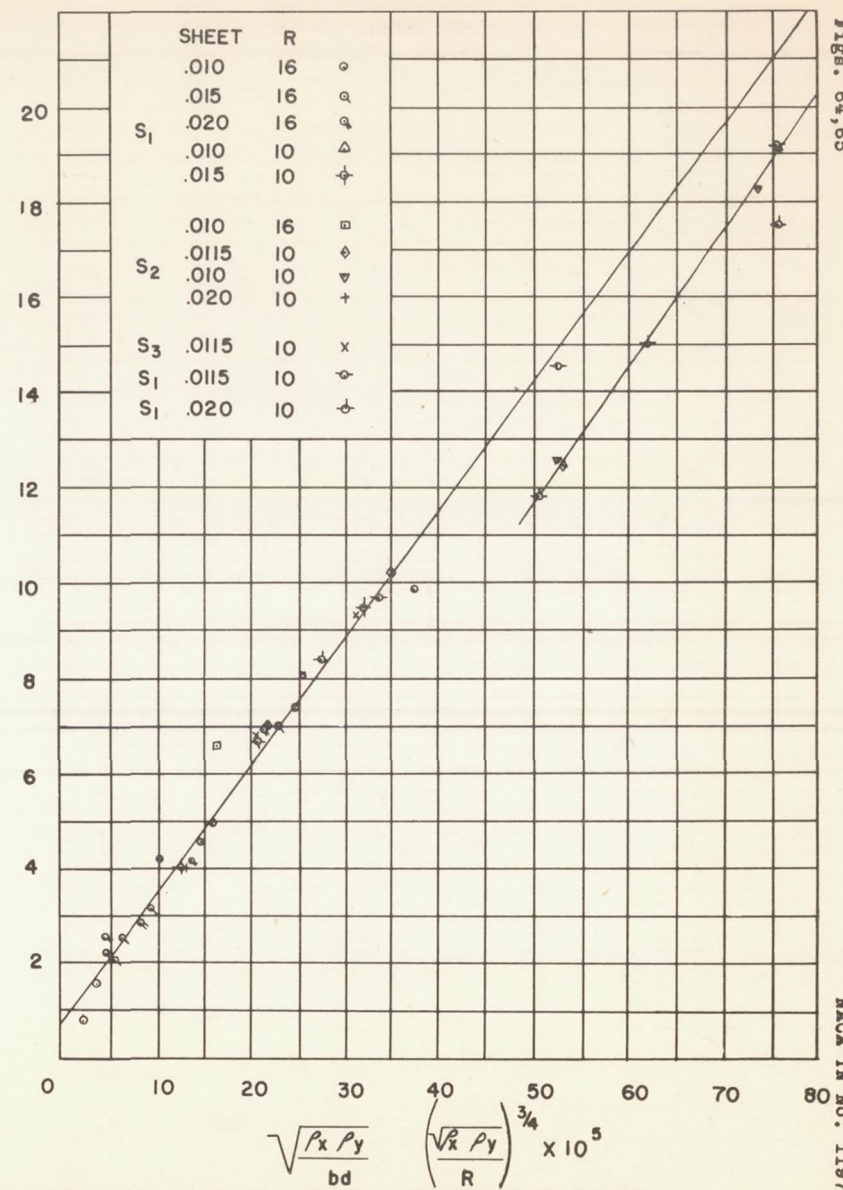
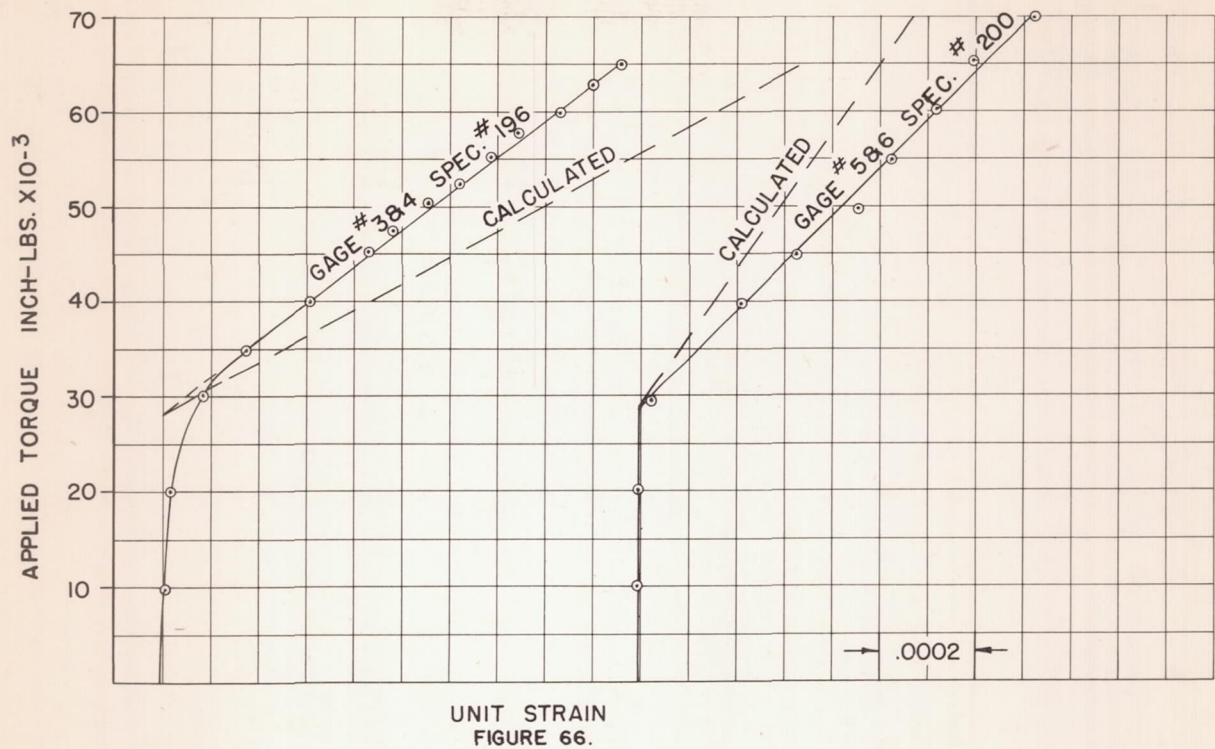
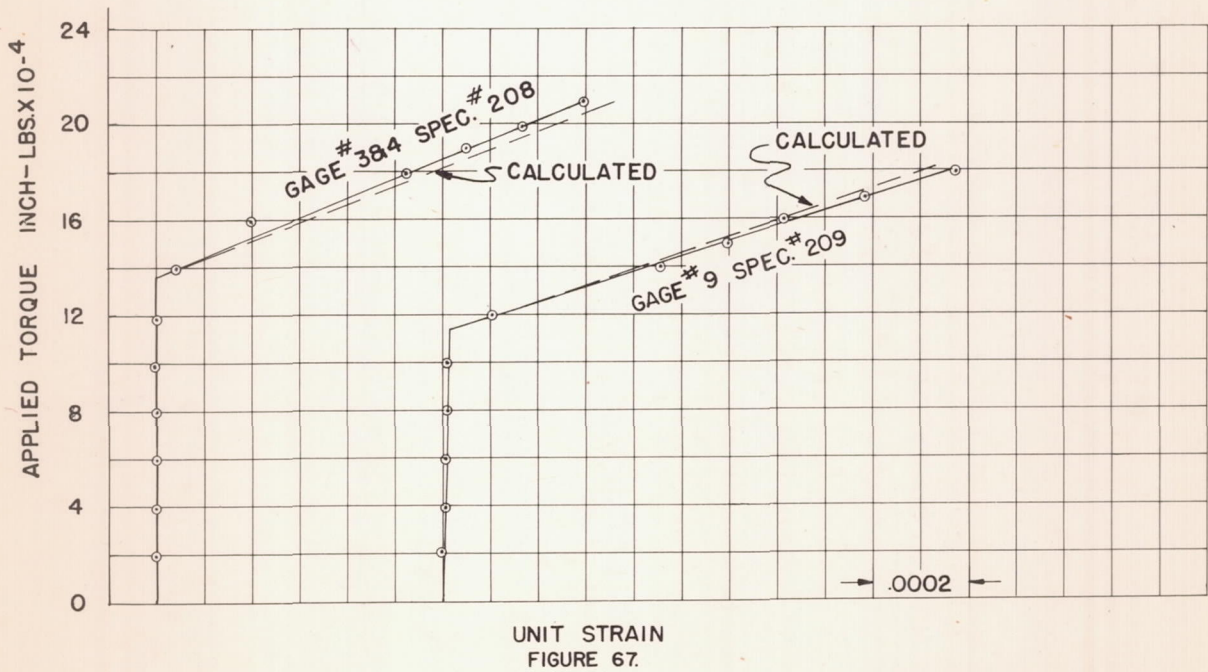


FIGURE 65.- GENERAL INSTABILITY FAILURE; PURE TORSION.

UNIT STRAIN  
FIGURE 66.UNIT STRAIN  
FIGURE 67.NATIONAL ADVISORY  
COMMITTEE FOR AERONAUTICS.